

UNIVERSITY OF CALIFORNIA, SAN DIEGO

**Interannual and decadal variations of Antarctic ice shelves using multi-mission
satellite radar altimetry, and links with oceanic and atmospheric forcings**

A dissertation submitted in partial satisfaction
of the requirements for the degree
Doctor of Philosophy

in

Earth Sciences

by

Fernando Serrano Paolo

Committee in charge:

Helen A. Fricker, Chair
Sarah T. Gille
Falko Kuester
Jean-Bernard Minster
Laurie Padman
David T. Sandwell

2015

Copyright

Fernando Serrano Paolo, 2015

All rights reserved.

The dissertation of Fernando Serrano Paolo is approved,
and it is acceptable in quality and form for publication on
microfilm and electronically:

Chair

University of California, San Diego

2015

DEDICATION

*To my grandma Nira,
my grandpa Horacio,
and my beautiful Charlotte.*

EPIGRAPH

It should never stand as argument the authority of any man, regardless of how excellent and illustrious he is... it is grossly unfair to fold one's own feeling to a submissive reverence toward another; it is worthy of mercenaries or slaves and contrary to the dignity of human freedom to suppress oneself and to be submissive; it is supreme stupidity to believe by inveterate custom; it is an irrational thing to conform with an opinion because of the number of those who have it... it has to be sought, instead, always a reason, true and necessary... and listen to the voice of nature.

—Giordano Bruno 1548–1600 (burned at the stake)

TABLE OF CONTENTS

Signature Page	iii
Dedication	iv
Epigraph	v
Table of Contents	vi
List of Figures	viii
List of Tables	ix
Acknowledgements	x
Vita	xi
Abstract of the Dissertation	xiii
Chapter 1 Introduction	1
1.1 Dissertation outline	1
1.2 Antarctic ice sheet, ice shelves and sea-level change	2
1.3 Satellite altimetry and ice-shelf change detection	5
1.4 Scientific objectives	10
1.5 Summary of results	12
1.6 Future research	13
Chapter 2 Time series of ice-shelf height	19
2.1 Abstract	19
2.2 Introduction	20
2.3 Satellite radar altimeter missions	21
2.4 Processing satellite radar altimeter data	23
2.5 Time series analysis	37
2.6 Results and discussion	44
2.7 Conclusions	48
Chapter 3 Trend analysis of ice-shelf height	57
3.1 Abstract	57
3.2 Introduction	57
3.3 Methods	58
3.4 Results and discussion	60
3.5 Conclusions	67
3.6 Supplementary material	67

Chapter 4	Variability analysis of ice-shelf height	83
4.1	Abstract	83
4.2	Introduction	84
4.3	Methods	86
4.4	Results and discussion	89
4.5	Conclusions	100
4.6	Supplementary material	100

LIST OF FIGURES

Figure 1.1:	Ice flow of the Antarctic Ice Sheet	3
Figure 1.2:	Configuration of an ice sheet and the interaction	4
Figure 1.3:	Configuration of the ice-shelf/ice-sheet interaction	5
Figure 1.4:	Schematic of an Antarctic ice shelf showing the primary	6
Figure 1.5:	Measurement principle of satellite radar altimetry	8
Figure 1.6:	Radar altimeter footprint and waveform	11
Figure 2.1:	ERS-1 radar-altimeter data coverage over the Weddell Sea	23
Figure 2.2:	Flowchart of our RA data processing scheme	25
Figure 2.3:	Representation of the multi-reference time-series approach	31
Figure 2.4:	Estimated radar altimeter extinction coefficient	33
Figure 2.5:	Correlation between backscatter (AGC), ice-shelf height	36
Figure 2.6:	Examples of single-grid-cell 18-year time series	39
Figure 2.7:	Regional time series of average Antarctic ice-shelf height	41
Figure 2.8:	Comparison of noise level between single-grid-cell	42
Figure 2.9:	Maps of rate and acceleration of Antarctic ice-shelf height	47
Figure 3.1:	Eighteen years of change in thickness and volume	61
Figure 3.2:	Variability in the rate of Antarctic ice-shelf thickness	62
Figure 3.3:	Time series of cumulative thickness change	63
Figure 3.4:	Evolution of the rate of thickness change	65
Figure 3.5:	Time series of cumulative thickness change for West	70
Figure 3.6:	Time series of cumulative thickness change for East	71
Figure 3.7:	Average rate and total thickness change for each Antarctic	72
Figure 3.8:	Polynomial versus line fit to 18-year-long records	73
Figure 3.9:	Error map for estimated rates of Antarctic ice-shelf	74
Figure 4.1:	Amundsen Sea ice shelves in Antarctica	86
Figure 4.2:	Decomposition of AS ice-shelf height time series	90
Figure 4.3:	Singular spectrum of AS ice-shelf height time series	92
Figure 4.4:	Modes of oscillation in the ice-shelf height RA time series	93
Figure 4.5:	Power spectrum of the reconstructed RA-derived ice-shelf	94
Figure 4.6:	Singular spectrum of the SOI time series	95
Figure 4.7:	Modes of oscillation in the SOI time series	96
Figure 4.8:	Power spectrum of the reconstructed SOI time series	97
Figure 4.9:	Dominant mode of interannual variability	98
Figure 4.10:	Maps of sea surface temperature (SST) anomaly	105
Figure 4.11:	Principal components retained after pre-PCA filtering	106
Figure 4.12:	Time series reconstruction using EOF 1–4	107
Figure 4.13:	Dominant mode of interannual variability (all time series)	108

LIST OF TABLES

Table 3.1: Average rates and total thickness change for Antarctic ice	75
Table 3.2: Comparison of our estimated thickness-change rates	77

ACKNOWLEDGEMENTS

I would like to acknowledge all the people who have assisted me throughout my dissertation research. In particular, my advisor Helen Fricker and co-advisor Laurie Padman, for their support and guidance throughout my entire PhD work. They were key for the success of my doctorate.

Additionally, I would like to express my sincere gratitude for the service of my committee members, David Sandwell, Jean-Bernard Minster, Sarah Gille and Falko Kuester, in addition to Helen and Laurie.

Finally, I would like to thank all the denizens of IGPP for being so supportive of me during my time at SIO. Many thanks to my good friends, Valerie Sahakian, Robert Petersen, Diego Melgar, Samer Naif, Soli Garcia, Katia Tymofyeyeva, Rachel Marcuson and Ashlee Henig. A very special thank you to Gedilani Oliveira and Catia Perciani; and of course, to my lovely Charlotte.

Chapter 2, in full, is in revision for publication of the material as it may appear in *Remote Sensing of Environment* 2015. Paolo, Fernando S.; Fricker, Helen A.; Padman, Laurie. The dissertation author was the primary investigator and author of this paper.

Chapter 3, in full, is a reprint of the material as it appears in *Science* 2015. Paolo, Fernando S.; Fricker, Helen A.; Padman, Laurie. The dissertation author was the primary investigator and author of this paper.

Chapter 4, in full, is currently being prepared for submission for publication of the material. Paolo, Fernando S.; Fricker, Helen A.; Padman, Laurie. The dissertation author was the primary investigator and author of this material.

VITA

2007	B.S. in Oceanography, University of São Paulo, Brazil
2009	M.S. in Geophysics, University of São Paulo, Brazil
2015	Ph.D. in Earth Sciences, University of California, San Diego Curricular group: Geophysics

AWARDS

2014	AGU Outstanding Student Paper Award, Cryosphere
2013–15	NASA Earth and Space Science Fellowship (NESSF)
2011	AAAS Student Award (1st place), Atmospheric & Oceanographic Sci.
2010	AGU Outstanding Student Paper Award, Cryosphere
2010	Honorable Mention (best M.S. Thesis in Geophysics), Univ. of São Paulo
2007–08	Brazilian Ministry of Sci. & Tech. Fellowship (Masters)
2007	Honorable Mention (2nd best B.S. Thesis), Univ. of São Paulo
2005–06	São Paulo Research Foundation Fellowship (Undergrad)
2004	Brazilian Ministry of Sci. & Tech. Fellowship (Undergrad)

PUBLICATIONS

F. S. Paolo, H. A. Fricker, L. Padman, “Developing improved decadal records of Antarctic ice-shelf height change from multiple satellite radar altimeters”, *Remote Sens. Environ.* (2015) in revision.

P. R. Holland, A. Brisbourne, H. F. J. Corr, D. McGrath, K. Purdon, J. Paden, H. A. Fricker, **F. S. Paolo**, A. Fleming, “Oceanic and atmospheric forcing of Larsen C Ice-Shelf thinning”, *The Cryosphere* (2015).

F. S. Paolo, H. A. Fricker, L. Padman, “Volume loss from Antarctic ice shelves is accelerating”, *Science* (2015).

F. S. Paolo, E. C. Molina, “Integrated marine gravity field along the Brazilian coast from altimeter-derived sea surface gradient and shipborne gravity”, *J. Geodyn.* (2010).

F. S. Paolo, “Satellite altimetry and marine gravity on the integrated representation of the gravity field along the Brazil coast”, *M.S. Thesis* (2009).

M. C. Bícego, E. Zanardi-Lamardo, S. Taniguchi, C. C. Martins, D. A. M. da Silva, S. T. Sasaki, A. C. R. Albergaria-Barbosa, **F. S. Paolo**, R. R. Weber, R. C. Montone, “Results from a 15-year study on hydrocarbon concentrations in water and sediment from Admiralty Bay, King George Island, Antarctica”, *Antarct. Sci.* (2009).

F. S. Paolo, M. M. Mahiques, “Utilization of acoustic methods in coastal dynamics studies: example in the Cananéia lagoonal mouth”, *Braz. J. Geophys.* (2008).

FIELDS OF STUDY

Studies in *Ice and the Climate System* — Prof. H. A. Fricker

Studies in *Physics of Global Warming* — Prof. R. Keeling

Studies in *Physics of Earth Materials (Continuum Mechanics)* — Prof. D. C. Agnew

Studies in *Internal Constitution of the Earth* — Profs. G. T. Masters & D. Stegman

Studies in *Applied Mathematics* — Prof. E. Lauga

Studies in *Inverse Theory* — Prof. C. Constable

Studies in *Geophysical Data Analysis* — Profs. R. L. Parker & D. C. Agnew

Studies in *Oceanographic Data Analysis* — Prof. D. Rudnick

Studies in *Computer Intensive Statistics* — Dr. J. Barlow

Studies in *Numerical Methods for Partial Differential Eqs.* — Prof. Y. Fialko

Studies in *Seismology* — Profs. G. T. Masters & J-B. Minster

Studies in *Geodynamics* — Prof. D. T. Sandwell

Studies in *Gravity and Geomagnetism* — Profs. R. L. Parker & C. Constable

Studies in *Satellite Remote Sensing* — Prof. D. T. Sandwell & H. A. Fricker

Studies in *Ethical & Professional Science* — Profs. S. Constable & C. Constable

ABSTRACT OF THE DISSERTATION

Interannual and decadal variations of Antarctic ice shelves using multi-mission satellite radar altimetry, and links with oceanic and atmospheric forcings

by

Fernando Serrano Paolo

Doctor of Philosophy in Earth Sciences

University of California, San Diego, 2015

Professor Helen A. Fricker, Chair

Antarctica's ice shelves, the floating extensions of the ice sheet, exert an important dynamic constraint on the flow of ice from the grounded ice sheet to the ocean, and hence on changes in global sea level. Thinning of an ice shelf reduces its ability to restrain the ice discharge from the grounded ice-sheet interior. Since the grounded ice sheet responds to perturbations in the ice shelves, predicting sea-level rise requires that we understand the processes that determine ice-shelf response to climate variability. Our understanding of these processes is, however, still too rudimentary to allow prediction of ice-sheet change under projected future climate states. This dissertation presents improved procedures to construct 18-year time series (1994-2012) of ice-shelf height around the entire Antarctic continent by merging data from multiple overlapping

satellite radar altimeter missions (ERS-1, ERS-2, and Envisat). The resulting data set has a temporal resolution of 3 months and a spatial resolution of \sim 30 km. Improved procedures for trend analysis are introduced, and a more accurate alternative for uncertainty estimation to the standard error propagation approach is proposed. Ice-shelf height variability is analyzed using orthogonal-component decomposition of multivariate time series, spectral estimation and background-noise statistical tests. The derived data set and method allow to estimate, reliably and with defined formal uncertainties, the temporal progression and spatial structure of changes in ice-shelf height and volume in Antarctica between 1994 and 2012. The results reveal that, overall, Antarctic ice-shelf volume loss is accelerating. Furthermore, significant interannual variability in the Amundsen Sea ice shelves is strongly correlated with the low-frequency mode of El Niño-Southern Oscillation. These findings may ultimately allow us to understand the processes driving ice-shelf changes sufficiently to improve our models for predicting future ice loss.

Chapter 1

Introduction

1.1 Dissertation outline

This dissertation is organized into four chapters. Each chapter was designed as a self-contained work to address the specific objectives proposed in this PhD research (below). *Chapter 1* presents an introduction to the scientific questions being addressed and the background needed to follow the work developed in *Chapters 2–4*. *Chapter 2* describes the full method implemented in this study (partially developed and partially modified from previous work) to construct the longest, continuous and high-resolution (in time and space) time series of changes in ice-shelf surface height from multiple satellite radar altimeters (RAs). In this chapter, the RA data and corrections are discussed, and new processing approaches are proposed. This chapter is in revision for the journal *Remote Sensing of Environment*. *Chapter 3* describes the trend analysis approach implemented in the ice-shelf height time-series product (derived in *Chapter 2*), as well as reporting and discussing some of the main findings of this dissertation, which have significantly advanced our understanding of the state of the Antarctic ice shelves. This chapter was published in the journal *Science*. *Chapter 4* focuses on the variability analysis of the ice-shelf height time series. This chapter investigates the origin of interannual fluctuations in ice-shelf thickness, and seeks to understand the links between observed ice-shelf changes and large-scale climate variability. The material in this chapter is currently being prepared for publication.

1.2 Antarctic ice sheet, ice shelves and sea-level change

The Antarctic Ice Sheet gains mass through snowfall and loses mass through submarine melting and iceberg calving of its ice shelves, the marginal floating extensions of inland glaciers and ice streams. Both these processes, melting and calving, contribute about equally to ice-shelf loss [Rignot et al. 2013; Depoorter et al. 2013]. The majority of Antarctica's ice drains through these ice shelves, where most of the mass lost from the ice sheet is transferred to the ocean (Fig. 1.1). The Antarctic Ice Sheet contains ice equivalent to ~ 58 m of global sea-level rise¹ [Fretwell et al. 2013], and has been losing mass at an average rate of ~ 71 Gt year⁻¹ (gigatonnes per year)² between 1992 and 2011 [Shepherd et al. 2012]. This is equivalent to a contribution of slightly over 6% to the total sea-level rise of ~ 3.2 mm year⁻¹. More important than the currently small contribution to sea-level rise, however, is the accelerated state of this ice-loss rate, as has been observed during the past decade [Shepherd et al. 2012; Sutterley et al. 2014; Velicogna 2009; Chen et al. 2009; Harig and Simons 2015], which raises significant concern about future ice-sheet behavior and its contribution to sea-level change.

Located at the boundary between the ice sheet, atmosphere and ocean, Antarctica's ice shelves are potentially vulnerable to changes in both atmospheric and oceanic conditions (Fig. 1.2), making them sensitive indicators of large-scale climate change. For more than two decades, rapid changes have been occurring in the extent and thickness of many Antarctic ice shelves, particularly along the Antarctic Peninsula and the Amundsen Sea sector of West Antarctica [Cook and Vaughan 2010; Pritchard et al. 2012; Shepherd et al. 2010; Wingham et al. 2009; Zwally et al. 2005; Fricker and Padman 2012]. It is through the ice shelves that variations in oceanic and atmospheric states are “felt” by the ice sheet, as forcing mechanisms to grounded-ice change.

In the past decade, considerable progress has been made in understanding the fundamental role that ice shelves play in restraining the grounded ice-sheet flow [e.g., Schoof 2007; Goldberg et al. 2009; Gudmundsson 2013]. Ice shelves exert a back-stress on grounded tributary glaciers and ice streams resulting from drag forces at the ice-bedrock interface. This resistive stress, known as the *buttressing effect*, holds back the ice

¹A moderate loss of 2% of the Antarctic Ice Sheet is sufficient to rise global sea level by ~ 1 m.

²360 Gt of ice corresponds roughly to 1 mm of sea-level rise.

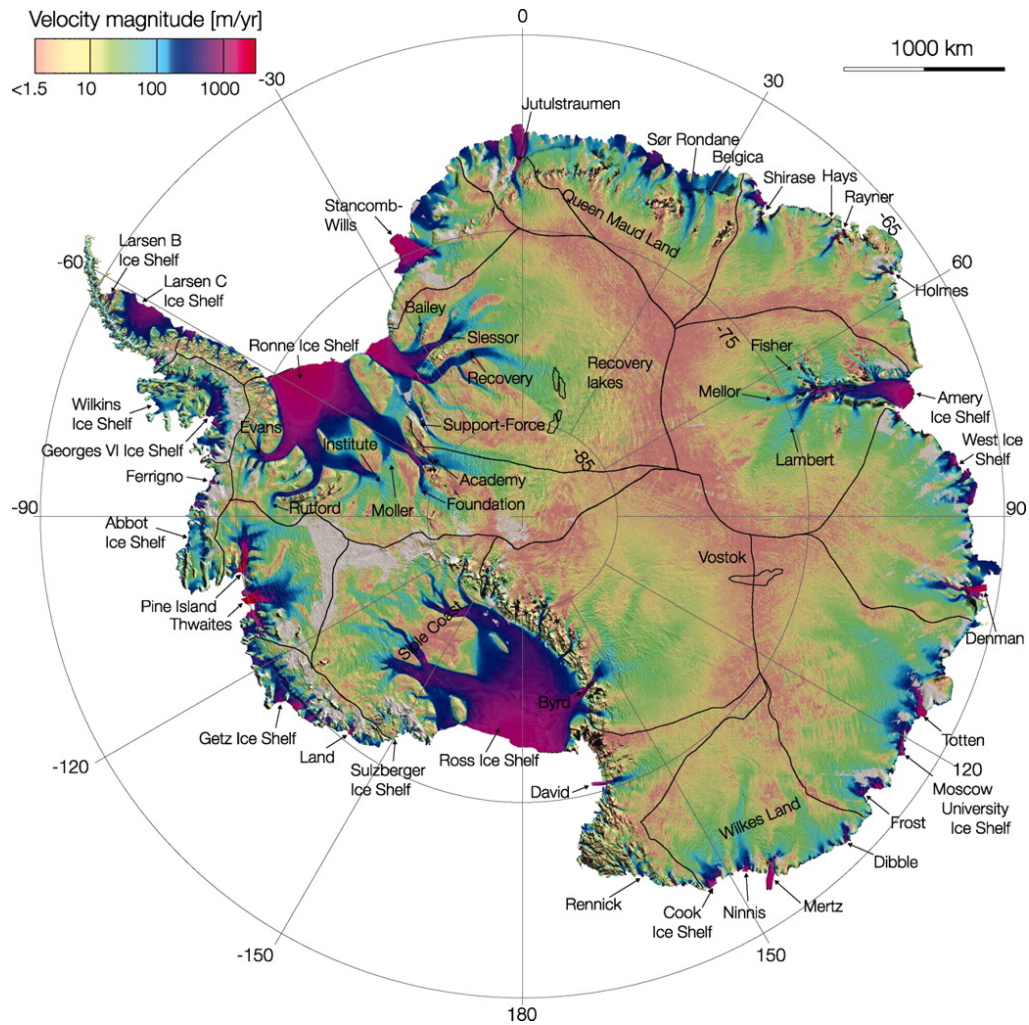


Figure 1.1: Ice flow of the Antarctic Ice Sheet. Color map represents the horizontal velocity field of the ice-sheet's surface (orange is near-zero velocity and purple is maximum velocity), as derived from Interferometric Synthetic Aperture Radar (InSAR). The pattern shows ice flowing from the inland catchment basins towards the ocean through the fringing ice shelves, where flow speed is highest. Credit: NASA; Rignot et al. [2011].

flow from the ice-sheet interior to the ocean (Fig. 1.3). With loss of back-stress due to ice-shelf shrinkage or breakup, ice discharge increases with grounding line (GL)³ thickness to compensate for the reduction in buttressing [Schoof 2007; Joughin et al. 2012]. This nonlinear dynamics, $\text{flow} \propto \text{thickness}^{n \geq 3}$ (at the GL), becomes particularly important in regions where (a) the ice sheet is grounded below sea level (marine ice sheet) and (b) the bed deepens inwards (retrograde bed slope) (Fig. 1.2). Such configuration gives

³The grounding line is the dynamic boundary between the grounded ice sheet and the floating ice shelves; where glaciers/ice streams detach from the bedrock and start to float.

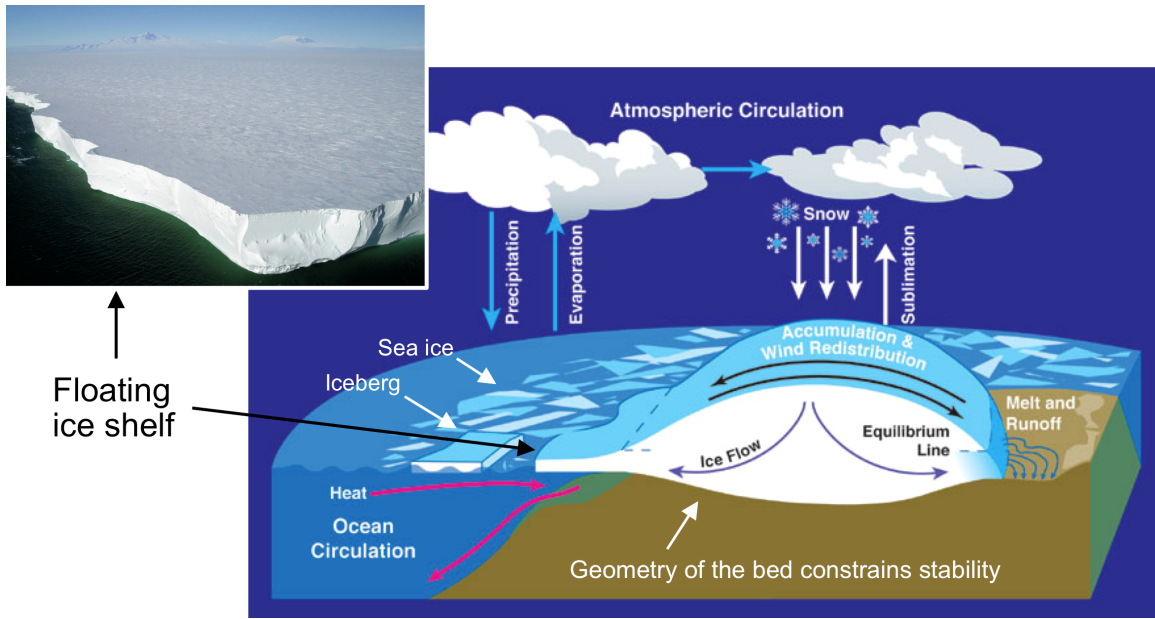


Figure 1.2: Configuration of an ice sheet and the interaction with its surrounding ocean and atmosphere. The left hand side of the ice sheet depicts the characteristic configuration of the Antarctic Ice Sheet, while the right hand side is more characteristic of the Greenland Ice Sheet. Note that ~90% of all ice shelves are in Antarctica. Credit: NASA.

rise to a condition of unstable equilibrium known as the *marine ice-sheet instability*, first proposed in the 1970s by, e.g., Weertman [1974]; Mercer [1978].

There have been recent rapid advances in identifying the dynamical processes by which the ocean can control ice-sheet mass loss and associated sea-level change (Fig. 1.4). Studies have shown that increased ocean-forced basal melting of ice shelves, leading to flow acceleration of adjacent grounded ice, is responsible for the majority of current Antarctic ice sheet loss [Rignot et al. 2008; Pritchard et al. 2009]. Dramatic grounding line retreat as a consequence of intensified basal melting has induced extensive land ice thinning [Wingham et al. 2009; Pritchard et al. 2009; Rignot et al. 2014], and faster flow rates have followed ice shelf collapses due to the reduction in buttressing [Rignot et al. 2004; Scambos et al. 2004]. In fact, 87% of all Antarctic Peninsula (AP) tidewater glaciers are known to be retreating [Cook et al. 2005], and dynamic thinning (increased strain rates due to flow acceleration) has occurred around the AP [Rignot et al. 2008; Pritchard et al. 2009]. These observations have been interpreted as evidence that ocean forcing can lead to rapid changes in ice-sheet dynamic flow and its subsequent contribution to sea-level rise. Despite this progress, our understanding

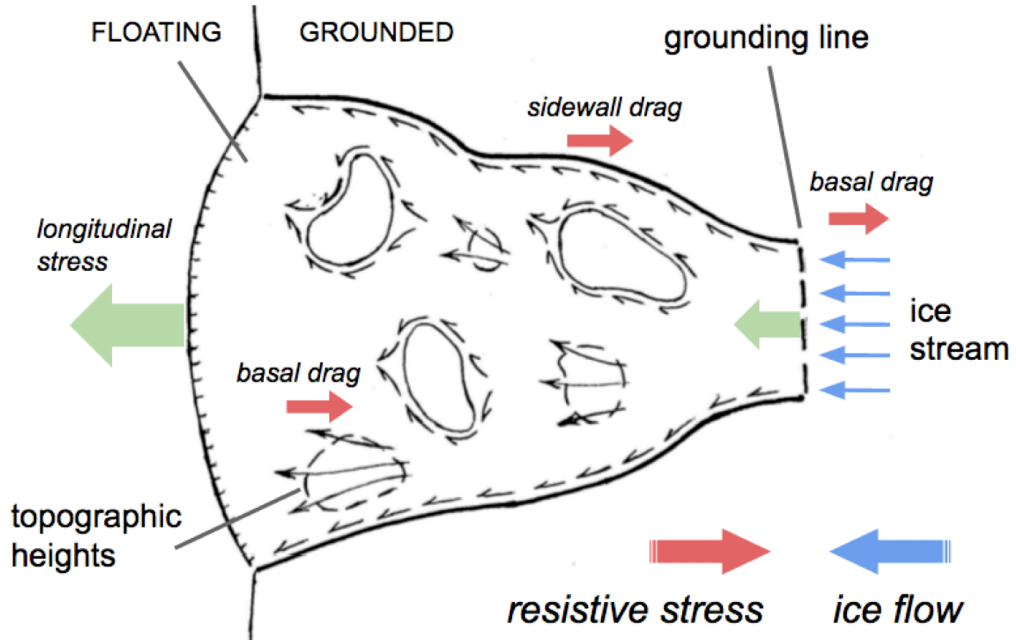


Figure 1.3: Configuration of the ice-shelf/ice-sheet interaction. The arrows show the various forces that interplay at the ice-shelf/ice-sheet transition, giving rise to the buttressing effect (ice-shelf's ability to restrain the grounded ice-sheet flow). *Credit: modified from Hughes et al. [2014].*

of these processes is still too rudimentary to allow prediction of ice-sheet change under projected future climate states.

In essence, since the grounded ice sheet changes in response to perturbations in the ice shelves, understanding variations in the state of the ice shelves is key to identifying relationships between observed ice loss and large-scale climate variability. There are two complementary ways forward: to develop our understanding of the actual mass loss processes, so they can be better represented in models; and to empirically relate observed ice-sheet change to ocean and atmospheric variability. This dissertation focuses on the second approach.

1.3 Satellite altimetry and ice-shelf change detection

Continuous observations of ice shelves over long periods of time are required to determine ice-shelf stability and monitor change. These observations can also be used to identify general relationships between ice-shelf changes and atmospheric and oceanic variability. Given the vast size of Antarctica, its remote location and challenging

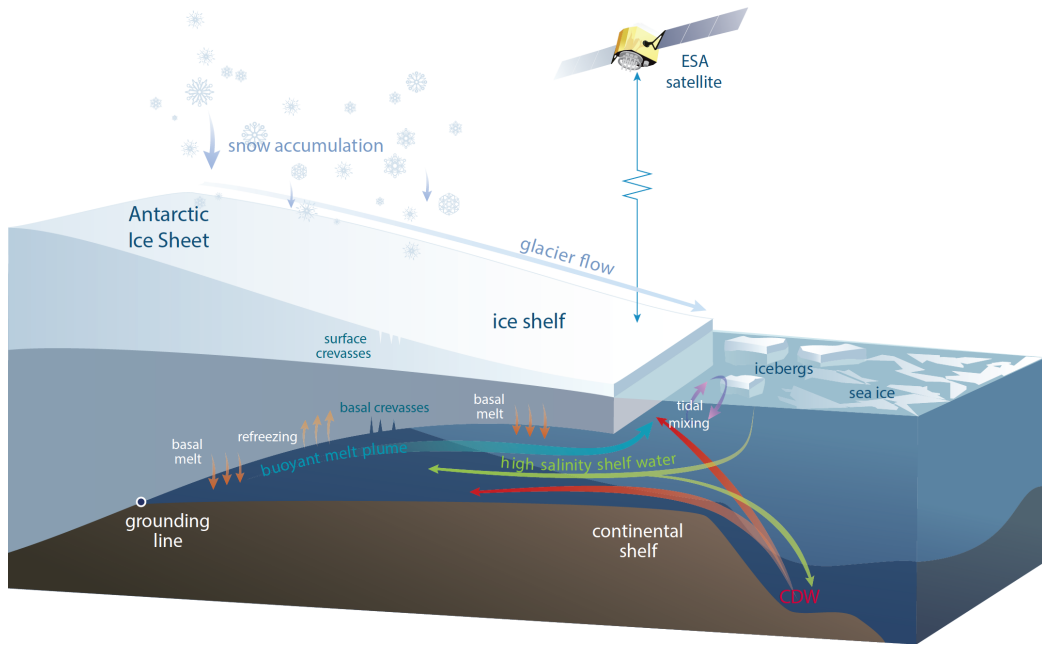


Figure 1.4: Schematic of an Antarctic ice shelf showing the primary processes causing ice-shelf volume changes. Ice is added to the ice shelf by glaciers flowing off the continent and by local snowfall that compresses to form additional ice. Ice is lost when icebergs break off the ice front, and by melting at the ice base in some regions as warm water flows into the ocean cavity under the ice shelf. Under some ice shelves, cold and fresh meltwater rises to a point where it refreezes onto the ice shelf. In this schematic, the grounding line is sitting on a “retrograde” slope (sloping downwards towards the continental interior). See Fig. 1.5 for explanation of satellite measurement.

field conditions, space-based techniques are the only practical way to monitor the ice shelves. Much of our current understanding of how ice-shelf processes couple ice-sheet changes to climate variability comes from analyses of trends in surface elevation change, $\partial h / \partial t$, derived from satellite radar and laser altimeter measurements (Fig. 1.4) [Zwally et al. 2005; Shepherd et al. 2010; Pritchard et al. 2012; Fricker and Padman 2012]. In particular, satellite radar altimeters have provided the longest set of continuous observations over the Antarctic and Greenland ice sheets, and have dramatically changed our ability to study these ice masses. Maps of ice-shelf height change at high spatial resolution have also been developed using measurements from a satellite laser altimeter (ICESat)⁴ [Pritchard et al. 2012], but the time span of the data set only covered the period 2003–2008 (5 years). In contrast, satellite radar altimeters have been providing

⁴ICESat (Ice, Cloud, and land Elevation Satellite), was a NASA satellite mission for measuring ice sheet mass balance, cloud and aerosol heights, as well as land topography and vegetation characteristics. It operated from 2003 to 2010.

measurements of the ice shelves since 1978⁵ [Zwally et al. 1983; Zwally et al. 1989; Davis et al. 1998; Martin et al. 1983]. Historical RA missions like Seasat (1978) and Geosat (1985–1989) were limited to orbit latitudes equatorward of 72° and, although insufficient for whole ice sheet studies, this coverage did capture a portion of the fringing ice shelves and marginal grounded ice [e.g., Fricker and Padman 2012].

More than two decades of modern RA missions, including ERS-1 (1992–1996), ERS-2 (1995–2003), Envisat (2002–2012), and Cryosat-2 (2010–present), have dramatically improved our understanding of ice-sheet mass balance and its relation to measured sea-level rise [e.g., Shepherd et al. 2012; Wingham et al. 2006]. In general, however, studies focusing on the ice shelves using RA have under-exploited these data, reporting linear height-trends for a fraction—and usually averaged over broad regions—of the complete (modern-era) RA data set [e.g., Shepherd et al. 2003; Shepherd et al. 2010; Zwally et al. 2005].

A satellite radar altimeter measures the satellite-to-surface round-trip travel time of the emitted electromagnetic waves (Fig. 1.5). The standard altimeters used in this study operated in the Ku-band (microwaves): 13.6–13.8 GHz frequency, 2.2–2.3 cm wavelength. As electromagnetic waves travel through the atmosphere, they can be delayed by water vapour or by free electrons. Once the data are corrected for these effects, the final range R is estimated with high precision⁶. The radar-altimeter’s response over ice surfaces is considerably more complex than over the oceans. Causal factors identified in the complex backscatter response over ice sheets include: sloping surfaces, surface undulations with characteristic wavelengths on the same spatial scale as the altimeter beam-limited footprint, off-track reflections, dynamic lag of the altimeter tracking circuit (on-board, which requires off-board post-processing—retracking), and spatio-temporal variations in the ice-surface properties (leading to backscatter fluctuations) [Martin et al. 1983].

⁵Although another radar altimeter flew before this date over the ice sheets (the GEOS-3), its experimental measurements were not useful for ice-sheet change determination.

⁶The strength of satellite radar altimeters is their single-measurement high precision, which is fundamental for estimating changes (more so than accuracy).

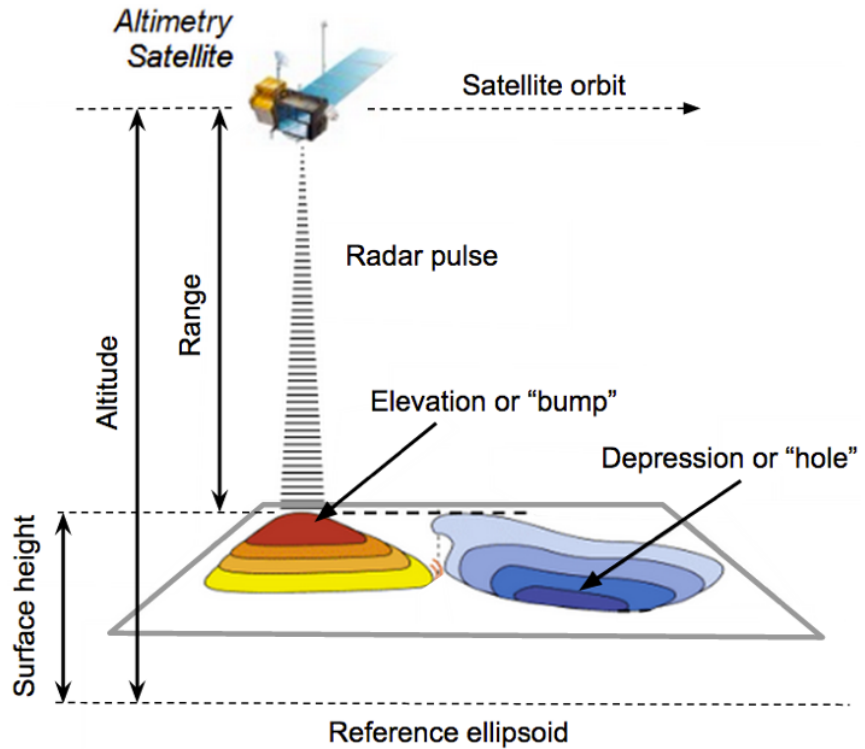


Figure 1.5: Measurement principle of satellite radar altimetry. (top) Radar altimeters estimate the height of surface reflectors (with respect to a reference ellipsoid, e.g., WGS84) by measuring the satellite-to-surface round-trip travel time of radar pulses. (bottom) The three European Space Agency satellites used in this study (from left to right): the European Remote Sensing Satellite-1 (ERS-1, 1992–1996), the European Remote Sensing Satellite-2 (ERS-2, 1995–2003), and the Environmental Satellite (Envisat, 2003–2012).

The ice-shelf height measured by an altimeter can be represented as:

$$h = A - (R - D) \quad (1.1)$$

where h is the surface height with respect to the ellipsoid, A is the satellite's altitude, R is the satellite-to-surface measured range, and D is the atmospheric path delay (Fig. 1.5). Surface height h is derived, along with other parameters, from the radar echo waveform (the shape of the return pulse; see Fig. 1.6). By performing repeated measurements over time we can track changes in the ice-shelf height that can be related to the ice-shelf mass balance as follows [Shepherd et al. 2004b; Padman et al. 2012]:

$$\frac{\partial h}{\partial t} = \underbrace{\frac{\partial \Delta}{\partial t}}_d - M \underbrace{\frac{\partial}{\partial t} \rho_w^{-1}}_e + \underbrace{\int_0^M dm \frac{\partial}{\partial t} \rho_f^{-1}(m)}_c + (\rho_i^{-1} - \rho_w^{-1}) \cdot (\dot{M}_s + \dot{M}_b + \mathbf{u} \cdot \nabla M + M \nabla \cdot \mathbf{u}) \quad (1.2)$$

where Δ is the ocean-surface height; M is ice-shelf mass per unit area; ρ_w , ρ_f and ρ_i are the densities of water, firn and ice, respectively; \mathbf{u} is the horizontal velocity; and ∇ is the gradient operator (∂_x, ∂_y). The individual terms in the equation represent (a) sea-level variations, (b) ocean-density changes, (c) firn compaction (air loss), (d) ice-ocean density contrast, (e) surface and basal ice-shelf accumulation rates, and (f) advection of thickness gradient and flow divergence.

The estimates for the Antarctic mass budget, derived from satellite observations over the past two decades, vary widely according to the method they are based upon—for example, from -250 to $+50$ Gt year $^{-1}$ for 1992–2009 [Zwally and Giovinetto 2011]. As reported by Zwally and Giovinetto [2011]:

Generally, the range of estimates in IPCC07⁷ encompassed the errors listed in the studies, but as noted in the report, a mid-range value does not indicate a more reliable estimate, and the composite errors listed in each

⁷Fourth Assessment Report (AR4) of the Intergovernmental Panel on Climate Change (IPCC), 2007: https://www.ipcc.ch/publications_and_data/publications_ipcc_fourth_assessment_report_synthesis_report.htm.

study do not define confidence limits because important components lack formal statistical derivation. This caution on the error estimates applies to all studies regardless of methods of data collection and analyses.

This highlights the need to account for uncertainties more consistently, as well as analyzing the inherently noisy and complex altimeter measurements within a robust statistical framework.

1.4 Scientific objectives

This dissertation seeks to address the following scientific questions. a) Has $\partial h/\partial t$ for Antarctic ice shelves been constant, or has it varied over time? b) Are the observed changes restricted to particular regions, or do they occur at a larger scale? c) What are the spatial patterns of coherence in $\partial h/\partial t$ around Antarctica? d) Are there links between interannual variations in the ice shelves and large-scale climate variability?

To answer these questions, this PhD research was designed around three main objectives, which became chapters of this dissertation:

- i. *Derive reliable time series of height change (Chapter 2).* Improve and extend the procedures for extracting height changes from multi-mission RA records, deriving reliable long-term, continuous time series in a high-resolution grid for consistent trend and variability analysis.
- ii. *Quantify long-term trends (Chapter 3).* Analyze long-term changes for all Antarctic ice shelves spanning a time period of nearly two decades, mapping in time and space the rate of change in ice-shelf height and volume, the acceleration and associated uncertainties.
- iii. *Analyze interannual variability (Chapter 4).* Use the extended time series and spatial maps to seek relationships between fluctuations in ice-shelf height and known modes of variability in the atmosphere and the ocean, such as the El Niño-Southern Oscillation.

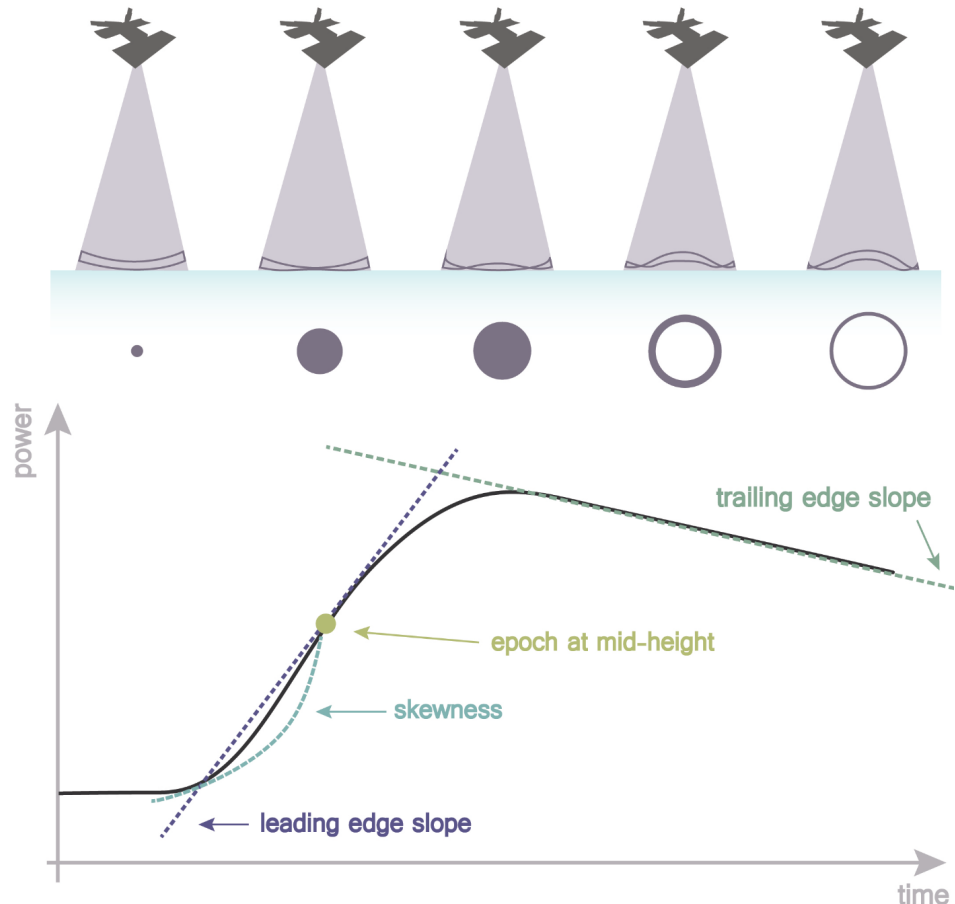


Figure 1.6: Radar altimeter footprint and waveform. (top) The radar altimeter receives the reflected wave (or echo), which varies in intensity over time. Over a flat surface the reflected wave's amplitude increases sharply from the moment the leading edge of the radar signal strikes the surface. (bottom) The echo waveform has a characteristic shape that can be described analytically (the Brown model [Brown 1977]). From this shape, several parameters can be deduced by comparing the real (averaged) waveform with the theoretical curve. *Epoch at mid-height*: this gives the time delay of the expected return of the radar pulse (estimated by the tracker algorithm) and thus the time that the radar pulse took to travel the satellite-surface distance (*Range*) and back again. *Amplitude of the useful signal*: this amplitude with respect to the emission amplitude gives the backscatter coefficient (σ_0). *Thermal noise*: the instrument's (internal) background noise. *Leading-edge slope*: this can be related to the significant wave height (SWH) or surface roughness. *Skewness*: the leading edge curvature. *Trailing-edge slope*: this is linked to any mispointing of the radar antenna (any deviation from nadir of the radar pointing). Credit: modified from ESA's Radar Altimetry Tutorial; Caroline Fleet.

1.5 Summary of results

This dissertation presents methods for improved analysis of ice-shelf height data from multiple satellite RAs and estimation of uncertainties in the resulting products. We constructed 18-year-long time series of height changes at ~ 3 month intervals and ~ 30 km grid cells over Antarctica's floating ice shelves. Our data set allowed us to estimate, reliably and with defined formal uncertainties, the temporal progression and spatial structure of changes in ice-shelf height in Antarctica between 1994 and 2012.

We have demonstrated that: i) substantial averaging both in time and space is required to construct reliable RA height records over floating ice shelves; ii) densification of the surface strongly affects the height-change estimate, and the backscatter correction significantly reduces this effect; iii) densification is a more important effect than penetration in biasing the height-change estimates over the ice shelves; iv) given the high interannual-to-decadal variability that is present, a simple straight-line fit fails to capture the underlying trends, some degree of curvature in the trend is needed; v) polynomial trends allow us to obtain information on the evolution and spatial structure of changes, for instance, instantaneous rate of change (derivative of the trend) and average acceleration (slope of the derivative); and vi) given the convoluted nature of the error sources, a top-down approach for uncertainty estimation (such as bootstrap applied to time-dependent data) constitutes a more accurate alternative for error analysis.

We have shown that Antarctic ice-shelf volume loss is accelerating. In the Amundsen Sea, some ice shelves buttressing regions of grounded ice that are prone to instability have experienced sustained rapid thinning for almost two decades. If the present climate forcing is sustained, we expect a drastic reduction in volume of the rapidly thinning ice shelves at decadal to century time scales, resulting in grounding-line retreat and potential ice-shelf collapse. Both of these processes further accelerate the loss of buttressing, with consequent increase of grounded-ice discharge and sea-level rise. On smaller scales, ice-shelf thickness variability is complex, demonstrating that results from single satellite missions with typical durations of a few years are insufficient to draw conclusions about the long-term response of ice shelves. Large changes occur over a wide range of time scales, with rapid variations of ice-shelf thickness suggesting that

ice shelves can respond quickly to changes in oceanic and atmospheric conditions.

We have presented a signal-detection procedure that (a) optimizes the fundamental signal-to-noise ratio problem through the combination of multivariate singular spectrum analysis, principal component analysis, maximum entropy and multi-taper methods; and (b) tests assumptions regarding the detectability of signals immersed in background noise, which is of fundamental importance in analyzing short and noisy records. We have shown that there is significant variability in ice-shelf height in the Amundsen Sea sector, particularly at the interannual scale. This interannual response is strongly correlated with the low-frequency mode of El Niño-Southern Oscillation (ENSO). Due to the convoluted nature of different modes of variability and lack of observations, an ENSO signature in Antarctica has been suggested but not unequivocally demonstrated so far. Thus, our results are the first direct observational evidence of a teleconnection between climate dynamics in the tropical Pacific Ocean and the mass balance of Antarctic ice shelves and, through the buttressing effect, the mass balance of the Antarctic Ice Sheet. This may ultimately allow us to improve our models for predicting future ice loss.

1.6 Future research

Our variability analysis, performed on the 18-year record of ice-shelf height changes in the Amundsen region, showed that there is significant interannual fluctuation in Antarctic ice-shelf volume. This variation in ice-shelf mass not only fingerprints the mechanisms by which oceanic and atmospheric forcing perturbs the ice-sheet flow, but also provides the basis for estimating changes in freshwater fluxes around Antarctica, an important and poorly constrained parameter for modeling the polar-ocean circulation and ice-sheet dynamics. In a planned postdoctoral project, we will focus on two complementary analyses based on the results and products presented in this dissertation. 1) We will extend our study on the ENSO-Amundsen linkage by including potential correlations of estimated ice-shelf “modes” of variability with other climatic variables such as sea-ice extent, wind velocity and sea-surface pressure off the coast of Antarctica. 2) We will convert our regional estimates of ice-shelf volume changes to equivalent “excess” freshwater flux to estimate and map the time-dependence of freshwater input

to Antarctic coastal regions (Ross, Amundsen, Bellingshausen, Larsen, Filchner-Ronne, Queen Maud, Amery, and Wilkes) previously defined by Paolo et al. [2015b].

References

- Brown, G. S. (1977). "The average impulse response of a rough surface and its applications". *IEEE Transactions on Antennas and Propagation* 25, 67–74.
- Chen, J. L., C. R. Wilson, D. Blankenship, and B. D. Tapley (2009). "Accelerated Antarctic ice loss from satellite gravity measurements". *Nature Geoscience* 2, 859–862.
- Cook, A. J., A. J. Fox, D. G. Vaughan, and J. G. Ferrigno (2005). "Retreating Glacier Fronts on the Antarctic Peninsula over the Past Half-Century". *Science* 308, 541–544.
- Cook, A. J. and D. G. Vaughan (2010). "Overview of areal changes of the ice shelves on the Antarctic Peninsula over the past 50 years". *The Cryosphere* 2002, 77–98.
- Davis, C. H., C. A. Kluever, and B. J. Haines (1998). "Elevation Change of the Southern Greenland Ice Sheet". *Science* 279, 2086–2088.
- Depoorter, M. A., J. L. Bamber, J. A. Griggs, J. T. M. Lenaerts, S. R. M. Ligtenberg, M. R. van den Broeke, and G. Moholdt (2013). "Calving fluxes and basal melt rates of Antarctic ice shelves". *Nature* 502, 89–92.
- Fretwell, P., H. D. Pritchard, D. G. Vaughan, J. L. Bamber, N. E. Barrand, R. Bell, C. Bianchi, R. G. Bingham, D. D. Blankenship, G. Casassa, G. Catania, D. Callens, H. Conway, A. J. Cook, H. F. J. Corr, D. Damaske, V. Damm, F. Ferraccioli, R. Forsberg, S. Fujita, Y. Gim, P. Gogineni, J. A. Griggs, R. C. A. Hindmarsh, P. Holmlund, J. W. Holt, R. W. Jacobel, A. Jenkins, W. Jokat, T. Jordan, E. C. King, J. Kohler, W. Krabill, M. Riger-Kusk, K. A. Langley, G. Leitchenkov, C. Leuschen, B. P. Luyendyk, K. Matsuoka, J. Mouginot, F. O. Nitsche, Y. Nogi, O. A. Nost, S. V. Popov, E. Rignot, D. M. Rippin, A. Rivera, J. Roberts, N. Ross, M. J. Siegert, A. M. Smith, D. Steinhage, M. Studinger, B. Sun, B. K. Tinto, B. C. Welch, D. Wilson, D. A. Young, C. Xiangbin, and A. Zirizzotti (2013). "Bedmap2: improved ice bed, surface and thickness datasets for Antarctica". *The Cryosphere* 7, 375–393.
- Fricker, H. A. and L. Padman (2012). "Thirty years of elevation change on Antarctic Peninsula ice shelves from multimission satellite radar altimetry". *Journal of Geophysical Research: Oceans* 117, C02026.
- Goldberg, D., D. M. Holland, and C. Schoof (2009). "Grounding line movement and ice shelf buttressing in marine ice sheets". *Journal of Geophysical Research: Earth Surface* 114, F04026.
- Gudmundsson, G. H. (2013). "Ice-shelf buttressing and the stability of marine ice sheets". *The Cryosphere* 7, 647–655.
- Harig, C. and F. J. Simons (2015). "Accelerated West Antarctic ice mass loss continues to outpace East Antarctic gains". *Earth and Planetary Science Letters* 415, 134–141.

- Hughes, T., A. Sargent, J. Fastook, K. Purdon, J. Li, J.-B. Yan, and S. Gogineni (2014). “Quantifying the Jakobshavn Effect: Jakobshavn Isbrae, Greenland, compared to Byrd Glacier, Antarctica”. *The Cryosphere Discuss.* 8, 2043–2118.
- Joughin, I., R. B. Alley, and D. M. Holland (2012). “Ice-Sheet Response to Oceanic Forcing”. *Science* 338, 1172–1176.
- Martin, T. V., H. J. Zwally, A. C. Brenner, and R. A. Bindschadler (1983). “Analysis and Retracking of Continental Ice Sheet Radar Altimeter Waveforms”. *Journal of Geophysical Research* 88, 1608–1616.
- Mercer, J. H. (1978). “West Antarctic ice sheet and CO₂ greenhouse effect: a threat of disaster”. *Nature* 271, 321–325.
- Padman, L., D. P. Costa, M. S. Dinniman, H. a. Fricker, M. E. Goebel, L. a. Huckstadt, A. Humbert, I. Joughin, J. T. M. Lenaerts, S. R. M. Ligtenberg, T. Scambos, and M. R. Van Den Broeke (2012). “Oceanic controls on the mass balance of Wilkins Ice Shelf, Antarctica”. *Journal of Geophysical Research: Oceans* 117, 1–17.
- Paolo, F. S., H. A. Fricker, and L. Padman (2015b). “Volume loss from Antarctic ice shelves is accelerating”. *Science* 348, 327–331.
- Pritchard, H. D., S. R. M. Ligtenberg, H. A. Fricker, D. G. Vaughan, M. R. van den Broeke, and L. Padman (2012). “Antarctic ice-sheet loss driven by basal melting of ice shelves”. *Nature* 484, 502–505.
- Pritchard, H. D., R. J. Arthern, D. G. Vaughan, and L. A. Edwards (2009). “Extensive dynamic thinning on the margins of the Greenland and Antarctic ice sheets.” *Nature* 461, 971–975.
- Rignot, E., G. Casassa, P. Gogineni, W. Krabill, A. Rivera, and R. Thomas (2004). “Accelerated ice discharge from the Antarctic Peninsula following the collapse of Larsen B ice shelf”. *Geophysical Research Letters* 31, L18401.
- Rignot, E., J. Mouginot, and B. Scheuchl (2011). “Ice flow of the Antarctic ice sheet.” *Science* 333, 1427–1430.
- Rignot, E., S. Jacobs, J. Mouginot, and B. Scheuchl (2013). “Ice-Shelf Melting Around Antarctica”. *Science* 341, 266–270.
- Rignot, E., J. Mouginot, M. Morlighem, H. Seroussi, and B. Scheuchl (2014). “Widespread, rapid grounding line retreat of Pine Island, Thwaites, Smith, and Kohler glaciers, West Antarctica, from 1992 to 2011”. *Geophysical Research Letters* 41, 3502–3509.
- Rignot, E., J. L. Bamber, M. R. van den Broeke, C. Davis, Y. Li, W. J. van de Berg, and E. van Meijgaard (2008). “Recent Antarctic ice mass loss from radar interferometry and regional climate modelling”. *Nature Geoscience* 1, 106–110.

- Scambos, T. A., J. A. Bohlander, C. A. Shuman, and P. Skvarca (2004). "Glacier acceleration and thinning after ice shelf collapse in the Larsen B embayment, Antarctica". *Geophysical Research Letters* 31, 2001–2004.
- Schoof, C. (2007). "Ice sheet grounding line dynamics: Steady states, stability, and hysteresis". *Journal of Geophysical Research: Earth Surface* 112, 1–19.
- Shepherd, A., D. Wingham, T. Payne, and P. Skvarca (2003). "Larsen ice shelf has progressively thinned." *Science* 302, 856–859.
- Shepherd, A., D. Wingham, and E. Rignot (2004b). "Warm ocean is eroding West Antarctic Ice Sheet". *Geophysical Research Letters* 31, L23402.
- Shepherd, A., D. Wingham, D. Wallis, K. Giles, S. Laxon, and A. V. Sundal (2010). "Recent loss of floating ice and the consequent sea level contribution". *Geophysical Research Letters* 37, 1–5.
- Shepherd, A., E. R. Ivins, G. A. V.R. Barletta, M. J. Bentley, S. Bettadpur, K. H. Briggs, D. H. Bromwich, R. Forsberg, N. Galin, M. Horwath, S. Jacobs, I. Joughin, M. A. King, J. T. M. Lenaerts, J. Li, S. R. M. Ligtenberg, A. Luckman, S. B. Luthcke, M. McMillan, R. Meister, G. Milne, J. Mouginot, A. Muir, J. P. Nicolas, J. Paden, A. J. Payne, H. Pritchard, E. Rignot, H. Rott, L. S. Sørensen, T. A. Scambos, B. Scheuchl, E. J. O. Schrama, B. Smith, A. V. Sundal, J. H. van Angelen, W. J. van de Berg, M. R. van den Broeke, D. G. Vaughan, I. Velicogna, J. Wahr, P. L. Whitehouse, D. J. Wingham, D. Yi, D. Young, and H. J. Zwally (2012). "A Reconciled Estimate of Ice-Sheet Mass Balance". *Science* 338, 1183–1189.
- Sutterley, T. C., I. Velicogna, E. Rignot, J. Mouginot, T. Flament, M. R. van den Broeke, J. M. van Wessem, and C. H. Reijmer (2014). "Mass loss of the Amundsen Sea Embayment of West Antarctica from four independent techniques". *Geophysical Research Letters* 41, 2014GL061940.
- Velicogna, I. (2009). "Increasing rates of ice mass loss from the Greenland and Antarctic ice sheets revealed by GRACE". *Geophysical Research Letters* 36, L19503.
- Weertman, J. (1974). "Stability of the junction of an ice sheet and an ice shelf". *Journal of Glaciology* 13, 3–11.
- Wingham, D. J., A. Shepherd, A. Muir, and G. J. Marshall (2006). "Mass balance of the Antarctic ice sheet." *Philosophical Transactions A* 364, 1627–1635.
- Wingham, D. J., D. W. Wallis, and A. Shepherd (2009). "Spatial and temporal evolution of Pine Island Glacier thinning, 1995–2006". *Geophysical Research Letters* 36, 5–9.
- Zwally, H. J., M. B. Giovinetto, J. Li, H. G. Cornejo, and M. A. Beckley (2005). "Mass changes of the Greenland and Antarctica ice sheets and shelves and contributions to sea level rise: 1992–2002". *Journal of Glaciology* 51, 509–509.

- Zwally, H. J. and M. B. Giovinetto (2011). “Overview and Assessment of Antarctic Ice-Sheet Mass Balance Estimates: 1992-2009”. *Surveys in Geophysics* 32, 351–376.
- Zwally, H. J., R. A. Bindschadler, A. C. Brenner, T. V. Martin, and R. H. Thomas (1983). “Surface elevation contours of greenland and Antarctic Ice Sheets”. *Journal of Geophysical Research: Oceans* 88, 1589–1596.
- Zwally, H. J., R. A. Bindschadler, A. C. Brenner, J. A. Major, and J. G. Marsh (1989). “Growth of Greenland Ice Sheet: Measurement”. *Science* 246, 1587–1589.

Chapter 2

Time series of ice-shelf height

This chapter, in full, is a reprint of:

Developing improved decadal records of Antarctic ice-shelf height change from multiple satellite radar altimeters, F.S. Paolo, H.A. Fricker, L. Padman, Remote Sens. Environ. in revision

2.1 Abstract

Antarctica's ice shelves, the floating extensions of the ice sheet, exert an important dynamic constraint on the flow of ice from the grounded ice sheet to the ocean, and hence on changes in global sea level. Thinning of an ice shelf reduces its ability to restrain the ice discharge from the grounded ice-sheet interior. However, our understanding of how ice-shelf processes couple ice-sheet changes to climate variability is still rudimentary. In part, this is due to the brevity and low resolution of surveys of ice-shelf thickness relative to the time scales on which ice-sheet mass fluctuates. We present improved procedures to construct 18-year (1994–2012) time series of ice-shelf height around the entire Antarctic continent, merging data from multiple overlapping satellite radar altimeter missions (ERS-1, ERS-2, and Envisat). We apply an averaging scheme to enhance the signal-to-noise ratio of height changes over the floating ice shelves, and extract low-order polynomial trends using a robust approach accounting for both bias and variance in the fit (regularized regression with cross-validation). We identify the main processes affecting the estimation of ice-shelf height from satellite

radar altimeters. We estimate uncertainties by bootstrap resampling of the residuals of the fit, allowing us to construct formal confidence intervals (unlike the standard error-propagation approach). Our results show that, for the ice shelves, densification of the surface is a more important effect than penetration of the radar signal in biasing the estimated height changes. The 18-year record of surface height allows us to map the temporal progression and spatial structure of changes in ice-shelf height, which provides insights on how ice shelves respond to the changing atmospheric and oceanic conditions.

2.2 Introduction

The Antarctic Ice Sheet contains ice above floatation equivalent to 58 m of global sea-level rise [Fretwell et al. 2013] and, over centennial-to-millennial time scales, plays an important role in pacing sea-level changes [Alley et al. 2005]. Satellite measurements over the past two decades show mass loss from the grounded ice sheet [Shepherd et al. 2012] including accelerating loss in the Amundsen Sea Embayment [Sutterley et al. 2014], a region with large potential to contribute to sea level rise [Rignot et al. 2014; Joughin et al. 2014]. There is an urgent need to understand the mechanisms behind these current changes as a step toward predicting Antarctica's contribution to global sea-level change over the next century.

Most ice mass loss from Antarctica takes place through iceberg calving and basal melting from the ice shelves, the floating extensions of the ice sheet [Depoorter et al. 2013; Joughin et al. 2012; Rignot et al. 2013]. Ice shelves restrain the discharge of grounded ice into the ocean through a buttressing effect [Joughin and Alley 2011; Schoof 2007]. Small perturbations in the adjacent oceanic and atmospheric conditions can have a large impact on the extent and thickness of ice shelves [Dutrieux et al. 2014; Rignot et al. 2004; Scambos et al. 2004], which reduces their buttressing capability. The response of ice shelves to climate change is, therefore, a key component in assessing future loss of grounded ice.

Our understanding of the many processes that affect ice-shelf mass balance is too rudimentary to allow prediction of ice-sheet change under projected future climate states. There are two complementary ways forward: to develop our theoretical frame-

work of the actual mass-loss processes so they can be better represented in models; and to empirically relate observed ice-sheet change to ocean and atmospheric variability. In a recent study [Paolo et al. 2015b, see chap. 3] we reported changes in Antarctic ice shelf height, and inferred thickness during the 18-year period 1994–2012. The temporal and spatial resolutions of that record were 3 months and 30 km, respectively. This record will be used to improve knowledge of ice-shelf response to climate by comparing measured variability of ice thickness with measured or modeled changes in the ocean and atmosphere. This continuous, highly-resolved record overcomes the limitations of previous studies of ice-shelf thickness, which analyzed much shorter records and/or predominantly reported simple linear trends for large areas [Pritchard et al. 2012; Shepherd et al. 2010; Zwally et al. 2005].

In this paper we document comprehensive methods for constructing continuous records from multiple satellite radar altimeters to obtain reliable time series of height change over the longest possible time period, providing detailed justification for the data processing approach used by Paolo et al. [2015b]. We present improved procedures for merging data from three overlapping satellite missions, enhancing the signal-to-noise ratio of changes in ice-shelf height, and extracting 18-year mean trends and acceleration. The method reveals complex patterns of ice-shelf height variability in both time and space. We introduce an alternative approach to the standard error propagation for the uncertainty analysis: bootstrapping applied to time-dependent data.

2.3 Satellite radar altimeter missions

We used data from three European Space Agency (ESA) satellite radar altimeter (RA) missions: the European Remote Sensing Satellite-1 and Satellite-2 (ERS-1, 1991–1996; and ERS-2, 1995–2003); and the Environmental Satellite (Envisat, 2002–2012). Each satellite carried a standard pulse-limited altimeter with a footprint size of ∼3–5 km over the predominant flatter portions of the ice sheets. For reasons explained below in Section 2.3, we do not use the first two years of ERS-1 data, resulting in an 18-year continuous record for 1994–2012.

ERS-1 was launched in July 1991 and operated between December 1991 and June 1996. It flew at an altitude of ∼785 km with an inclination of 98.5 degrees (lat-

itudinal limit of 81.5°), with three different orbital repeat periods: 3-day (Ice Phase, December 1991 to March 1992 and December 1993 to April 1993), 35-day (Multidisciplinary Phase, April 1992 to December 1993 and March 1995 to June 1996) and 168-day (Geodetic Phase, April 1994 to March 1995). ERS-2 was launched in April 1995 and operated from May 1995 to June 2003 in an orbit with a repeat period of 35 days, following the ERS-1 35-day orbit. In June 2003 the on-board tape recorder used for the RA data failed, and the mission continued without altimetry until July 2011. The RA system on these two satellites was based on a linearly polarized antenna at 13.8 GHz Ku-band, yielding along-track measurements that are ~ 340 m apart (sampling rate of 20 Hz; each measurement is the average of several radar echoes).

The ERS-1/ERS-2 orbit covered about 85% of the Antarctic ice-shelf area, missing only the southern portions of the large Filchner-Ronne (Fig. 2.1) and Ross ice shelves. Over the ice shelves, ERS-1 and ERS-2 operated in both a standard ‘ocean mode’ and a specialized ‘ice mode’, alternating between them. The range window (the segment of return echo that is recorded) for ice mode was four times wider than for ocean mode, increasing the chances of capturing return signals over rough topographic surfaces. However the broader range window resulted in four times coarser sampling of the return waveform, leading to a less precise estimation of arrival time and, therefore, of the surface height.

Envisat was launched in March 2002 into the same 35-day orbit as ERS-1 and ERS-2, providing data at the same 20 Hz sampling rate. The altimeter on this satellite (RA-2) [Roca et al. 2009], a linearly-polarized radar, operated via a single antenna dish on the Ku-band (13.6 GHz) and S-band (3.2 GHz). This dual frequency enables the correction of height-measurement errors introduced by the ionosphere. RA-2 had an improved precision over ice surfaces compared to the ERS altimeters, and operated with three sampling modes: ‘fine’, ‘medium’ and ‘coarse’, which differ in their sampling of the waveform of the return echo. Envisat stopped operating in April 2012.

We obtained Level-2 RA data as Ice Data Records (IDR) for each mission from NASA’s Goddard Space Flight Center (GSFC) Ice Altimetry group (<http://icesat4.gsfc.nasa.gov/>). At GSFC, the RA waveforms were retracked using a multi-parameter range-retracking algorithm (the β -retracker) [Zwally and Brenner 2001]. The following corrections were applied by GSFC: atmospheric range corrections; instrument corrections;

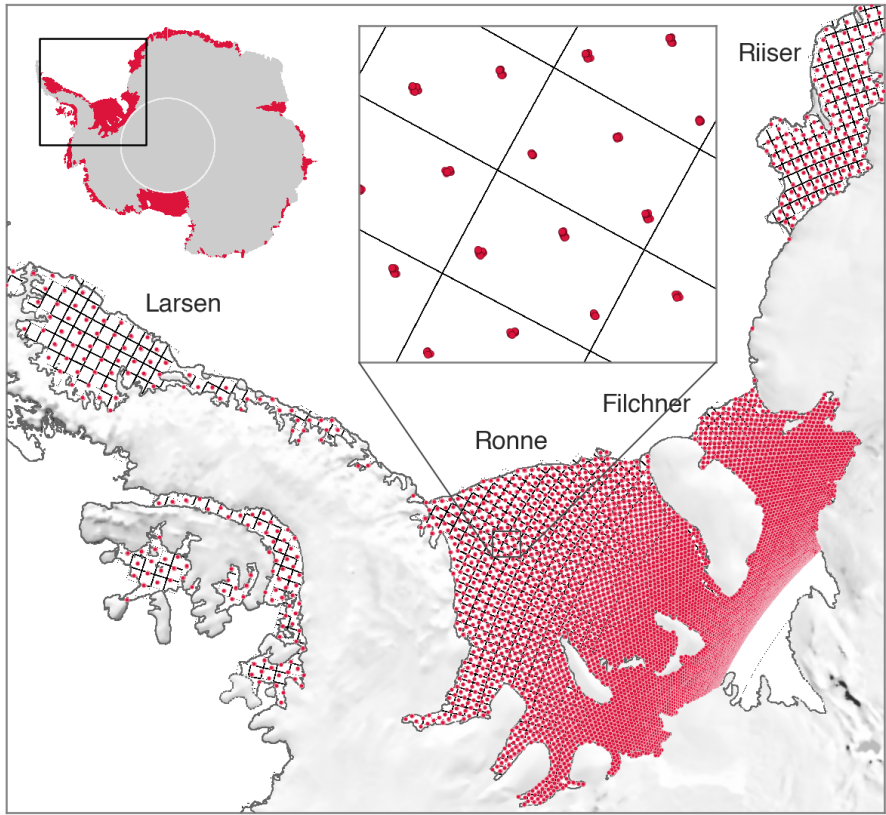


Figure 2.1: ERS-1 radar-altimeter data coverage over the Weddell Sea region of Antarctica, for a typical 3-month period with the 35-day repeat orbit. Red dots are crossover locations on the ice shelves. The ~30-km grid that we used to average the crossovers is overlaid. ice shelves.

slope corrections; ocean and solid earth tides [Brenner et al. 1983; Zwally and Brenner 2001; Zwally et al. 2005]; (for ERS) removal of a 40.9 cm bias from ERS-1 heights to account for a change in instrument parameter used for ERS-2 [Femenias 1996]; corrections for drifts in the ultra-stable oscillator and bias changes in the scanning point target response that are obtained from ESA; and upgraded orbits (DGM-E04 orbits for ERS) which have a radial orbit precision of 5-6 cm [Scharroo and Visser 1998].

2.4 Processing satellite radar altimeter data

Our determination of height changes over the ice shelves from multi-mission satellite RA data is based on crossover analysis [e.g., Davis and Ferguson 2004; Wingham et al. 2009; Zwally et al. 2005], which estimates change in surface height at

intersections between time-separated ascending and descending satellite tracks. Along-track (or repeat-cycle) analysis methods that provide higher point density have recently been introduced [Flament and Rémy 2012; Moholdt et al. 2010; Pritchard et al. 2012]; however, crossover analysis remains the most precise technique, since differences are derived from precisely co-located height estimates on the ascending and descending tracks. For crossover analysis interpolation is performed between measurements ~ 340 m apart in the along-track direction (where there is a much more defined profile from a consistent set of measurements, i.e., one orbit); in contrast for repeat-cycle analysis each measurement is projected onto a reference ground track, with the actual orbits varying up to ~ 2 km from each other from repeat to repeat (so interpolation is performed in the across-track direction without having a good estimate of the slope). The spacing of crossovers becomes much smaller as latitude approaches the satellite's turning point (Fig. 2.1).

In this section we describe the steps required to process RA data from multiple satellite missions. Steps include (see flowchart in Fig. 2.2): subsetting data over floating ice; data editing and additional corrections required for floating ice and for radar signal interactions with the surface layer on the ice shelves; crossover analysis; methods for merging data records from the different missions; and the averaging scheme required to achieve satisfactory data coverage and accuracy. The output is 18-year long records of ice-shelf surface height, which we then analyzed using statistical techniques to derive long-term trends, acceleration and uncertainties.

2.4.1 Initial RA data selection and editing

Antarctic ice shelf mask

For this study we are interested only in Antarctica's floating ice shelves; therefore, we subsetted all of our RA datasets based on a 1-km resolution Antarctic ice-sheet mask [Depoorter et al. 2013] that was constructed using a composite of InSAR [Rignot et al. 2011], ICESat [Brunt et al. 2010; Fricker et al. 2009], MODIS MOA [Scambos et al. 2007] and ASAID [Bindschadler et al. 2011] products. This high-resolution product allows us to exclude all grounded ice, which includes islands, ice rises and ripples that are completely surrounded by ice shelves.

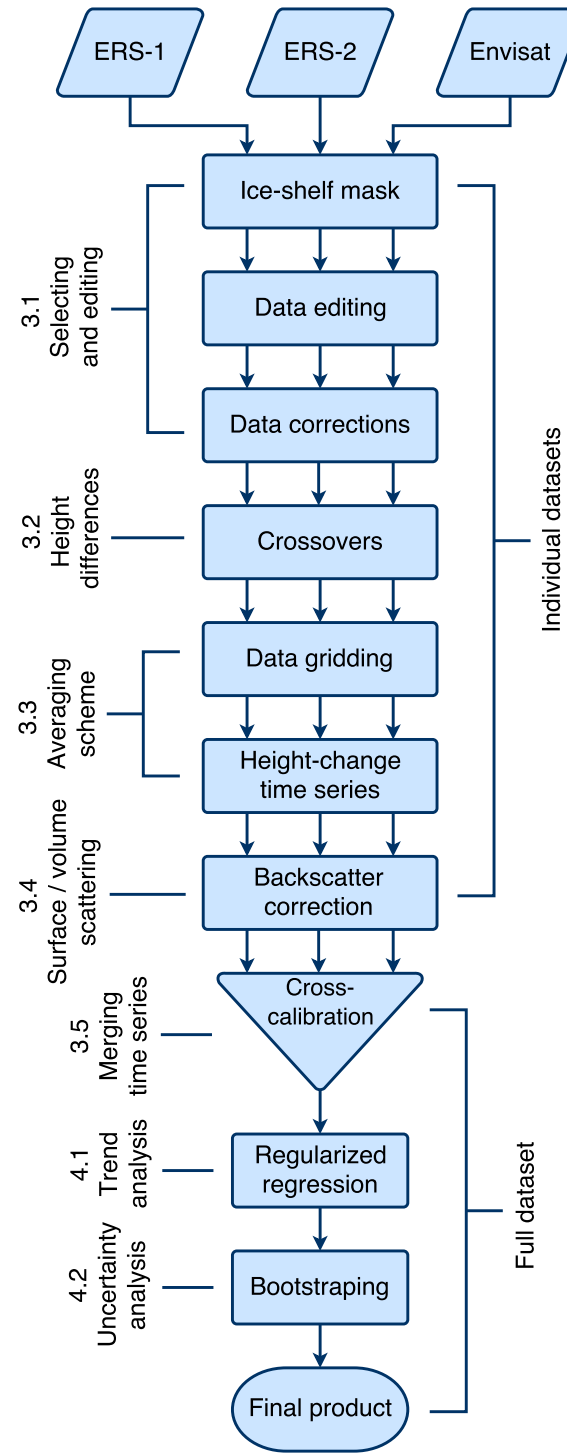


Figure 2.2: Flowchart of our RA data processing scheme, showing the steps performed to construct an 18-year record of ice-shelf surface-height change from multiple satellite altimeters. Each step is described in Sections 2.4.1 and 2.4.2.

We considered only the portions of ice shelves that were present and afloat through the entire 18-year observation period. We excluded regions where ice front advance or retreat occurred during the 18 years and portions of a few ice shelves that became ungrounded between 1994 and 2012.

Altimeter data editing

We excluded data if any of the following conditions were met: the return waveform had no leading edge, or had specular shape indicating surface melt ponds and melt streams [Phillips 1998] as indicated by flags in the IDR; any geophysical correction was missing from the IDR; the crossover point was less than 3 km from any ice-shelf boundary (grounding line and ice front). The last criterion was designed to avoid biasing estimates (i) with high topographic gradients within the pulse-limited radar footprint, (ii) with changes in grounded ice that are an order of magnitude higher than over floating ice, and (iii) where geophysical corrections for ocean processes such as tides are unreliable, especially close to the grounding line where the ice is not in full hydrostatic equilibrium [Fricker and Padman 2006].

Additional data corrections

The ocean tide corrections applied to the IDR (from the CSR3 global tide model) are not accurate in Antarctica [King and Padman 2005]; for that reason, we removed this correction from the data and applied an improved tide correction using the regional Circum-Antarctic Tidal Simulation model (CATS2008a; an updated version of the inverse tide model described by Padman et al. [2002]). This tide model has higher resolution (~ 4 km) and a more accurate land mask than global models, resulting in more accurate tide prediction close to the coast. We also corrected for the ocean tidal loading (the elastic deformation of the seabed in response to the tide load) using the TPXO7.2 model [Egbert and Erofeeva 2002].

Estimating height differences

To estimate the height differences at crossovers we first precisely locate the intersection points between each ascending and descending satellite tracks. We then find

the two data points on either side of this intersection for each track pair, interpolate these to estimate the height at actual crossover location, and difference values from both tracks. When some data are missing along the satellite track, we only estimated crossover height-differences if the gap between data points on either side of the intersection point was less than 3 km. This criterion ensured that the RA pulse-limited footprints at both ends of the gap still overlapped enough so that interpolated heights along both tracks at the precise crossover location were consistent representations of the same location on the ice surface.

Our approach to developing time series of ice-shelf height with respect to an initial epoch t_0 , $h(t - t_0)$, uses a multi-reference time scheme [Khvorostovsky 2012; Li and Davis 2006] applied to each satellite mission separately. This method computes crossover height differences for each pair of ascending and descending tracks, $\Delta h(t_i, t_j)$, throughout the entire record for a specific mission regardless of time separation between track pairs. For example, in the 9-year Envisat record, time separation of differences, $\Delta t = t_j - t_i$, at crossovers range from close to zero to nine years.

For ERS-1, where data were acquired in different modes ('ice' and 'ocean') at different times over the ice shelves, we analyzed the crossovers $\Delta h(t_i, t_j)$ estimated from pairs of tracks with the same operation mode (ice-mode crossed with ice-mode or ocean-mode crossed with ocean-mode). Results for both modes were practically identical. In contrast, estimates of $\Delta h(t_i, t_j)$ obtained from a mixed-mode crossover (one track in ice-mode, the other in ocean-mode), were not consistent with the same-mode pairings. We also found that ice-mode data by themselves were insufficient to provide near-full coverage over the ice shelves for the first few years of ERS-1 operation. Hence, for ERS-1 we retained both types of same-mode crossovers (ice-ice and ocean-ocean). For Envisat, we used the fine-mode data only.

2.4.2 Averaging to enhance the signal-to-noise ratio

For a given change in ice thickness, the estimated height-change signal over a floating ice shelf is about an order of magnitude smaller than the same signal over grounded ice. This is because, outside of a narrow ice-flexure zone roughly 1–10 km wide seaward of the grounding line, ice shelves are in hydrostatic equilibrium, with

a density that is about 10% less than seawater. Since ice thickness and mass are the primary variables we wish to document, this reduced signal implies that there is a need to reduce the noise in the height estimates over ice shelves, a problem that is compounded when the goal is to identify variability over short time scales.

To enhance the signal-to-noise ratio over floating ice we implemented two averaging steps to reduce the variance in the height estimates, as described below.

Spatial gridding and temporal binning

We defined blocks of height data, $h(\mathbf{x}, t_i)$, consisting of all ascending and descending tracks within non-overlapping 3-month time bins and spatial grid cells of $0.75^\circ \times 0.25^\circ$ in longitude and latitude, respectively ($\sim 30 \times 30$ km at 71°S). At shorter time intervals, e.g., one month, the data records are often discontinuous. Aggregating data over 3-month bins provides continuous records while still resolving the annual cycle. The choice of grid-cell size (~ 30 km) was a compromise between characteristic spatial scales of ice-shelf processes and the spatial distribution of crossovers (Fig. 2.1). We identify each 3-dimensional block (one time bin and spatial cell), by its central time, $t_i \rightarrow i = 0, 1, 2, \dots, N$, where N is the total number of time bins within each satellite record, and by its central location, $\mathbf{x} \rightarrow 0^\circ < \text{longitude} < 360^\circ$ and $-81.5^\circ < \text{latitude} < -64.5^\circ$ (the center of the grid cells).

For each pair of blocks for the same cell but for separate time bins t_i and t_j , we developed the set of all crossover height differences, $\Delta h(t_i, t_j)$, found by differencing all height values from the two data blocks. During this process we excluded crossover values higher than 15 m (gross outliers). For all pairs of t_i, t_j , we therefore obtained average height changes at each location as:

$$\overline{\Delta h}(\mathbf{x}, t_i, t_j) = \frac{1}{n_{ad} + n_{da}} \left\{ n_{ad} \text{Md} [\Delta h_{ad}(t_i, t_j)] + n_{da} \text{Md} [\Delta h_{da}(t_i, t_j)] \right\} \quad (2.1)$$

where $\overline{\Delta h}$ is the weighted-mean height-change estimate between times t_i and t_j , Δh_{ad} and Δh_{da} are height changes formed by differencing ascending-descending and descending-ascending satellite ground tracks, respectively, n_{ad} and n_{da} are the number of crossovers of each type per block, and $\text{Md}[\cdot]$ is the median operator. We used

the median instead of the mean because individual values of $\Delta h(t_i, t_j)$ can have large errors and their distribution can be non-Gaussian. It is necessary to use the average between ascending/descending and descending/ascending crossovers to remove any time-invariant biases, such as those introduced by the combination of satellite orientation, antenna polarization and ice surface anisotropy.

If we assume that true temporal variations in h are small for small time separations (within the time bin itself, i.e., less than three months), then the statistics of $\Delta h(t_i, t_j)$ are a measure of noise in the height difference estimates. This noise value may be spatially dependent; for example, relatively smooth and flat regions of ice shelf may have smaller noise in Δh than regions where the ice-shelf surface is sloping or rough.

Derivation of height-change time series

The simplest way to obtain a time series of height change for a specific spatial cell is to difference the first block of data consecutively with all subsequent blocks [e.g., Zwally et al. 1989]. This approach, however, results in all height differences in the resulting record being dependent upon the quality and data availability of the reference epoch (the first block). Instead, for each cell we evaluated all possible combinations between time bins within each satellite mission [Zwally and Brenner 2001; Li and Davis 2006], and further combinations between the formed differences as in Khvorostovsky [2012]. This procedure was carried out as follows.

For each grid cell we constructed a set of $N - 1$ time series of average height differences with respect to each of the $N - 1$ separate epochs, and then formed a full matrix (one per cell) containing one height-change record per row. For example, taking t_0 to be the reference epoch (any time could be chosen) we then have:

$$[\Delta h] = \begin{pmatrix} h_{0,1} & h_{0,2} & h_{0,3} & \cdots & h_{0,N} \\ -- & h_{0,1} + h_{1,2} & h_{0,1} + h_{1,3} & \cdots & h_{0,1} + h_{1,N} \\ h_{0,2} - h_{1,2} & -- & h_{0,2} + h_{2,3} & \cdots & h_{0,2} + h_{2,N} \\ h_{0,3} - h_{1,3} & h_{0,3} - h_{2,3} & -- & \cdots & h_{0,3} + h_{3,N} \\ \cdots & \cdots & \cdots & \cdots & \cdots \\ h_{0,N} - h_{1,N} & h_{0,N} - h_{2,N} & h_{0,N} - h_{3,N} & \cdots & -- \end{pmatrix} \quad (2.2)$$

where $h_{i,j} = \overline{\Delta h}(\mathbf{x}, t_i, t_j)$ from Eq. 2.1. In the example above, every row constitutes a time series of height change with respect to t_0 . This (final) matrix is constructed by (i) forming the upper triangle of the matrix from the calculated average differences (this is a one-sided matrix containing the height differences between all possible time combinations), (ii) forming the lower triangle as the negative of the upper one (this is the transposed of the previous one-sided matrix multiplied by -1), and (iii) adding the two single-sided matrices to form a full matrix and then adding each element j of the reference row (first one in this example, time series with respect to t_0) to the respective row $i = j$ (Fig. 2.3). We note that any row in the matrix could be used as the reference series (i.e., any epoch); the optimal one, however, will cover the largest time span in the presence of data gaps.

Next, we weight-averaged the matrix rows by the number of crossovers used to form each average difference to produce a mean time series per cell, with reduced statistical error:

$$h(\mathbf{x}, \tau) = \langle [\Delta h] \rangle \quad (2.3)$$

where $\tau = t - t_0$. We propagated individual errors in the averaging procedure assuming normality [Li and Davis 2006].

To evaluate possible signal aliasing we used a small region to test aggregating data in 3-month bins that were overlapped by $1/3$ as in Khvorostovsky [2012]. The overlapping approach required a much longer computation time, and the resulting average time series were roughly the same as the ones derived from the non-overlapping approach, and so we did not apply this to the full dataset.

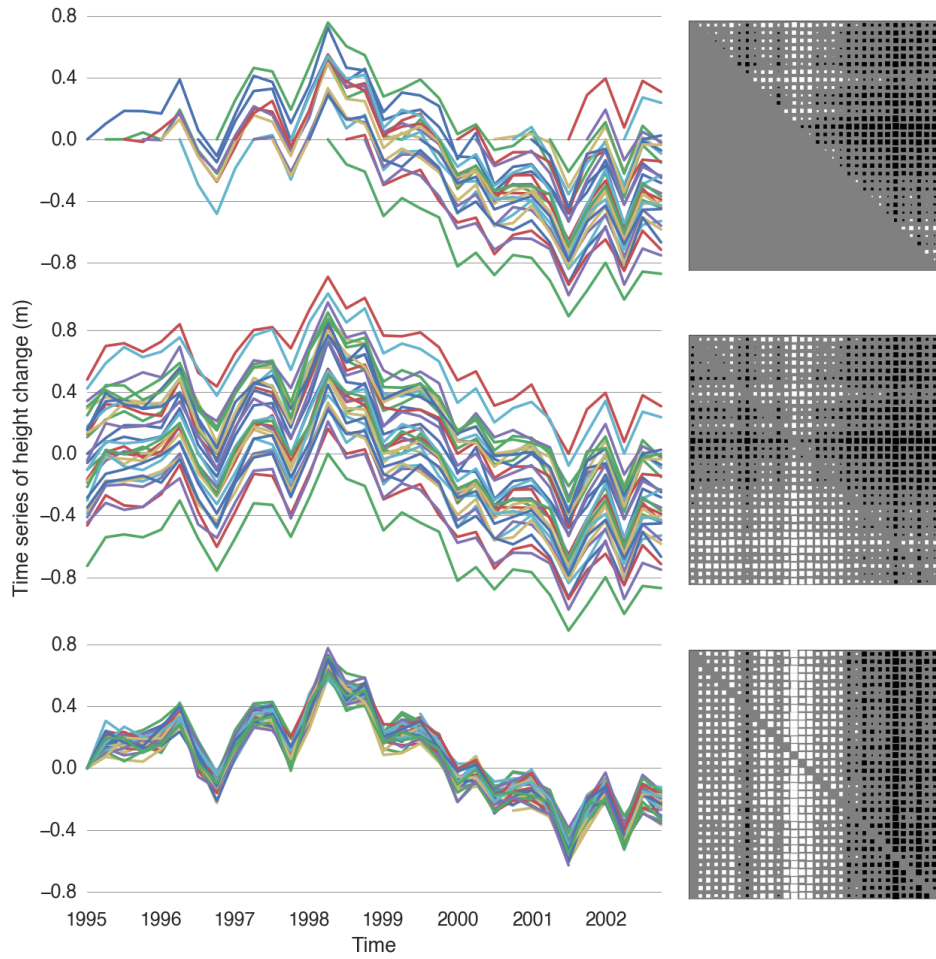


Figure 2.3: Representation of the multi-reference time-series approach. (left) Individual time series of cumulative change. (right) Diagram representing the matrix formed with the time series on the left (one time series per row). From top to bottom is depicted the process of forming single-grid-cell average time series: (top) the one-sided matrix of average differences; (middle) the two-sided matrix; (bottom) referencing all the rows (time series) to a common epoch for posterior averaging (this matrix is Eq. 2.2).

2.4.3 Surface and volume scattering variation

Interpreting heights derived from RA data over snow-covered ice surfaces requires an understanding of the complex interaction of the radar wave with the snowpack and firn (compressed snow that has not yet formed into solid ice). Over ice sheets, part of the incident radar energy penetrates into the snowpack/firn [Ridley and Partington 1988] by an amount that depends on the properties of the surface layers including temperature, density, grain-size and moisture content [Davis and Moore 1993], leading to volume scattering with reflections within sub-surface layers and ice lenses. Volume

scattering increases the path length of the radiation and, therefore, its travel-time back to the satellite and the inferred height. The waveform shape in the presence of volume scattering is also different than if only surface scattering occurred. In some cases, most of the echo can be from a well-defined sub-surface horizon within the snowpack [Thomas et al. 2008], leading to a surface-like waveform shape, but a height estimate that is still lower than the true surface.

The penetration depth (where the radar pulse decays by $1/e$ of its initial intensity) varies with density, grain-size, and water content of the snow/firn. Penetration depth can be several meters over the colder and dryer parts of the Antarctic plateau where grain sizes are smaller, but is much lower (on the order of centimeters) over the warmer and wetter ice shelves where grain sizes are larger [Davis 1996]. Note that the dependence is on the bulk electromagnetic properties (and not grain size as such). To demonstrate this we used the [Davis and Moore 1993] surface/volume algorithm to estimate the extinction coefficient (k_e ; which is inversely proportional to penetration depth) for the entire Antarctic area under the ERS-1 satellite's coverage, using ERS-1 altimeter level-1 ocean-mode waveforms (Phase C) (Fig. 2.4). In general, k_e is on the order of 4–5 times higher over the ice shelves than elsewhere on the ice sheet. This means that the penetration bias is not as large over the ice shelves as it is over the ice sheet interior.

The return radar waveform used to estimate the surface height is the sum of surface echo (energy scattered by the surface) and volume echo (energy scattered within the snowpack). Perturbations in the return radar waveform occur due to changes in the properties of the snowpack, which alter the effective backscatter layer, potentially leading to a biased surface-height estimate. Two competing effects (with opposite signs) play a significant role in altering the shape of the return waveform: i) penetration of the signal into the firn layer increases volume scattering (increasing the waveform's leading-edge width); and ii) densification of the surface increases the air-snow dielectric contrast (decreasing the leading-edge width). We investigated corrections to minimize these effects as described in Section 2.4.3 below.

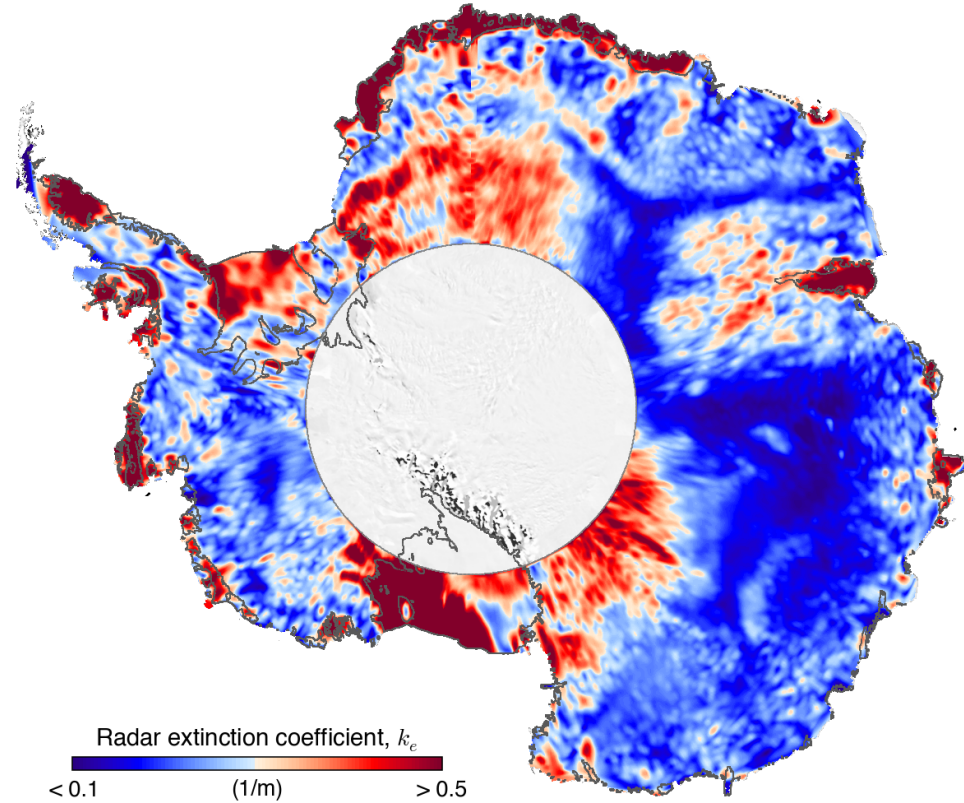


Figure 2.4: Estimated radar altimeter extinction coefficient (k_e) over the Antarctic ice sheet. k_e was derived from ERS-1 Phase C ocean-mode return waveforms over the ice sheet and ice shelves using a surface/volume scattering algorithm [Davis and Moore 1993]. Note that the k_e (which is inversely related to the penetration depth) is generally higher in the ice shelves than on the plateau. This difference can mostly be explained in terms of grain sizes: on the ice shelf, individual particles are larger than those on the plateau, due to much warmer temperatures, combined with successive melt-freeze cycles (i.e., wet snow metamorphosis) [Zwally and Fiegles 1994]; therefore k_e is high. On the plateau, grain sizes depend on surface temperature and accumulation rate. In general, as elevation and distance from the coast (continentally) increases, temperatures decrease; therefore the grain sizes and k_e decrease.

Correction for changes in backscatter

Although much progress has been made in understanding the relation between backscatter fluctuation (resulting mainly from variations in near-surface properties) and altimeter-derived height [Arthern et al. 2001; Davis and Moore 1993; Legresy 1998; Partington et al. 1989; Remy et al. 2012; Ridley and Partington 1988], it is still an active area of investigation, and its full impact on the RA measurement error remains poorly known [Remy et al. 2012]. To attempt to minimize the impact of fluctuations in backscatter on the estimated height, an empirical adjustment using backscatter information is performed [as have been applied by, Davis and Ferguson 2004; Khvorostovsky

2012; Rémy and Parouty 2009; Wingham et al. 2006; Wingham et al. 1998; Zwally et al. 2005].

We used the altimeter automatic gain control (AGC; proportional to the log of the gain) as a measure of backscattered power to adjust our height-change time series using corresponding series of changes in AGC, $g(\mathbf{x}, \tau)$ [Zwally et al. 2005]. We formed these backscatter-change time series for each grid cell in the same way as the height-change series described above. We derived a spatially varying sensitivity factor to scale the backscatter values at each grid-cell:

$$S(\mathbf{x}) = \frac{\Delta h(\mathbf{x})}{\Delta g(\mathbf{x})} \quad (2.4)$$

where h and g are all the height and backscatter differences formed at location \mathbf{x} . In other words, this sensitivity is the regression slope of the correlation between height and backscatter changes that we derived independently at each grid cell and for each RA mission. We then corrected each time series as:

$$h(\mathbf{x}, \tau)_{\text{cor}} = h(\mathbf{x}, \tau) - S(\mathbf{x}) g(\mathbf{x}, \tau) - h_0(\mathbf{x}) \quad (2.5)$$

where h_{cor} is backscatter-corrected height-change, S is the sensitivity factor (altimeter dependent), g is proportional to gain change, and h_0 is the regression intercept (not needed for correcting full independent records relative to some epoch). For the regression procedure we used a robust method, ‘maximum likelihood-type estimator’ [Huber 1981, p. 43], instead of the commonly used least-squares approach, which can be sensitive to outliers (especially when few data are available).

In selecting an optimal backscatter correction scheme we tested three different approaches. We correlated series of backscatter and height changes: i) using the cross-calibrated full 18-year records, ii) using data within 2 and 3-year sliding windows (similar to Khvorostovsky [2012]) and iii) using independent single-mission records. For each approach we performed the correlation using both the original time series (absolute values) and the differenced series (derivative). We found that the third approach was the only one to perform consistently under a variety of conditions (e.g., high vs. low variance, high vs. low correlation, high vs. low heteroscedasticity). Note that using differenced series is equivalent to using high-pass filtered records and, therefore, higher

correlations are expected since backscatter change is primarily a function of seasonality. However, in correlating differenced series only the short-term fluctuations in backscatter are taken into account. Hence, we corrected our height-change records by correlating series of absolute values using method (iii).

Densification from changes in the firn column

One approach to account for changing surface mass balance over an ice shelf, specifically firn compaction/densification, is to use an atmospheric-based model to predict how the firn column evolves under modeled climate conditions. For example, a laser altimeter study by Pritchard et al. [2012] used modeling of changes in the firn column to isolate the part of the signal due to fluctuations in the snowpack. We performed a correlation analysis between our backscatter-uncorrected time series, which contain the seasonal response of the ice-shelf surface as detected by the altimeter's automatic gain control (backscatter), and the height changes derived from a firn densification model (FDM). To construct the firn height-change record we used the Ligtenberg et al. [2011]'s FDM from which we (i) extracted firn height-change series for each location in our grid; (ii) averaged the 48-hour firn records with a 3-month moving window; and (iii) retained the discrete time-values that corresponded to our 3-month ice-shelf height records.

We found no correlation between the firn-height changes from the model and the (backscatter-uncorrected) RA-derived changes in ice-shelf height at the fine resolution required for this study (individual grid cells of ~ 30 km). Since backscatter changes are indicative (among other processes) of the seasonal fluctuation in the firn height (see text below), some degree of correlation between the uncorrected RA records (which contain at least part of the seasonal firn-height cycle) and the FDM is expected. The firn model was able to provide, however, an estimate of the expected seasonal variation of the firn height at the larger scale (Fig. 2.5). Additionally, since some degree of penetration through fresh snow is expected at the frequency of the Ku-band altimeter, satellite RAs are less sensitive than laser altimeters to fluctuations in surface mass balance. For these reasons we found no justification to use an FDM to make any firn-change correction on RA height estimates.

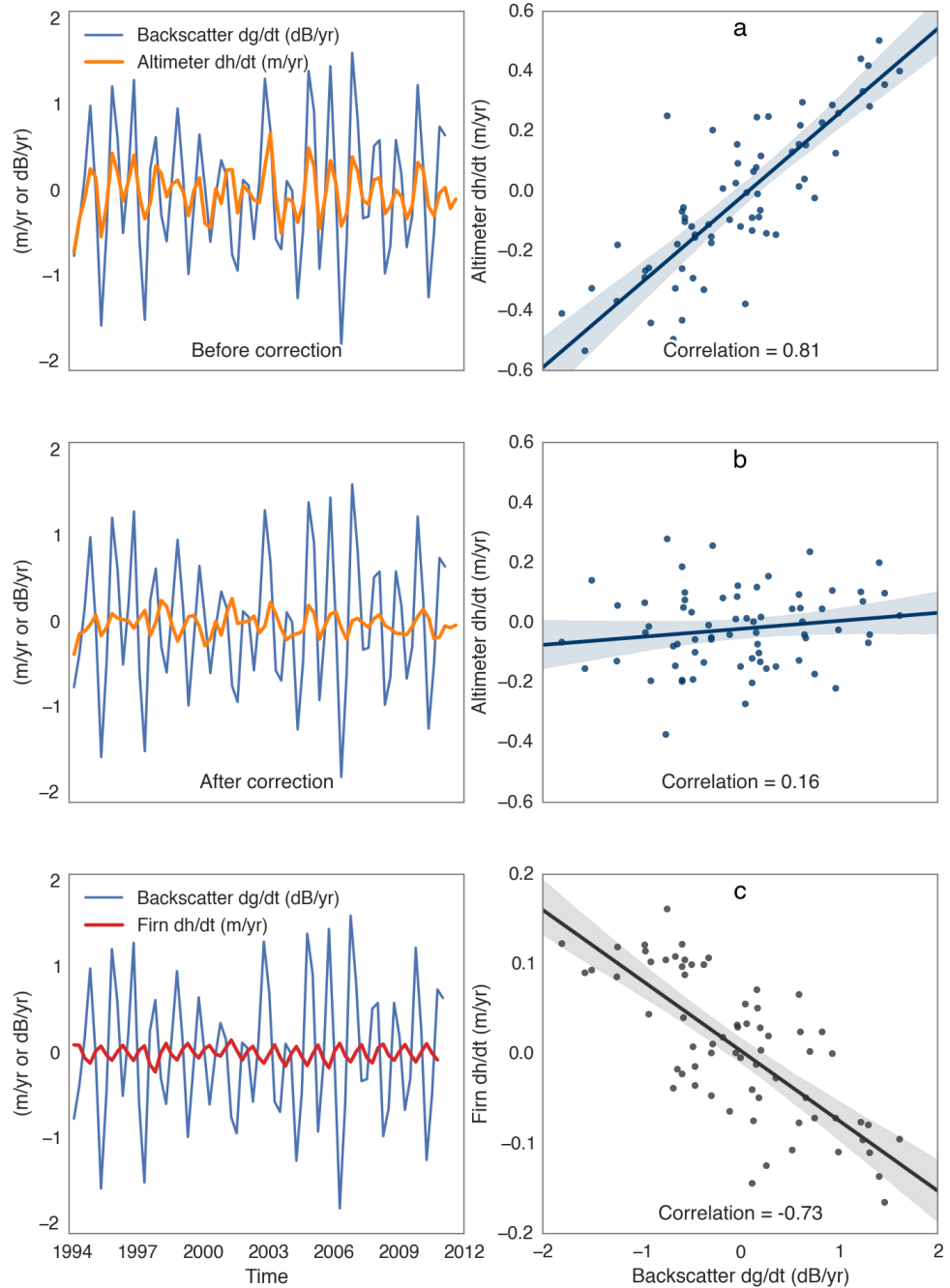


Figure 2.5: Correlation between backscatter (AGC), ice-shelf height and firn-height change derived from a firn densification model. (left column) Derivative of circum-Antarctic-wide average time series; (right column) respective correlations. From top to bottom, correlations between the derivative of backscatter and derivatives of: (a) uncorrected ice-shelf height; (b) corrected ice-shelf height (at the grid-cell level); and (c) firn-column height time series.

2.4.4 Merging individual satellite mission time series

The analyses described in Sections 2.4.1 to 2.4.3 led to independent time series for each of the three satellite missions. These time series then needed to be concatenated and further quality-controlled to generate the long multi-mission record of ice-shelf height. At each grid cell we cross-calibrated the records from the three satellite missions by computing the offsets (weighted-average of differences) between the time series during the periods when consecutive missions overlapped (ERS-1 to ERS-2: 1995–1996 and ERS-2 to Envisat: 2002–2003). We excluded the first two years of ERS-1 data (1992–1994) from our analysis because they show an apparent strong negative anomaly that extends over several sectors of Antarctica, and this anomaly also appears in the altimeter’s backscatter. In the absence of evidence supporting such a strong continental-scale signal, we assume this feature is an artifact of the data. Our final dataset therefore spans 18 years from 1994 to 2012.

We corrected a few step changes greater than 3 m (usually associated with anomalous backscatter) by leveling the segments on each side by the difference in their medians, and removed any peak greater than 3 standard deviations from the polynomial trend (see below). We rejected full 18-year records if time series from any of the three missions did not overlap due to data gaps, or if the full data set spanned less than 70% of the 18-year time interval.

2.5 Time series analysis

Estimating the evolution of changes in ice-shelf height is an important step for fingerprinting the oceanic and atmospheric processes driving such changes. A challenging task in analysis of any climate data is the extraction of underlying trends from relatively short and noisy records, particularly when there is considerable change in variance within the record itself (heterocedasticity). Ice shelves couple with the atmosphere (temperature, radiation balance, precipitation and wind stress), ocean (circulation, temperatures and waves), and sea ice (concentration and thickness), over a wide range of time scales [Paolo et al. 2015b]. Estimated trends are, therefore, strongly dependent upon length of the time interval over which the trends are calculated.

Previous authors have adopted a variety of approaches for trend extraction such as fitting simple straight lines [Pritchard et al. 2012; Shepherd et al. 2010], quadratics [Wingham et al. 2009], cubics [Schenk and Csatho 2012], sinusoids [Zwally et al. 2005], and using autoregressive models [Davis et al. 2005]. We took a different approach by (i) selecting the best fit from a range of possible models (polynomial of degree 0, 1, 2 or 3), and (ii) taking into account both bias and variance in the fitting procedure (i.e., regularization).

2.5.1 Extracting trends from height-change time series

We fitted low-order polynomial models to each time series (Fig. 2.6), allowing the degree m to vary from 0 (constant height) to 3 (cubic fit), using the lasso approach for regularized regression [Tibshirani 1996]. The regularization parameter (and, therefore, degree of the polynomial) was selected by ten-fold cross-validation, where the optimal fit is the one that minimizes the average ‘mean square prediction error’ across folds (i.e., on each fold a model is fitted to 90% of the data, testing a series of 100 regularization parameters; the MSE¹ of each fitted model/parameter tested is then computed with respect to the 10% of the data left out) [Friedman et al. 2010]. With this bias-variance-tradeoff approach, our objective is to allow a degree of curvature for estimating potential acceleration of height-change rate while avoiding the rapid oscillations introduced by ordinary least-squares polynomial fits [Paolo et al. 2015b]. The polynomials are defined as (dropping the spatial variable for generalization):

$$\hat{h}(\tau) = \sum_{m=0}^3 \beta_m \tau^m \quad (2.6)$$

where \hat{h} is the polynomial model, and β_m are the coefficients of the polynomial. We then calculated average and instantaneous rates of change as the slope of the secant and tangent lines, respectively, to the fitted polynomial by finite difference approximation.

In estimating ice surface-height trends we allow for a trend \dot{p} in sea-surface height due to the inverse barometer effect associated with a regional atmospheric-pressure trend [Padman et al. 2003] (source: ERA-Interim [Dee et al. 2011]), and a

¹Mean Square Error.

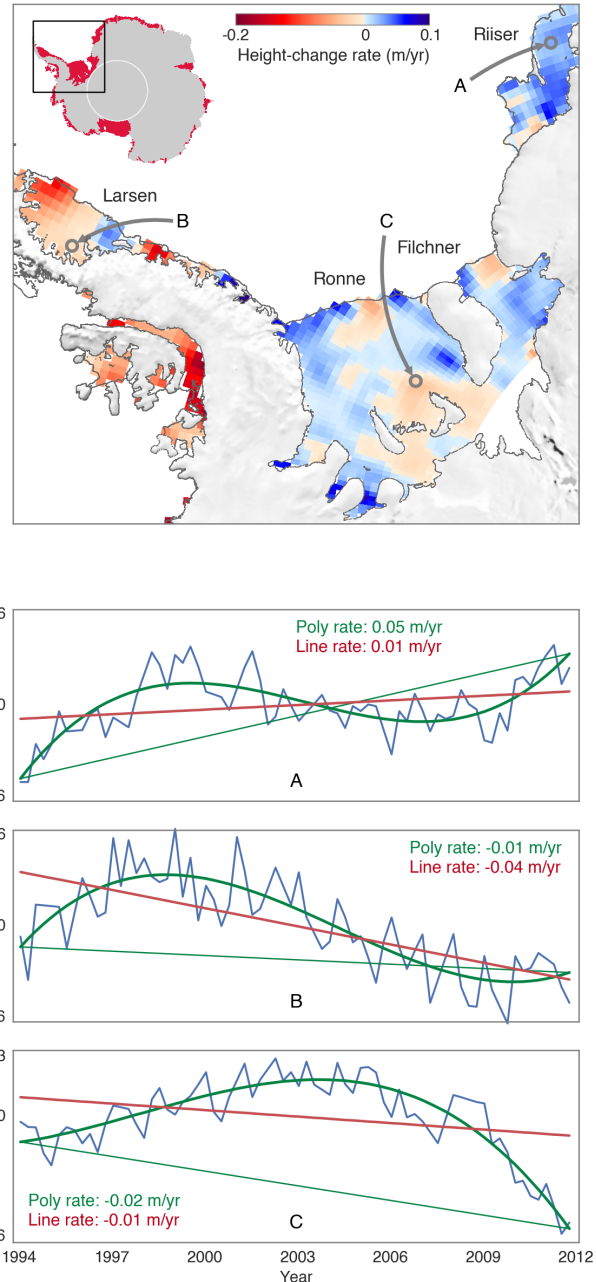


Figure 2.6: Examples of single-grid-cell 18-year time series over the Antarctic ice shelves. (top) Map showing individual grid cells with estimated 18-year mean polynomial trends over the ice shelves for one sector of Antarctica (inset map). The grid was smoothed and interpolated using a Gaussian Kernel with sigma equal to grid-cell size. (lower panels) Comparison of polynomial versus straight-line fits for trend determination on three individual height-change time series (locations shown in map). The average polynomial rate is estimated from the slope of the line connecting the polynomial end points (Eq. 2.7).

regional sea-level trend $\dot{\eta}$ (source: AVISO [Le Traon et al. 1998]). The average rate of change $\Delta\hat{h}/\Delta\tau$ between two times τ_i and τ_j is then given by:

$$\frac{\Delta\hat{h}}{\Delta\tau} = \frac{\hat{h}(\tau_j) - \hat{h}(\tau_i)}{\tau_j - \tau_i} + \dot{p} + \dot{\eta} \quad (2.7)$$

To estimate average acceleration we calculated the mean slope of the (numerical) derivative of the polynomial fit (second derivative). We performed the regularized regression procedure in two ways: a) on each individual grid-cell time series (over 2650 cells), which we used to construct spatial maps of average ice-shelf height changes (Fig. 2.6); and b) on ice-shelf-wide and region-wide average time series for estimating regional trends (Fig. 2.7; [Paolo et al. 2015b]).

Performing regularized regression on regional-average time series, where each point is the average of many other points, is preferred over aggregating estimates of trends from fitted polynomials on individual grid cells. In the latter the regularized regression is not as well constrained due to a lower signal-to-noise ratio (Fig. 2.8). A consequence of this analysis approach to trend estimation is that the sum of ice-shelf/regional values does not equal the total value computed for all of Antarctica. This is because different region sizes lead to different constraints in the regression (i.e., the all-Antarctica trend comes from its own lasso polynomial estimate while each individual ice-shelf trend also has its own lasso regression); all estimates are consistent, however, within the formal errors.

2.5.2 Estimating uncertainties

Time series error bars

Our averaging procedure facilitates the formal derivation of statistical error for individual height values within each mean time series. Two factors contribute to lower the uncertainty in the height estimates: i) the large number of crossovers that contribute to the final height estimate per location per time step ($\sim 10-100$); and ii) the long-period records (18 years), which makes the derivation of long-term slopes robust to high-frequency fluctuations (e.g., seasonality).

Our uncertainties are meant to reflect: (a) the sampling error (number of crossovers);

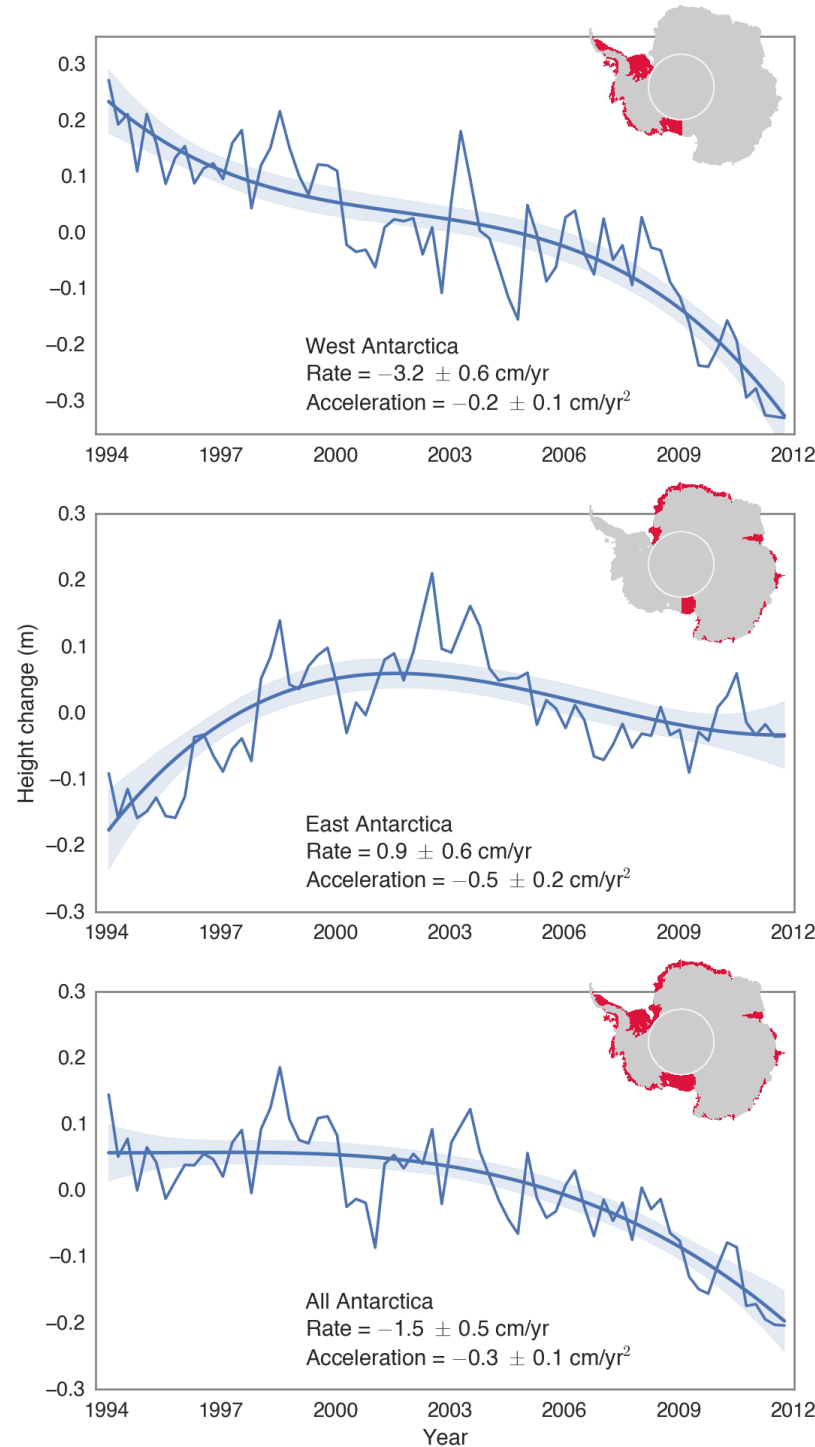


Figure 2.7: Regional time series of average Antarctic ice-shelf height for: (top) West Antarctic ice shelves; (middle) East Antarctic ice shelves; and (bottom) all Antarctic ice shelves. Adapted from Paolo et al. [2015b].

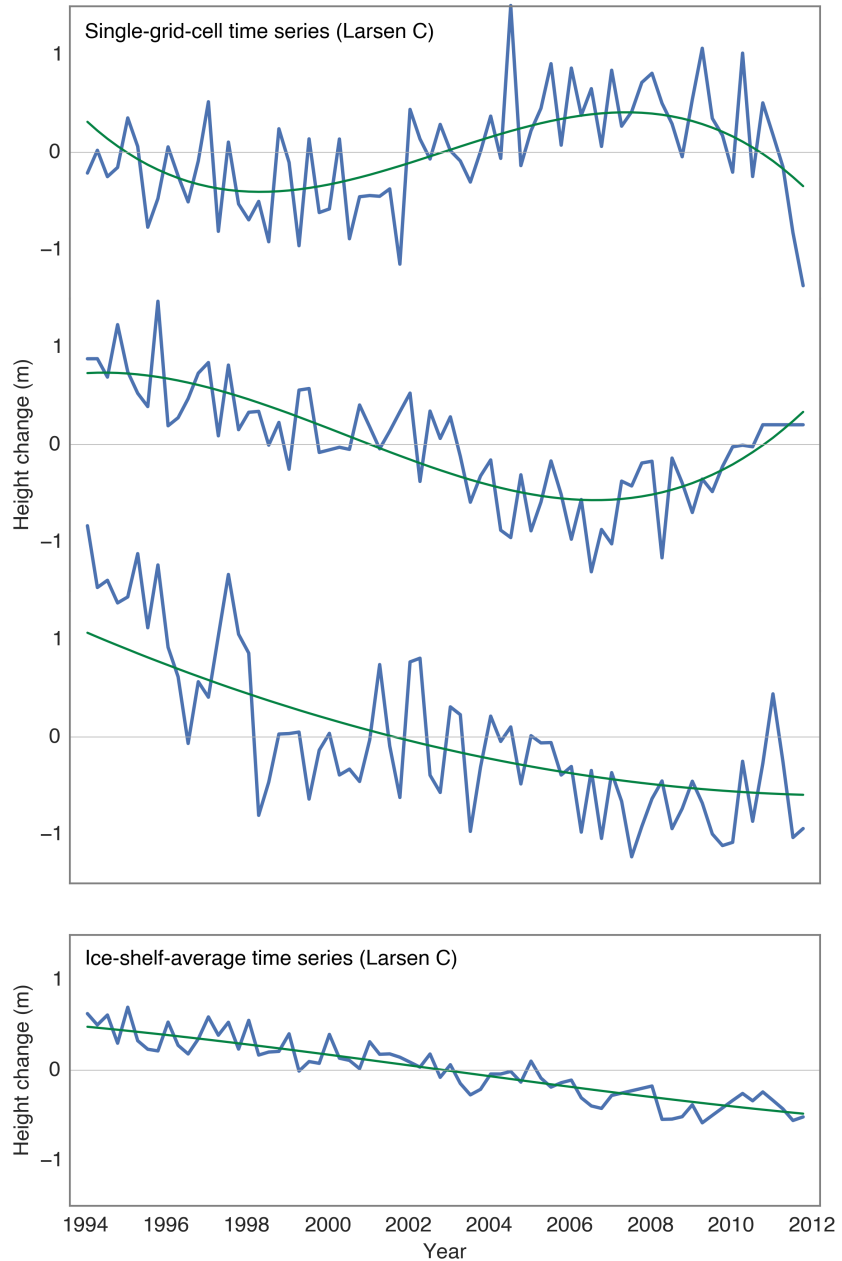


Figure 2.8: Comparison of noise level between single-grid-cell and ice-shelf-average time series. (top) Example of time series derived for three individual grid cells on Larsen-C Ice Shelf. Green lines show polynomial fits. Differences between single-cell time series represent both true spatial variations (signal) and contributions from noise. (bottom) Time series generated by averaging all individual-grid-cell time series over the entire Larsen-C Ice Shelf. The polynomial is fitted to the averaged time series (it is not the average of single-cell fits).

and (b) the backscatter-related error. Hence, we derived the time-series error bars as:

$$\delta h(\mathbf{x}, \tau) = \sqrt{\text{SE}[\Delta h(\mathbf{x}, \tau)]^2 + \text{SE}[h(\mathbf{x})_{\text{cor}} - h(\mathbf{x})_{\text{unc}}]^2} \quad (2.8)$$

where $\text{SE}[\cdot]$ is the standard error, $\Delta h(\mathbf{x}, \tau)$ represents all height differences at time τ and grid-cell location \mathbf{x} (these are the crossovers being averaged at each block in Eq. 2.2), and $h(\mathbf{x})$ is the formed height record at each grid cell, backscatter corrected (cor) and uncorrected (unc). The first term on the right-hand side represents the noise at the grid-cell level (time and spatially dependent). The second term assesses the magnitude of the backscatter-series to height-series correlation (spatially dependent) by looking at the difference between the corrected and uncorrected records. Both terms refer to the mean time series (Eq. 2.3 and 2.5).

Trend and acceleration error bars

We estimated the uncertainties in the derived trends from the polynomial fits based on the variance of the residuals. In general this provides a higher uncertainty than that derived from the individual data points. This is because the spread of the residuals arises from true natural variability in addition to observational uncertainty. Furthermore, the spread of the residuals contain valuable information on whether the polynomial fit is a good statistical model for the data. We computed the residuals as:

$$\varepsilon(\tau) = h(\tau) - \hat{h}(\tau) \quad (2.9)$$

where ε are the residuals, h is the observed time series of height changes and \hat{h} is the polynomial fit. We then used the ‘bootstrap’ approach [Efron and Tibshirani 1993] in which the residuals of the polynomial fit are randomly resampled with replacement. That is, every subsample of the residuals contains data from the original sample that can appear multiple times, so that each subsample have the same number of elements as the original data set, but with less information about the noise (with respect to the fit). We then added back each resampled residual to the original fitted model to construct the bootstrap samples:

$$h^*(\tau) = \hat{h}(\tau) + \varepsilon^*(\tau) \quad (2.10)$$

where h^* is the bootstrap time series and ε^* are the resampled residuals. We refit the polynomial model (as previously described) to each bootstrap time series and calculated the following: average rate of change, the derivative of the polynomial and the average rate of change of the derivative (average acceleration). By doing this repeatedly, we constructed an empirical distribution for each parameter of interest. We then estimated formal confidence intervals (95%) from this distribution. We constructed 1000 bootstrap samples for each individual ice-shelf/region time series, and 500 for each grid-cell time series (a total of $\sim 1,330,000$ sets of calculations).

The total uncertainty in the estimated ice-shelf height rate also includes the systematic component coming from the regional sea-level change and inverse barometer effect. However, these terms are an order of magnitude smaller than the bootstrap-derived component. The uncertainty is then given by:

$$\delta\dot{h} = \sqrt{(\delta\dot{h}^*)^2 + (\delta\dot{\eta})^2 + (\delta\dot{p})^2} \quad (2.11)$$

where $\delta\dot{h}^*$ is the uncertainty in the rate of height change at the 95% confidence level from the bootstrap distribution, $\delta\dot{\eta}$ and $\delta\dot{p}$ are the uncertainties in regional sea-level and regional atmospheric pressure trends, respectively.

Estimating uncertainties using bootstrapping is a ‘top-down’ approach, which has the advantage of not relying on the assumption that characteristics of the noise are known (e.g., normally distributed), or requiring that the relationships between the different sources of error are specified since an algebraic solution of error propagation (‘bottom-up’ approach) is not required.

2.6 Results and discussion

2.6.1 Comparison between backscatter and height

Our comparison of the height-change time series with changes in backscatter for all ice-shelf grid cells around Antarctica (Fig. 2.5) showed that the majority of the grid cells presented a positive correlation (indicative of densification of the surface) instead of a negative one (indicative of penetration). The backscatter variation impacts significantly the estimated height-changes (correlation $r \approx 0.81$) and the respective cor-

rection greatly reduces this effect (correlation $r \approx 0.16$). The anti-correlation between backscatter variation and modeled firn-height changes (correlation $r \approx -0.73$) implies that backscatter increases with firn compaction (densification of the surface), which fluctuates with the seasons. That is, for an increase in backscatter (presumably due to densification) there is an apparent increase in height even though surface densification implies compaction of the firn layer (surface lowering).

2.6.2 Trend and acceleration in ice-shelf height change

We derived two main products from our 18-year long, high-resolution (~ 3 months and ~ 30 km) record of ice-shelf height change.

Regionally-averaged time series. Regional averaging increases the statistical significance of the information that can be recovered from the available data (e.g., acceleration from the curvature of the fit). We computed circum-Antarctic average time series of height change from 1994 to 2012 for West Antarctic, East Antarctic and all Antarctic ice shelves (Fig. 2.7). These results have revealed accelerated losses in total Antarctic ice-shelf volume at decadal time scale (these results are discussed by Paolo et al. [2015b]).

High-resolution spatial maps. With analysis at the grid-cell level it is possible to map, for most of the Antarctic ice-shelf area, the spatial structure of the 18-year average rate of change, average acceleration and instantaneous rates in ice-shelf surface height (Fig. 2.9). Mapping higher-order terms such as average acceleration (slope of the derivative of the trend) reveals the regional contribution to the accelerated loss. The primary factor in the overall acceleration of the Antarctic rate of ice-shelf loss is the cessation (or deceleration) of earlier gains in the East Antarctic ice shelves [Paolo et al. 2015b].

2.6.3 Processes affecting RA-derived ice-shelf height

The main sources of uncertainty affecting our ability to use RA-derived height estimates (instantaneous and/or trend) over the Antarctic ice shelves are as follows

(order of magnitude given for instantaneous values):

- i. *Surface and volume scattering variation, $O(1)$ m.* Despite considerable progress, ongoing investigation on the interaction of the radar wave with the snow/firn/ice surface and how the surface properties change over time is essential, particularly for the modern CryoSat-2 radar mission and its innovative Doppler-delay altimeter system [Wingham et al. 2006].
- ii. *Firn-column changes, $O(0.01\text{--}1)$ m.* This effect is important to separate the mass-loss-driven changes from the surface-compaction-driven changes in the RA observation. However, there is still no reliable model-derived correction to account for this effect at the small spatial scales (tens of kilometers) that we are considering.
- iii. *Atmospheric pressure, $O(0.01\text{--}0.1)$ m.* Since ice shelves are floating, depressions on the sea-surface height force by changes in atmospheric pressure (inverse barometer effect) will be included in the altimeter ice-shelf-height measurement. There is considerable fluctuation and significant trend in the atmospheric pressure around the Antarctic ice shelves [Padman et al. 2003], especially on the time scales of a few years that we attempt to resolve here.
- iv. *Regional sea level trend, $O(0.01\text{--}0.1)$ m.* The trend in sea-level rise (which includes changes in the geoid) varies considerably from the global average (~ 3 mm/yr) at the regional scale [Church et al. 2004]; and this becomes particularly important when making inferences of ice-shelf height over long time periods (e.g., decades).
- v. *Advection of surface topographic features, $O(1\text{--}100)$ m.* The relatively large footprint size (~ 3 km) of pulse-limited RAs can lead to moving topographic features (e.g., megaripples and crevasses) being misinterpreted as interannual fluctuations in ice-shelf surface and derived changes in basal mass balance (melting).
- vi. *Errors in ocean tide and load tide corrections, $O(0.01\text{--}0.1)$ m.* Ocean tide height changes can be large, up to ~ 8 m at spring tides under the southern Ronne Ice Shelf. Standard tide model corrections reduce the tide-induced height error to <0.1 m [King and Padman 2005; King et al. 2011; Stammer et al. 2014]. Further

reduction by averaging is not effective because the ocean tide is a long-wavelength process. Instead, improvements in tide models are required.

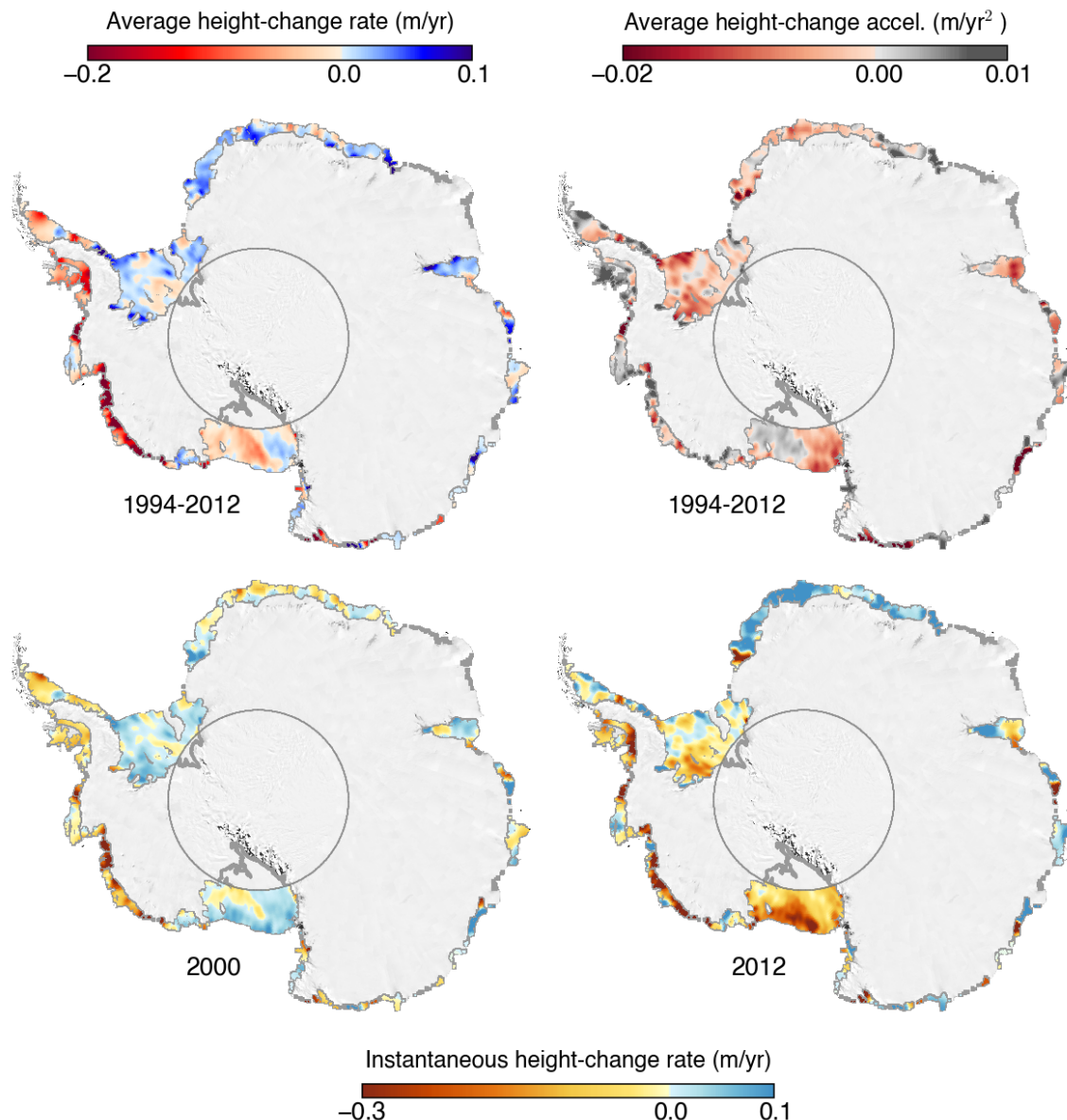


Figure 2.9: Maps of rate and acceleration of Antarctic ice-shelf height change. (top) 18-year average rate and acceleration of ice-shelf height change; (bottom) instantaneous rate of change in surface height for 2000 and 2012. Rates and acceleration were derived from polynomial models, such that (a) negative acceleration represents either increase loss-rate or decrease gain-rate (and vice-versa for positive acceleration), and (b) instantaneous rates reflect the decadal fluctuations.

2.6.4 Methodological limitations

We are unable to sample near the ice-shelf grounding line. Our grid-cell size is limited by the spatial distribution of the satellite ground-track crossing points (Fig. 2.1). We have eliminated all crossovers within 3 km of the grounding line where data may be corrupted due to the floating-to-grounded transition (high slopes, crevasses, and flexure so that hydrostatic corrections for ocean height do not work). These sampling issues are most severe for small ice shelves that have large melt rates in the grounding zone (such as Pine Island and Dotson), and they imply that estimated ice-shelf loss could be higher than our analyses suggest.

During the observation period, some ice shelves experienced significant grounding-line retreat [Rignot et al. 2014], without a commensurate retreat of their ice fronts, meaning that those ice shelves increased in area. This ice-shelf migration could impact the average value of volume loss if the new ice-shelf thickness is taken into account, although these area changes are small relative to the total ice-shelf area (less than 7%). Since our objective is to map and quantify the varying impacts of the ocean and atmosphere to ice loss around the Antarctic ice shelves, we used a fixed area approach (i.e., Eulerian reference frame).

2.7 Conclusions

We have presented a method for improved analyses of height data from multiple satellite RAs and quantifying uncertainties in the resulting data products. Using this method, we constructed an 18-year time series of height changes at \sim 3 month intervals and \sim 30 km grid cells over Antarctica's floating ice shelves. Our data set allowed us to estimate the temporal progression and spatial structure of ice-shelf height changes in Antarctica between 1994 and 2012.

We have demonstrated the following. Substantial averaging both in time and space is required to construct reliable RA height records over floating ice shelves. Densification of the surface strongly affects the height-change estimate, and the backscatter correction significantly reduces this effect. Densification is a more important effect than penetration in biasing the height-change estimates over the ice shelves. Given the high

interannual-to-decadal variability that is present, a simple straight-line fit fails to capture the underlying trends, some degree of curvature in the trend is needed. Polynomial trends allow us to obtain information on the evolution and spatial structure of changes, e.g., instantaneous rate of change (derivative of the trend), and average acceleration (slope of the derivative). Given the convoluted nature of the error sources, we propose that a top-down approach for uncertainty estimation (e.g., bootstrap applied to time-dependent data) constitutes a more accurate alternative for error analysis.

Acknowledgements

This work was funded by NASA [awards NNX12AN50H 002 (93735A), NNX10A-G19G and NNX13AP60G]. This is ESR contribution XXX. We thank J. Zwally's Ice Altimetry group at the NASA Goddard Space Flight Center for distributing their RA data sets for all satellite radar altimeter missions (<http://icesat4.gsfc.nasa.gov>). We are grateful to G. Hyland of the Australian Antarctic Division in Hobart for running the Davis S/V algorithm used to make Fig. 2.4. We thank C. Davis and D. Wingham for RA processing advice. We thank A. Shepherd for helpful comments that improved the manuscript. We also thank the San Diego Supercomputing Center for their assistance in HPC.

Chapter 2, in full, is in revision for publication of the material as it may appear in *Remote Sensing of Environment* 2015. Paolo, Fernando S.; Fricker, Helen A.; Padman, Laurie. The dissertation author was the primary investigator and author of this paper.

References

- Alley, R. B., P. U. Clark, P. Huybrechts, and I. Joughin (2005). “Ice-Sheet and Sea-Level Changes”. *Science* 310, 456–460.
- Arthern, R. J., D. J. Wingham, and A. L. Ridout (2001). “Controls on ERS altimeter measurements over ice sheets: Footprint-scale topography, backscatter fluctuations, and the dependence of microwave penetration depth on satellite orientation”. *Journal of Geophysical Research: Atmospheres* 106, 33471–33484.
- Bindschadler, R., H. Choi, a. Wichlacz, R. Bingham, J. Bohlander, K. Brunt, H. Corr, R. Drews, H. Fricker, M. Hall, R. Hindmarsh, J. Kohler, L. Padman, W. Rack, G. Rotschky, S. Urbini, P. Vornberger, and N. Young (2011). “Getting around Antarctica: New high-resolution mappings of the grounded and freely-floating boundaries of the Antarctic ice sheet created for the International Polar Year”. *The Cryosphere* 5, 569–588.
- Brenner, A. C., R. A. Bindschadler, R. H. Thomas, and H. J. Zwally (1983). “Slope-induced errors in radar altimetry over continental ice sheets”. *Journal of Geophysical Research: Oceans* 88, 1617–1623.
- Brunt, K. M., H. A. Fricker, L. Padman, T. A. Scambos, and S. O’Neel (2010). “Mapping the grounding zone of the Ross Ice Shelf, Antarctica, using ICESat laser altimetry”. *Annals of Glaciology* 51, 71–79.
- Church, J. A., N. J. White, R. Coleman, K. Lambeck, and J. X. Mitrovica (2004). “Estimates of the Regional Distribution of Sea Level Rise over the 1950–2000 Period”. *Journal of Climate* 17, 2609–2625.
- Davis, C. H. (1996). “Comparison of ice-sheet satellite altimeter retracking algorithms”. *IEEE Transactions on Geoscience and Remote Sensing* 34, 229–236.
- Davis, C. H. and A. C. Ferguson (2004). “Elevation change of the antarctic ice sheet, 1995-2000, from ERS-2 satellite radar altimetry”. *IEEE Transactions on Geoscience and Remote Sensing* 42, 2437–2445.
- Davis, C. H. and R. K. Moore (1993). “A combined surface- and volume-scattering model for ice-sheet radar altimetry”. *Journal of Glaciology* 39, 675–686.
- Davis, C. H., Y. Li, J. R. McConnell, M. M. Frey, and E. Hanna (2005). “Snowfall-driven growth in East Antarctic ice sheet mitigates recent sea-level rise.” *Science* 308, 1898–1901.
- Dee, D. P., S. M. Uppala, A. J. Simmons, P. Berrisford, P. Poli, S. Kobayashi, U. Andrae, M. A. Balmaseda, G. Balsamo, P. Bauer, P. Bechtold, A. C. M. Beljaars, L. van de Berg, J. Bidlot, N. Bormann, C. Delsol, R. Dragani, M. Fuentes, A. J. Geer, L. Haimberger, S. B. Healy, H. Hersbach, E. V. Hólm, L. Isaksen, P. Kållberg, M. Köh-

- ler, M. Matricardi, A. P. McNally, B. M. Monge-Sanz, J.-J. Morcrette, B.-K. Park, C. Peubey, P. de Rosnay, C. Tavolato, J.-N. Thépaut, and F. Vitart (2011). “The ERA-Interim reanalysis: configuration and performance of the data assimilation system”. *Quarterly Journal of the Royal Meteorological Society* 137, 553–597.
- Depoorter, M. A., J. L. Bamber, J. A. Griggs, J. T. M. Lenaerts, S. R. M. Ligtenberg, M. R. van den Broeke, and G. Moholdt (2013). “Calving fluxes and basal melt rates of Antarctic ice shelves”. *Nature* 502, 89–92.
- Dutrieux, P., J. D. Rydt, A. Jenkins, P. R. Holland, H. K. Ha, S. H. Lee, E. J. Steig, Q. Ding, E. P. Abrahamsen, and M. Schröder (2014). “Strong Sensitivity of Pine Island Ice-Shelf Melting to Climatic Variability”. *Science* 343, 174–178.
- Efron, B. and R. J. Tibshirani (1993). *An introduction to the Bootstrap*. Chapman and Hall/CRC.
- Egbert, G. D. and S. Y. Erofeeva (2002). “Efficient Inverse Modeling of Barotropic Ocean Tides”. *Journal of Atmospheric and Oceanic Technology* 19, 183–204.
- Femenias, P (1996). *ERS QLOPR and OPR range processing, ESA/ESRIN Tech. Note ER-TN-RS-RA-0022, Eur. Space Agency/Eur. Space Res. Inst., Frascati, Italy*.
- Flament, T. and F. Rémy (2012). “Dynamic thinning of Antarctic glaciers from along-track repeat radar altimetry”. *Journal of Glaciology* 58, 830–840.
- Fretwell, P., H. D. Pritchard, D. G. Vaughan, J. L. Bamber, N. E. Barrand, R. Bell, C. Bianchi, R. G. Bingham, D. D. Blankenship, G. Casassa, G. Catania, D. Callens, H. Conway, A. J. Cook, H. F. J. Corr, D. Damaske, V. Damm, F. Ferraccioli, R. Forsberg, S. Fujita, Y. Gim, P. Gogineni, J. A. Griggs, R. C. A. Hindmarsh, P. Holmlund, J. W. Holt, R. W. Jacobel, A. Jenkins, W. Jokat, T. Jordan, E. C. King, J. Kohler, W. Krabill, M. Riger-Kusk, K. A. Langley, G. Leitchenkov, C. Leuschen, B. P. Luyendyk, K. Matsuoka, J. Mouginot, F. O. Nitsche, Y. Nogi, O. A. Nost, S. V. Popov, E. Rignot, D. M. Rippin, A. Rivera, J. Roberts, N. Ross, M. J. Siegert, A. M. Smith, D. Steinhage, M. Studinger, B. Sun, B. K. Tinto, B. C. Welch, D. Wilson, D. A. Young, C. Xiangbin, and A. Zirizzotti (2013). “Bedmap2: improved ice bed, surface and thickness datasets for Antarctica”. *The Cryosphere* 7, 375–393.
- Fricker, H. A. and L. Padman (2006). “Ice shelf grounding zone structure from ICESat laser altimetry”. *Geophysical Research Letters* 33, L15502.
- Fricker, H. A., R. Coleman, L. Padman, T. A. Scambos, J. Bohlander, and K. M. Brunt (2009). “Mapping the grounding zone of the Amery Ice Shelf, East Antarctica using InSAR, MODIS and ICESat”. *Antarctic Science* 21, 515–532.
- Friedman, J., T. Hastie, and R. Tibshirani (2010). “Regularization Paths for Generalized Linear Models via Coordinate Descent”. *Journal of Statistical Software* 33, 1–22.
- Huber, P.J. (1981). *Robust Statistics*. John Wiley & Sons.

- Joughin, I. and R. B. Alley (2011). "Stability of the West Antarctic ice sheet in a warming world". *Nature Geoscience* 4, 506–513.
- Joughin, I., R. B. Alley, and D. M. Holland (2012). "Ice-Sheet Response to Oceanic Forcing". *Science* 338, 1172–1176.
- Joughin, I., B. E. Smith, and B. Medley (2014). "Marine Ice Sheet Collapse Potentially Under Way for the Thwaites Glacier Basin, West Antarctica". *Science* 344, 735–738.
- Khvorostovsky, K (2012). "Merging and analysis of elevation time series over Greenland ice sheet from satellite radar altimetry". *IEEE Transactions on Geoscience and Remote Sensing* 50, 1–14.
- King, M. A. and L. Padman (2005). "Accuracy assessment of ocean tide models around Antarctica". *Geophysical Research Letters* 32, L23608.
- King, M. A., L. Padman, K. Nicholls, P. J. Clarke, G. H. Gudmundsson, B. Kulessa, and A. Shepherd (2011). "Ocean tides in the Weddell Sea: New observations on the Filchner-Ronne and Larsen C ice shelves and model validation". *Journal of Geophysical Research: Oceans* 116, C06006.
- Le Traon, P.Y., F. Nadal, and N. Ducet (1998). "An Improved Mapping Method of Multisatellite Altimeter Data". *Journal of Atmospheric and Oceanic Technology* 15, 522–534.
- Legresy, B. (1998). "Using the temporal variability of satellite radar altimetric observations to map surface properties of the Antarctic ice sheet". *Journal of Glaciology* 44, 197–206.
- Li, Y. and C. H. Davis (2006). "Improved methods for analysis of decadal elevation-change time series over Antarctica". *IEEE Transactions on Geoscience and Remote Sensing* 44, 2687–2697.
- Ligtenberg, S. R. M., M. M. Helsen, and M. R. Van Den Broeke (2011). "An improved semi-empirical model for the densification of Antarctic firn". *The Cryosphere* 5, 809–819.
- Moholdt, G., C. Nuth, J. O. Hagen, and J. Kohler (2010). "Recent elevation changes of Svalbard glaciers derived from ICESat laser altimetry". *Remote Sensing of Environment* 114, 2756–2767.
- Padman, L., H. A. Fricker, R. Coleman, S. Howard, and L. Erofeeva (2002). "A new tide model for the Antarctic ice shelves and seas". *Annals of Glaciology* 34, 247–254.
- Padman, L., M. King, D. Goring, H. Corr, and R. Coleman (2003). "Ice-shelf elevation changes due to atmospheric pressure variations". *Journal of Glaciology* 49, 521–526.

- Paolo, F. S., H. A. Fricker, and L. Padman (2015b). “Volume loss from Antarctic ice shelves is accelerating”. *Science* 348, 327–331.
- Partington, K. C., J. K. Ridley, C. G. Rapley, and H. J. Zwally (1989). “Observations of the surface properties of the ice sheets by satellite radar altimetry”. *Journal of Glaciology* 35, 267–275.
- Phillips, H. A. (1998). “Surface meltstreams on the Amery Ice Shelf, East Antarctica”. *Annals of Glaciology* 27, 177–181.
- Pritchard, H. D., S. R. M. Ligtenberg, H. A. Fricker, D. G. Vaughan, M. R. van den Broeke, and L. Padman (2012). “Antarctic ice-sheet loss driven by basal melting of ice shelves”. *Nature* 484, 502–505.
- Remy, F., T. Flament, F. Blarel, and J. Benveniste (2012). “Radar altimetry measurements over antarctic ice sheet: A focus on antenna polarization and change in backscatter problems”. *Advances in Space Research* 50, 998–1006.
- Rémy, F. and S. Parouty (2009). “Antarctic ice sheet and radar altimetry: A Review”. *Remote Sensing* 1, 1212–1239.
- Ridley, J. K. and K. C. Partington (1988). “A model of satellite radar altimeter return from ice sheets”. *International Journal of Remote Sensing* 9, 601–624.
- Rignot, E., G. Casassa, P. Gogineni, W. Krabill, A. Rivera, and R. Thomas (2004). “Accelerated ice discharge from the Antarctic Peninsula following the collapse of Larsen B ice shelf”. *Geophysical Research Letters* 31, L18401.
- Rignot, E., J. Mouginot, and B. Scheuchl (2011). “Ice flow of the Antarctic ice sheet.” *Science* 333, 1427–1430.
- Rignot, E., S. Jacobs, J. Mouginot, and B. Scheuchl (2013). “Ice-Shelf Melting Around Antarctica”. *Science* 341, 266–270.
- Rignot, E., J. Mouginot, M. Morlighem, H. Seroussi, and B. Scheuchl (2014). “Widespread, rapid grounding line retreat of Pine Island, Thwaites, Smith, and Kohler glaciers, West Antarctica, from 1992 to 2011”. *Geophysical Research Letters* 41, 3502–3509.
- Roca, M., S. Laxon, and C. Zelli (2009). “The EnviSat RA-2 Instrument Design and Tracking Performance”. *IEEE Transactions on Geoscience and Remote Sensing* 47, 3489–3506.
- Scambos, T. A., J. A. Bohlander, C. A. Shuman, and P. Skvarca (2004). “Glacier acceleration and thinning after ice shelf collapse in the Larsen B embayment, Antarctica”. *Geophysical Research Letters* 31, 2001–2004.

- Scambos, T.A., T.M. Haran, M.A. Fahnestock, T.H. Painter, and J. Bohlander (2007). “MODIS-based Mosaic of Antarctica (MOA) data sets: Continent-wide surface morphology and snow grain size”. *Remote Sensing of Environment* 111, 242–257.
- Scharroo, R. and P. Visser (1998). “Precise orbit determination and gravity field improvement for the ERS satellites”. *Journal of Geophysical Research: Oceans* 103, 8113–8127.
- Schenk, T. and B. Csatho (2012). “A New Methodology for Detecting Ice Sheet Surface Elevation Changes From Laser Altimetry Data”. *IEEE Transactions on Geoscience and Remote Sensing* 50, 3302–3316.
- Schoof, C. (2007). “Ice sheet grounding line dynamics: Steady states, stability, and hysteresis”. *Journal of Geophysical Research: Earth Surface* 112, 1–19.
- Shepherd, A., D. Wingham, D. Wallis, K. Giles, S. Laxon, and A.V. Sundal (2010). “Recent loss of floating ice and the consequent sea level contribution”. *Geophysical Research Letters* 37, 1–5.
- Shepherd, A., E.R. Ivins, G.A. V.R. Barletta, M.J. Bentley, S. Bettadpur, K.H. Briggs, D.H. Bromwich, R. Forsberg, N. Galin, M. Horwath, S. Jacobs, I. Joughin, M.A. King, J.T.M. Lenaerts, J. Li, S.R.M. Ligtenberg, A. Luckman, S.B. Luthcke, M. McMillan, R. Meister, G. Milne, J. Mouginot, A. Muir, J.P. Nicolas, J. Paden, A.J. Payne, H. Pritchard, E. Rignot, H. Rott, L.S. Sørensen, T.A. Scambos, B. Scheuchl, E.J.O. Schrama, B. Smith, A.V. Sundal, J.H. van Angelen, W.J. van de Berg, M.R. van den Broeke, D.G. Vaughan, I. Velicogna, J. Wahr, P.L. Whitehouse, D.J. Wingham, D. Yi, D. Young, and H.J. Zwally (2012). “A Reconciled Estimate of Ice-Sheet Mass Balance”. *Science* 338, 1183–1189.
- Stammer, D., R.D. Ray, O.B. Andersen, B.K. Arbic, W. Bosch, L. Carrère, Y. Cheng, D.S. Chinn, B.D. Dushaw, G.D. Egbert, S.Y. Erofeeva, H.S. Fok, J.a.M. Green, S. Griffiths, M.A. King, V. Lapin, F.G. Lemoine, S.B. Luthcke, F. Lyard, J. Morison, M. Müller, L. Padman, J.G. Richman, J.F. Shriver, C.K. Shum, E. Taguchi, and Y. Yi (2014). “Accuracy assessment of global barotropic ocean tide models”. *Reviews of Geophysics* 52, 243–282.
- Sutterley, T.C., I. Velicogna, E. Rignot, J. Mouginot, T. Flament, M.R. van den Broeke, J.M. van Wessem, and C.H. Reijmer (2014). “Mass loss of the Amundsen Sea Embayment of West Antarctica from four independent techniques”. *Geophysical Research Letters* 41, 2014GL061940.
- Thomas, R., C. Davis, E. Frederick, W. Krabill, Y. Li, S. Manizade, and C. Martin (2008). “A comparison of Greenland ice-sheet volume changes derived from altimetry measurements”. *Journal of Glaciology* 54, 203–212.
- Tibshirani, R. (1996). “Regression shrinkage and selection via the lasso”. *Journal of the Royal Statistical Society, Series B* 58, 267–288.

- Wingham, D. J., A Shepherd, A Muir, and G. J. Marshall (2006). "Mass balance of the Antarctic ice sheet." *Philosophical Transactions A* 364, 1627–1635.
- Wingham, D. J., D. W. Wallis, and A. Shepherd (2009). "Spatial and temporal evolution of Pine Island Glacier thinning, 1995-2006". *Geophysical Research Letters* 36, 5–9.
- Wingham, D. J., A. J. Ridout, R. Scharroo, R. J. Arthern, and C. K. Shum (1998). "Antarctic Elevation Change from 1992 to 1996". *Science* 282, 456–458.
- Zwally, H. J., M. B. Giovinetto, J Li, H. G. Cornejo, and M. A. Beckley (2005). "Mass changes of the Greenland and Antarctica ice sheets and shelves and contributions to sea level rise: 1992-2002". *Journal of Glaciology* 51, 509–509.
- Zwally, H. J. and A. C. Brenner (2001). "Chapter 9 Ice Sheet Dynamics and Mass Balance". In: *International Geophysics*. Ed. by L.-L. F. a. A. Cazenave. Vol. 69. Academic Press, 351–xxvi.
- Zwally, H. J., R. A. Bindschadler, A. C. Brenner, J. A. Major, and J. G. Marsh (1989). "Growth of Greenland Ice Sheet: Measurement". *Science* 246, 1587–1589.
- Zwally, J. H. and S. Fiegles (1994). "Extent and Duration of Antarctic Surface Melting". *Journal of Glaciology* 40, 463–476.

Chapter 3

Trend analysis of ice-shelf height

This chapter, in full, is a reprint of:

Volume loss from Antarctic ice shelves is accelerating, F.S. Paolo, H.A. Fricker, L. Padman, Science (2015). doi:10.1126/science.aaa0940

3.1 Abstract

The floating ice shelves surrounding the Antarctic Ice Sheet restrain the grounded ice-sheet flow. Thinning of an ice shelf reduces this effect, leading to an increase in ice discharge to the ocean. Using 18 years of continuous satellite radar altimeter observations, we have computed decadal-scale changes in ice-shelf thickness around the Antarctic continent. Overall, average ice-shelf volume change accelerated from negligible loss at 25 ± 64 cubic kilometers per year for 1994–2003 to rapid loss of 310 ± 74 cubic kilometers per year for 2003–2012. West Antarctic losses increased by $\sim 70\%$ in the past decade, and earlier volume gain by East Antarctic ice shelves ceased. In the Amundsen and Bellingshausen regions, some ice shelves have lost up to 18% of their thickness in less than two decades.

3.2 Introduction

The Antarctic Ice Sheet gains mass through snowfall and loses mass at its margin through submarine melting and iceberg calving. These losses occur primarily from ice

shelves, the floating extensions of the ice sheet. Antarctica's grounded-ice loss has increased over the past two decades [Shepherd et al. 2012; Sutterley et al. 2014], with the most rapid losses being along the Amundsen Sea coast [Joughin and Alley 2011] concurrent with substantial thinning of adjoining ice shelves [Shepherd et al. 2010; Pritchard et al. 2012] and along the Antarctic Peninsula after ice-shelf disintegration events [Scambos et al. 2004]. Ice shelves restrain ("buttress") the flow of the grounded ice through drag forces at the ice-rock boundary, including lateral stresses at sidewalls and basal stresses where the ice shelf rests on topographic highs [Schoof 2007; Goldberg et al. 2009]. Reductions in ice-shelf thickness reduce these stresses, leading to a speed-up of ice discharge. If the boundary between the floating ice shelf and the grounded ice (the grounding line) is situated on a retrograde bed (sloping downwards inland), this process leads to faster rates of ice flow, with potential for a self-sustaining retreat [Schoof 2007; Favier et al. 2014; Joughin et al. 2014].

Changes in ice-shelf thickness and extent have primarily been attributed to varying atmospheric and oceanic conditions [Scambos et al. 2003; Dutrieux et al. 2014]. Observing iceshelf thickness variability can help identify the principal processes influencing how changing large-scale climate affects global sea level through the effects of buttressing on the Antarctic Ice Sheet. The only practical way to map and monitor ice-shelf thickness for this vast and remote ice sheet at the known space and time scales of ice-shelf variability is with satellite altimetry. Previous studies have reported trends based on simple line fits to time series of ice-shelf thickness (or height) averaged over entire ice shelves or broad regions [Shepherd et al. 2010; Zwally et al. 2005] or for short (\sim 5-year) time intervals [Pritchard et al. 2012; Rignot et al. 2013; Depoorter et al. 2013]. Here, we present a record of ice-shelf thickness that is highly resolved in time (\sim 3 months) and space (\sim 30 km), using the longest available record from three consecutive overlapping satellite radar altimeter missions (ERS-1, 1992–1996; ERS-2, 1995–2003; and Envisat, 2002–2012) spanning 18 years from 1994 to 2012.

3.3 Methods

Our technique for ice-shelf thickness change detection is based on crossover analysis of satellite radar altimeter data, in which time-separated height estimates are

differenced at orbit intersections [Zwally et al. 2005; Davis and Ferguson 2004; Wingham et al. 2009]. To cross-calibrate measurements from the different satellite altimeters, we used the roughly 1-year overlap between consecutive missions. The signal-to-noise ratio of altimeter-derived height differences for floating ice in hydrostatic equilibrium is roughly an order of magnitude smaller than over grounded ice, requiring additional data averaging to obtain comparable statistical significance. We aggregated observations in time (3-month bins) and space (\sim 30-km cells). Because the spatial distribution of crossovers changes with time (due, for example, to non-exact repeat tracks and nadir mispointing), we constructed several records at each cell location and stacked them in order to produce a mean time series with reduced statistical error¹. We converted our height-change time series and rates to thickness changes by assuming that observed losses occurred predominantly at the density of solid ice (basal melting) [Shepherd et al. 2010; Pritchard et al. 2012; Wingham et al. 2009]. This is further justified by the relative insensitivity of radar measurements to fluctuations in surface mass balance¹. For volume changes, we tracked the minimum (fixed) area of each ice shelf¹. We assessed uncertainties for all estimates using the bootstrap approach (resampling with replacement of the residuals of the fit) [Efron and Tibshirani 1993], which allows estimation of formal confidence intervals. All our uncertainties are stated at the 95% confidence level (discussion of uncertainties are provided in [¹] and the several corrections applied are stated in [²]).

We estimated 18-year trends in ice-shelf thickness by fitting low-order polynomials (degree $n \leq 3$) to the data using a combination of lasso regularized-regression [Tibshirani 1996] and cross-validation for model-parameter selection (the shape of the fit is determined by the data). This combined approach allowed us to minimize the effect of short-term variability on the 18-year trends. Relative to previous studies [Shepherd et al. 2010; Pritchard et al. 2012; Zwally et al. 2005; Fricker and Padman 2012], we have improved estimations by (i) using 18-year continuous records, (ii) implementing a time series averaging scheme so as to enhance the signal-to-noise ratio, and (iii) using

¹Materials and methods are available as supplementary materials on *Science Online*, and reproduced in part at the end of this chapter and the majority of it in *Chapter 2*.

²Corrections include lag of the satellite's leading-edge tracker (retracking), surface scattering variations, surface slope, dry atmospheric mass, water vapor, the ionosphere, solid Earth tide, ocean tide and loading, atmospheric pressure, and regional sea-level variation¹.

a robust approach to trend extraction.

3.4 Results and discussion

The 18-year average rate of thickness change varies spatially (Fig. 3.1). On shorter time scales, trends are highly variable but spatially coherent (Fig. 3.2 and movie³). We divided our data set into eight regions on the basis of spatial coherence of long-term ice-shelf behavior and calculated time series of ice-shelf thickness change (relative to series mean) for each region (Fig. 3.3). The largest regional thickness losses were in the Amundsen and Bellingshausen seas, with average (and maximum) thinning rates of 19.4 ± 1.9 (66.5 ± 9.0) m/decade and 7.4 ± 0.9 (64.4 ± 4.9) m/decade, respectively. These values correspond to ~ 8 and 5% of thickness loss over the 18 years for the two regions, respectively. These two regions account for less than 20% of the total West Antarctic ice-shelf area but, combined, contribute more than 85% of the total ice-shelf volume loss from West Antarctica. The area-averaged time records of ice-shelf thickness and volume for the West and East Antarctic sectors (Fig. 3.1, bottom left), broad regions (Fig. 3.3), and single ice shelves (Fig. 3.5 and ??) at 3-month time intervals show a wide range of temporal responses with large interannual-to-decadal fluctuations, stressing the importance of long records for determining the long-term state of the ice shelves. Comparing our long records with simple linear trends obtained for the periods of single satellite missions (such as the 5-year ICESat time span used in Pritchard et al. [2012]) shows that it is often not possible to capture the persistent signals in the shorter records (Fig. 3.3, 3.5 and ??).

³<https://www.youtube.com/watch?v=ii8enEyfFlo>

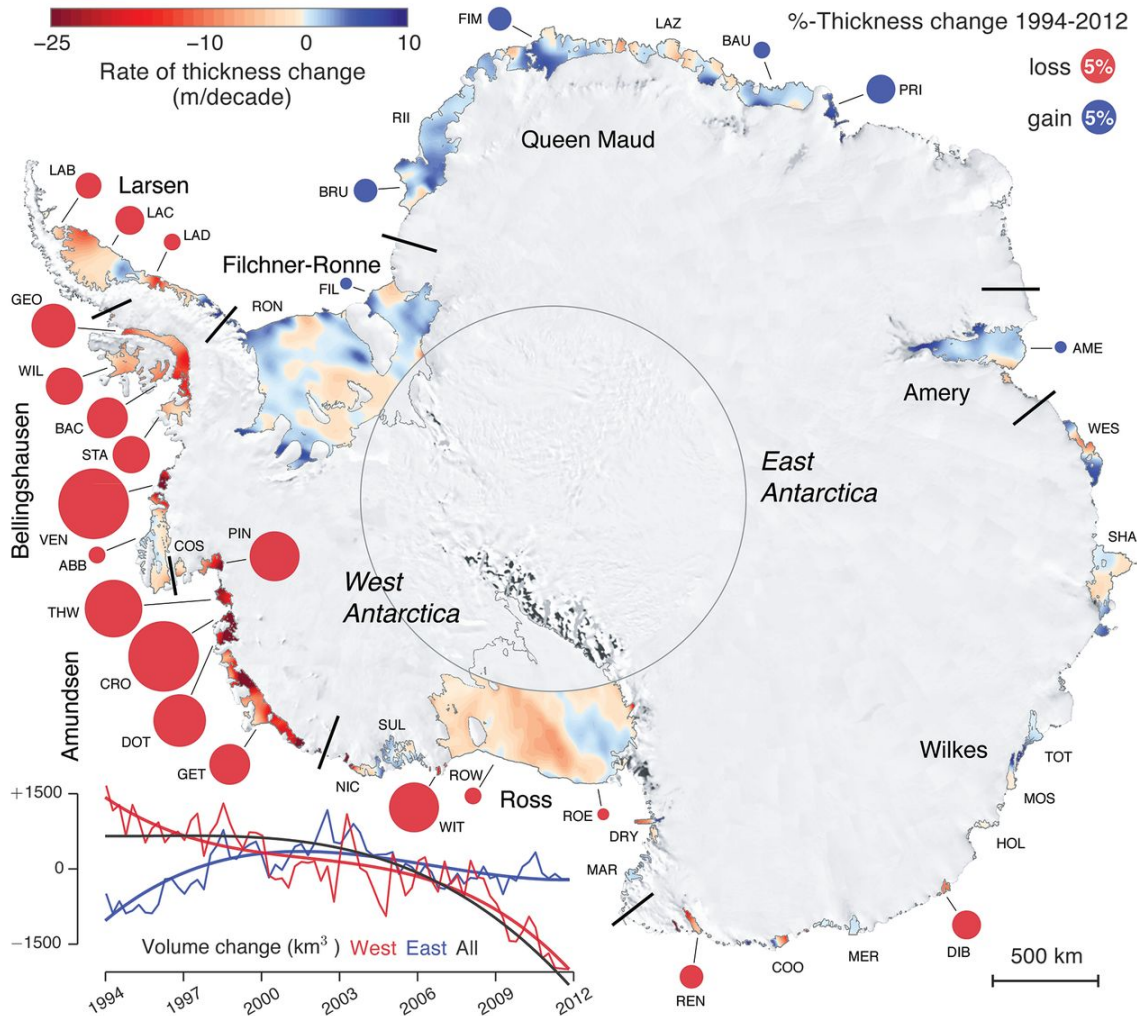


Figure 3.1: Eighteen years of change in thickness and volume of Antarctic ice shelves. Rates of thickness change (meters per decade) are colorcoded from -25 (thinning) to +10 (thickening). Circles represent percentage of thickness lost (red) or gained (blue) in 18 years. Only significant values at the 95% confidence level are plotted (Table 3.1). (Bottom left) Time series and polynomial fit of average volume change (cubic kilometers) from 1994 to 2012 for the West (in red) and East (in blue) Antarctic ice shelves. The black curve is the polynomial fit for All Antarctic ice shelves. We divided Antarctica into eight regions (Fig. 3.3), which are labeled and delimited by line segments in black. Ice-shelf perimeters are shown as a thin black line. The central circle demarcates the area not surveyed by the satellites (south of 81.5°S). Original data were interpolated for mapping purposes (percentage area surveyed of each ice shelf is provided in Table 3.1). Background is the Landsat Image Mosaic of Antarctica (LIMA).

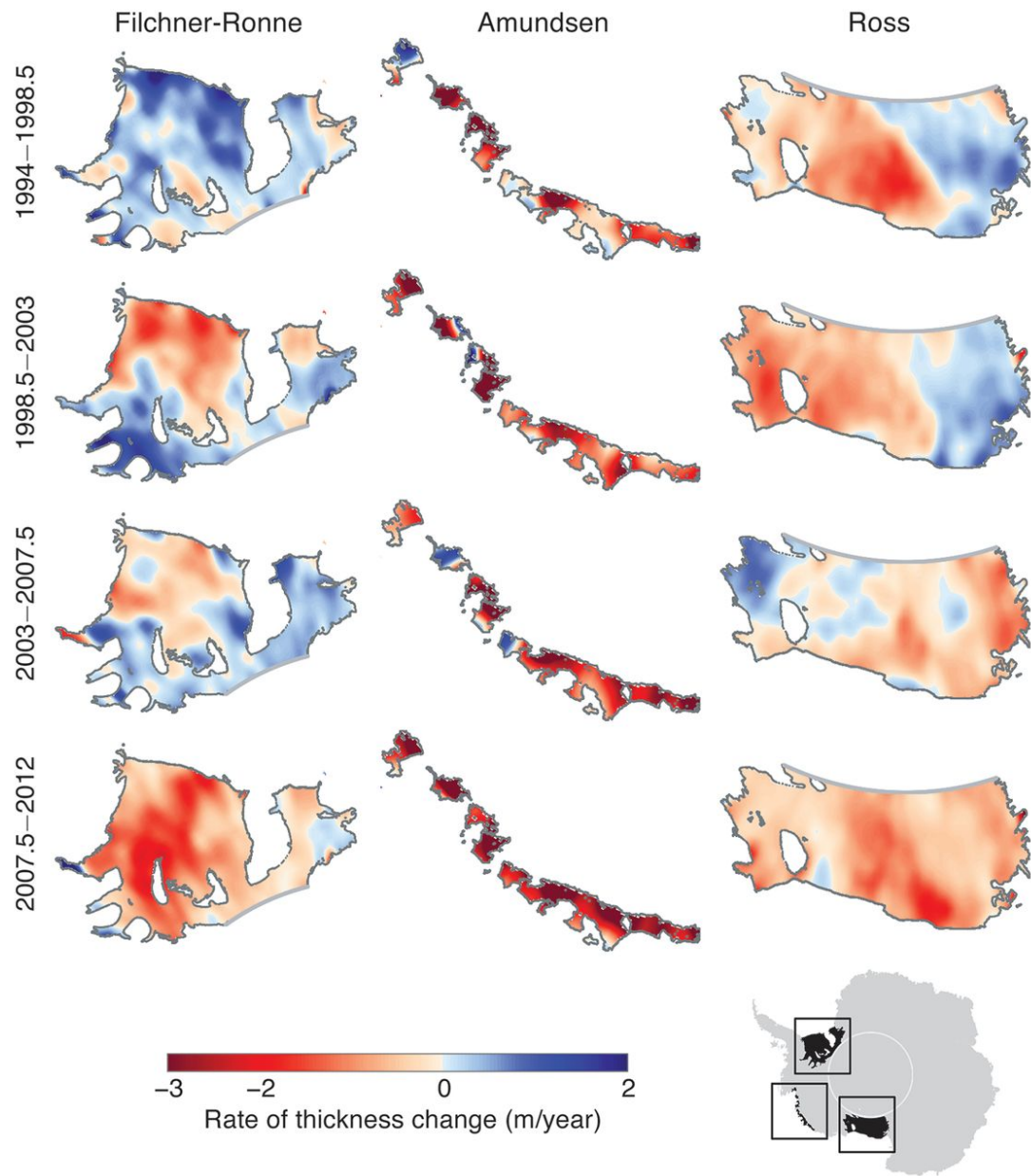


Figure 3.2: Variability in the rate of Antarctic ice-shelf thickness change (meters per year). Maps for (columns from left to right) Filchner-Ronne, Amundsen, and Ross ice shelves (locations in the bottom right corner) showing average rate of thickness change for (rows) four consecutive 4.5-year intervals (1994–1998.5, 1998.5–2003, 2003–2007.5, and 2007.5–2012). Shorter-term rates can be higher than those from an 18-year interval. Ice-shelf perimeters are thin black lines, and the thick gray line demarcates the limit of satellite observations.

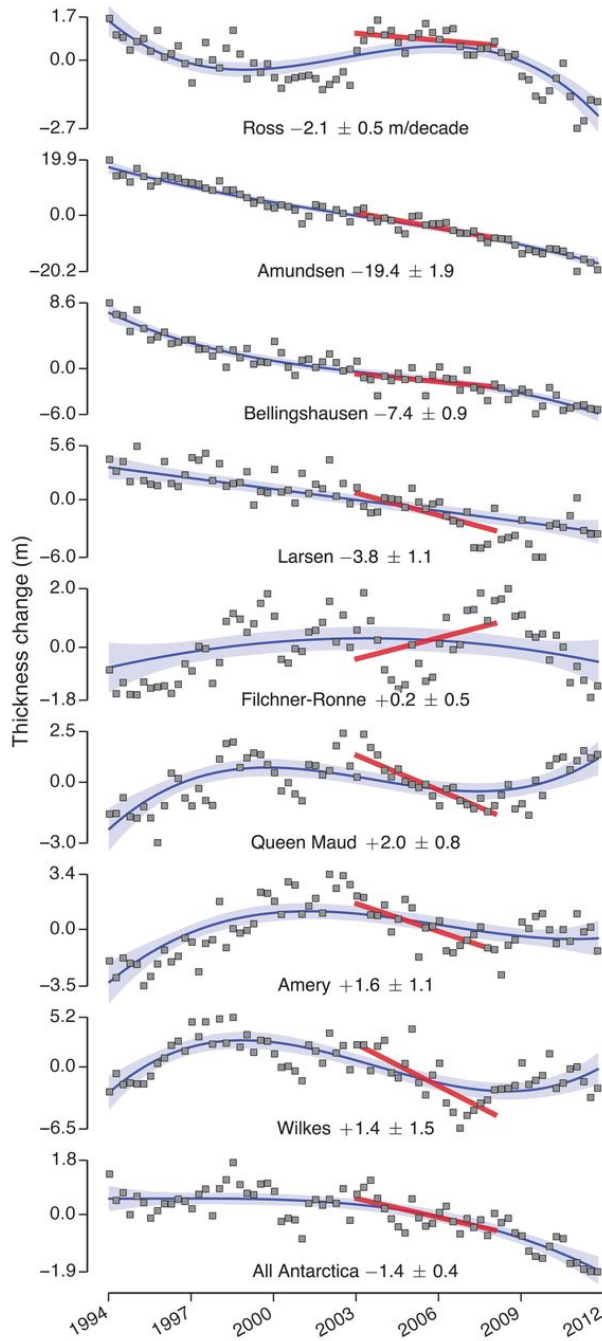


Figure 3.3: Time series of cumulative thickness change relative to series mean for Antarctic ice-shelf regions (1994–2012). Time series correspond to averages for all ice-shelf data within the Antarctic regions defined in Fig. 3.1. Dots represent average thickness change every 3 months. Error bars are small (in many cases, smaller than the symbols themselves, thus omitted from the plots), making the interannual fluctuation shown by the dots significant. The blue curve is the long-term trend from polynomial regression with the 95% confidence band, and the red line shows the regression line to the segment of our data set that overlaps with the period used for a prior ICESat-based analysis (2003–2008) [Pritchard et al. 2012]. Average rates (in meters per decade) are derived from the end points of the polynomial models.

Ice-shelf average thinning rates from the 18-year polynomial fits in the Amundsen Sea region (AS) range from 1.5 ± 0.9 m/decade for Abbot to 31.1 ± 5.4 m/decade for Crosson, with local maximum thinning of 66.5 ± 9.0 m/decade on Getz (Fig. 3.5 and Table 3.1). Crosson and Getz have lost ~ 18 and 6% of their thicknesses, respectively, over the 18-year period. If this thinning persists for these two ice shelves, we can expect volume losses of ~ 100 and 30%, respectively, in the next 100 years. Getz is the single largest contributor to the overall volume loss of Antarctic ice shelves, with an average change of -54 ± 5 km³/year, accounting for $\sim 30\%$ of the total volume loss from the West Antarctic ice shelves (Table 3.1). We find the most dramatic thickness reduction on Venable Ice Shelf in the Bellingshausen Sea (BS), with an average (and maximum) thinning rate of 36.1 ± 4.4 (64.4 ± 4.9) m/decade, respectively (Fig. 3.5 and Table 3.1). This ice shelf has lost 18% of its thickness in 18 years, which implies complete disappearance in 100 years.

For the ice shelves in the AS, observed rates are highest near the deep grounding lines, with lower rates found toward the shallower ice fronts (Fig. 3.2, Table 3.1, and movie⁴). This pattern is consistent with enhanced melting underneath the ice shelf forced by an increased flux of circumpolar deep water (CDW) from across the continental shelf and into the sub-ice-shelf cavity [Dutrieux et al. 2014; Jacobs et al. 2011; Thoma et al. 2008]. The consequent loss of ice-shelf buttressing from increased ocean-forced melting may have driven the grounding lines inland [Rignot et al. 2014] to a point on a retrograde bed slope at which the marine ice-sheet instability mechanism can take over the dynamics of ice export [Schoof 2007; Weertman 1974]. Hence, observed ice-shelf thinning reflects both ocean-induced basal melting and increased strain rates resulting from faster flows. Our analysis shows that thinning was already under way at a substantial rate at the start of our record in 1994.

On the eastern side of the Antarctic Peninsula [comprising Larsen B (Scar Inlet remnant), Larsen C, and Larsen D], the regional ice-shelf thinning rate of 3.8 ± 1.1 m/decade (Fig. 3.3) is about half of that on the western side (BS) (Fig. 3.1). The onset of thinning for Larsen C has progressed southward (Fig. 3.4), which is consistent with climate-driven forcing discussed in earlier studies [Fricker and Padman 2012; Cook and Vaughan 2010]. The highest thinning rates on Larsen C (with local maximum thinning

⁴<https://www.youtube.com/watch?v=ii8enEyfFlo>

of 16.6 ± 8.1 m/decade) are near Bawden Ice Rise (Fig. 3.1 and 3.4). Assuming that half of this observed thinning is due to air loss within the firn column, and considering that the ice shelf is ~ 40 m above flotation over the ice rise [Holland et al. 2015], we can expect Larsen C to fully unground from this pinning point within the next 100 years, with potential consequences on the ice-shelf stability [Borstad et al. 2013].

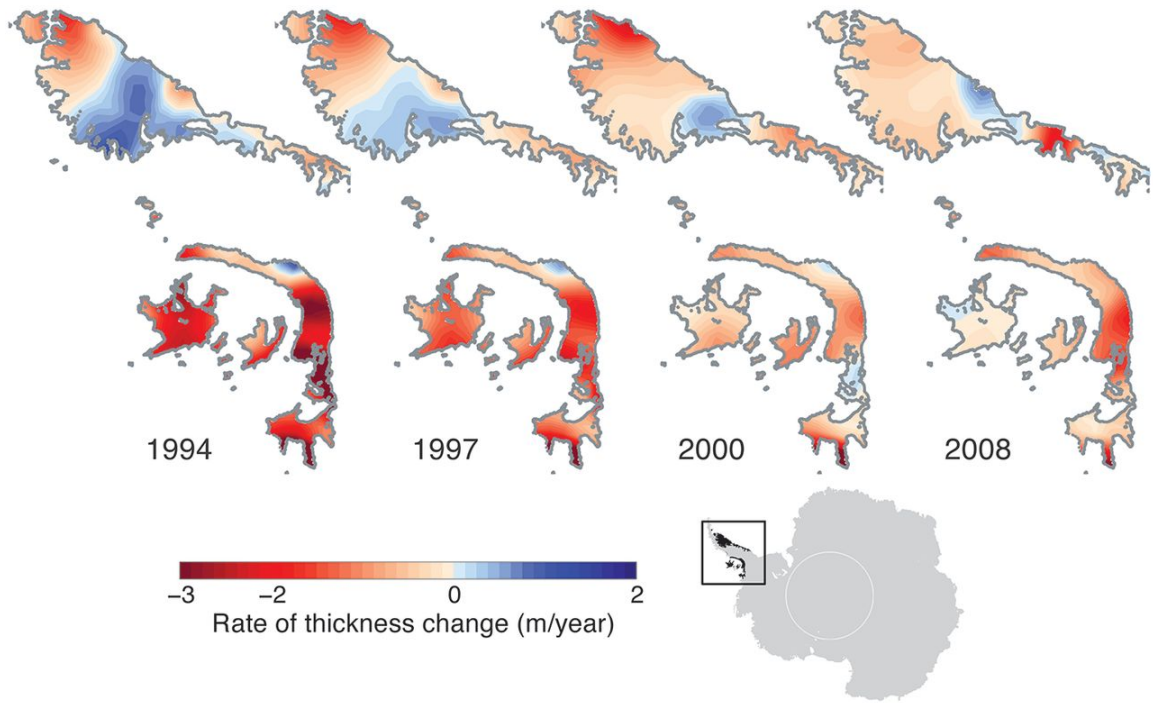


Figure 3.4: Evolution of the rate of thickness change in the Antarctic Peninsula. Instantaneous rate-of-thickness change (meters per year) for four specific times (1994, 1997, 2000, and 2008) is calculated as the derivative of the polynomial fit to the thickness-change time series. The rate increases spatially with time from north to south in the Larsen Ice Shelf (see movie⁵). The eastern (Weddell Sea) side of the Antarctic Peninsula (top) shows independent behavior from the western (Bellingshausen Sea) side (bottom).

The regional time-varying trends for the ice shelves in the three East Antarctic regions (Queen Maud, Amery, and Wilkes) are coherent (Fig. 3.3). Ice shelves in the Wilkes region are challenging for conventional radar altimeters because many of them are small, contained in narrow embayments, and have rough surfaces so that altimeter-derived height changes do not necessarily reflect thickness change accurately. Our estimate of overall thickness change for the Wilkes ice shelves is 1.4 ± 1.5 m/decade, which is not significantly different from zero. The Queen Maud region ice shelves show an overall increase in thickness of 2.0 ± 0.8 m/decade.

Like the AS ice shelves, Totten and Moscow University ice shelves in the Wilkes region buttress a large marine-based section of the East Antarctic ice sheet so that their stability is potentially important to grounded-ice loss. Although these ice shelves were previously reported as thinning [Pritchard et al. 2012] on the basis of a straight-line fit to a 5-year record from a satellite laser altimeter (ICESat, 2003–2008), our results show that those estimates are not representative of the longer-term trends (Fig. ??). Our estimate of thickness loss during 2003–2008 is similar to the ICESat-based result, but the full 18-year period shows thickness trends that are not significantly different from zero (Fig. ??).

For most ice shelves, our estimates are significantly different from previous results (Table 3.2). Several factors contribute to this. (i) The areas of ice shelves over which measurements are averaged vary between studies, affecting estimates on small ice shelves with large thickness-change signals. (ii) Because of our grid resolution, ice-shelf mask, and limited data coverage, we cannot sample near the grounding line of some ice shelves (such as Pine Island or Dotson); in such cases, our estimated changes are likely to represent a lower bound (changes could be larger). (iii) Radar altimeters are less sensitive than are laser altimeters to variations in surface mass balance owing to penetration of the radar signal into the firn layer. (iv) Short records and previous trend-extraction approaches could not capture and account for fluctuations in the underlying trend (Fig. 3.5 and ??). This is the dominant factor affecting comparisons between our results and previous studies.

The total volume of East Antarctic ice shelves increased during 1994–2003 by $148 \pm 45 \text{ km}^3/\text{year}$, followed by moderate loss ($56 \pm 37 \text{ km}^3/\text{year}$), whereas West Antarctic ice shelves exhibited persistent volume loss over the 18 years, with marked acceleration after 2003 (Fig. 3.1). Before and after 2003, this region lost volume by 144 ± 45 and $242 \pm 47 \text{ km}^3/\text{year}$, respectively, corresponding to $\sim 70\%$ increase in the average loss rate. The total circum-Antarctic ice-shelf volume loss was negligible ($25 \pm 64 \text{ km}^3/\text{year}$) during 1994–2003 and then declined rapidly by $310 \pm 74 \text{ km}^3/\text{year}$ after 2003. Overall, from 1994 to 2012 Antarctic ice-shelf volume changed on average by $-166 \pm 48 \text{ km}^3/\text{year}$, with mean acceleration of $-31 \pm 10 \text{ km}^3/\text{year}^2$ ($-51 \pm 33 \text{ km}^3/\text{year}^2$ for the period 2003–2012).

3.5 Conclusions

We have shown that Antarctic ice-shelf volume loss is accelerating. In the Amundsen Sea, some ice shelves buttressing regions of grounded ice that are prone to instability have experienced sustained rapid thinning for almost two decades. If the present climate forcing is sustained, we expect a drastic reduction in volume of the rapidly thinning ice shelves at decadal to century time scales, resulting in grounding-line retreat and potential ice-shelf collapse. Both of these processes further accelerate the loss of buttressing, with consequent increase of grounded-ice discharge and sea-level rise. On smaller scales, ice-shelf thickness variability is complex, demonstrating that results from single satellite missions with typical durations of a few years are insufficient to draw conclusions about the long-term response of ice shelves. Large changes occur over a wide range of time scales, with rapid variations of ice-shelf thickness suggesting that ice shelves can respond quickly to changes in oceanic and atmospheric conditions.

3.6 Supplementary material

Part of the supplementary material in the original manuscript is reproduced in *Chapter 2*, and thus omitted from this section to avoid repetition.

Estimating thickness and volume changes from height time series

We converted our height-change time series and rates to thickness changes assuming that (i) the ice shelf is in hydrostatic equilibrium and (ii) observed changes occur at the density of solid ice (e.g., basal melting) [Shepherd et al. 2010; Pritchard et al. 2012; Wingham et al. 2009]. The latter assumption is justified since, as discussed above, radar-altimeter measurements are relatively insensitive to changes in surface mass balance. We used an ice density of 917 kg/m^3 and ocean water density of 1028 kg/m^3 .

To map the spatial patterns of thickness changes, we fitted polynomials to the thickness-change time series for each grid cell and derived averaged rates as described above. We then smoothed and interpolated the rate-of-change spatial field using a Gaussian kernel with sigma equal to the grid-cell size. To estimate full-ice-shelf and

regional mean values we integrated the individual time series, limited to the surveyed area only and weighted by grid-cell area (i.e., ice-shelf area within each grid cell). The surveyed area is the fixed area of cells covered by the satellites' orbits for which data are available throughout 1994–2012, therefore excluding ice shelves south of 81.5°S and regions of advancing and retreating ice fronts and grounding lines. Overall, we were able to sample about 86% of the ice-shelf area covered by the ERS/Envisat orbit. Our area-average thickness-change time series are then:

$$H(t) = C \sum_k w_k h_k(t) \quad (3.1)$$

where $H(t)$ is mean time series of thickness change, $C = \rho_w (\rho_w - \rho_i)^{-1}$ is the height-to-thickness scaling factor, w are the weights for each cell k in the area-weighted average, and $h(t)$ is the observed height-change time series for each grid cell. To estimate the associated total ice-volume change for each ice shelf, we multiplied the derived changes (from the polynomial fits) on the surveyed area of each ice shelf by the full areas estimated using the 1-km-resolution ice-shelf mask, as:

$$\frac{\Delta V}{\Delta t} = AC \frac{\Delta \hat{h}}{\Delta t} \quad (3.2)$$

where A is total ice-shelf/region area.

The extreme case for temporal changes in ice-shelf area is the addition of ~ 600 km 2 to the area of the Crosson and Dotson ice shelves due to grounding-line retreat during the period of 1992–2012 [Rignot et al. 2014], corresponding roughly to 7% area increase. This area, which is excluded by our analysis, is small compared to the area that we cannot survey due to other constraints such as missing data, narrow embayments, rough topography, proximity to ice-shelf margins, and grid resolution. There are several ice shelves with more than 10% area unsurveyed (see Table 3.1). The error is also small relative to the height-to-volume conversion uncertainty due to inability to partition volume loss between basal melt, ice divergence and surface firn state. Uncertainties in the rate of thickness/volume change for the surveyed minimum ice-shelf area are significantly larger than any potential ice-shelf volume change by a retreating grounding line.

For calculating fractional change in ice-shelf volume we estimated the average

thickness of each ice shelf using the *Bedmap2* dataset [Fretwell et al. 2013]. To estimate average acceleration we calculated the average rate of change (slope of the secant line) of the derivative of the fitted polynomial.

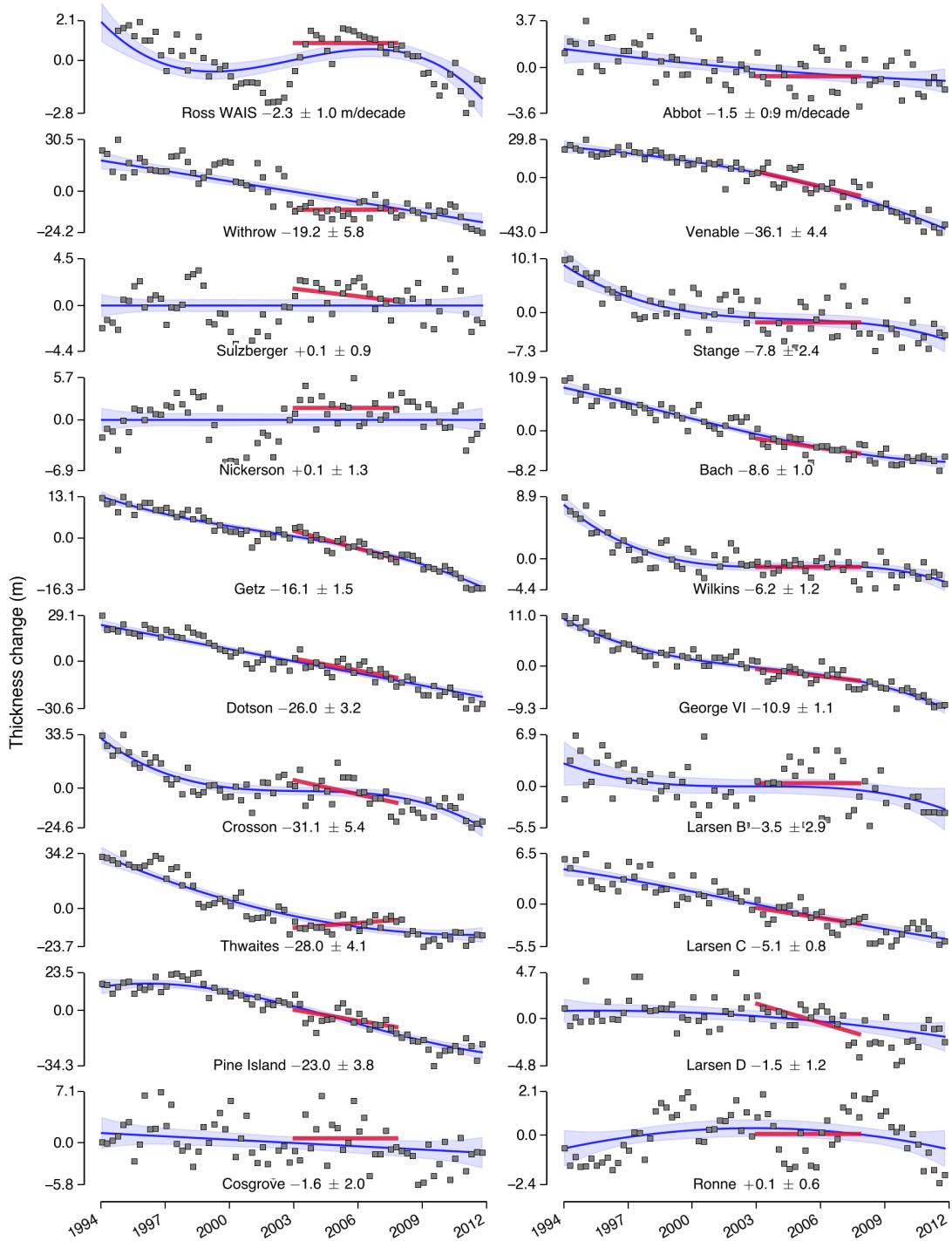


Figure 3.5: Time series of cumulative thickness change for West Antarctic ice shelves relative to series means. Thickness change was averaged over the extent of each ice shelf (sampled area only) for the period 1994–2012. Clock-wise from Ross-WAIS to Ronne. Locations are shown in Fig. 3.1. Black dots are 3-month-average thickness changes relative to series mean, blue curve is the 18-year polynomial trend with the 95% confidence band, and red line shows the regression line to the segment of our dataset that overlaps with the period used for a prior ICESat-based analysis (2003–2008) [Pritchard et al. 2012]. Average rates (in m/decade) are derived from the end points of the polynomial models.

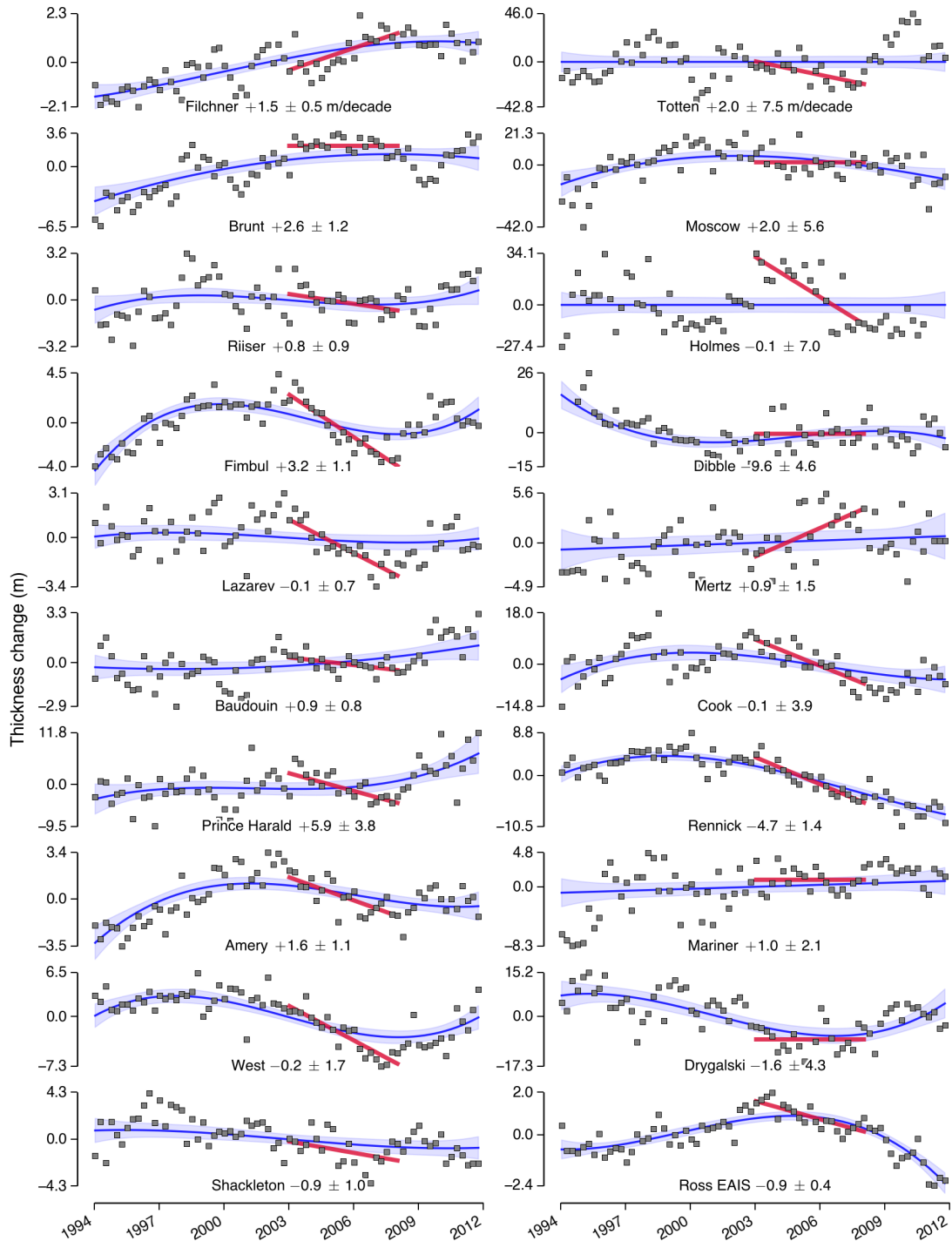


Figure 3.6: Time series of cumulative thickness change for East Antarctic ice shelves relative to series mean. Thickness change was averaged over the extent of each ice shelf (sampled area only) for the period 1994–2012. Clock-wise from Filchner to Ross-EAIS. Locations are shown in Fig. 3.1. Black dots are 3-month-average thickness changes relative to series mean, blue curve is the 18-year polynomial trend with the 95% confidence band, and red line shows the regression line to the segment of our dataset that overlaps with the period used for a prior ICESat-based analysis (2003–2008) [Pritchard et al. 2012]. Average rates (in m/decade) are derived from the end points of the polynomial models.

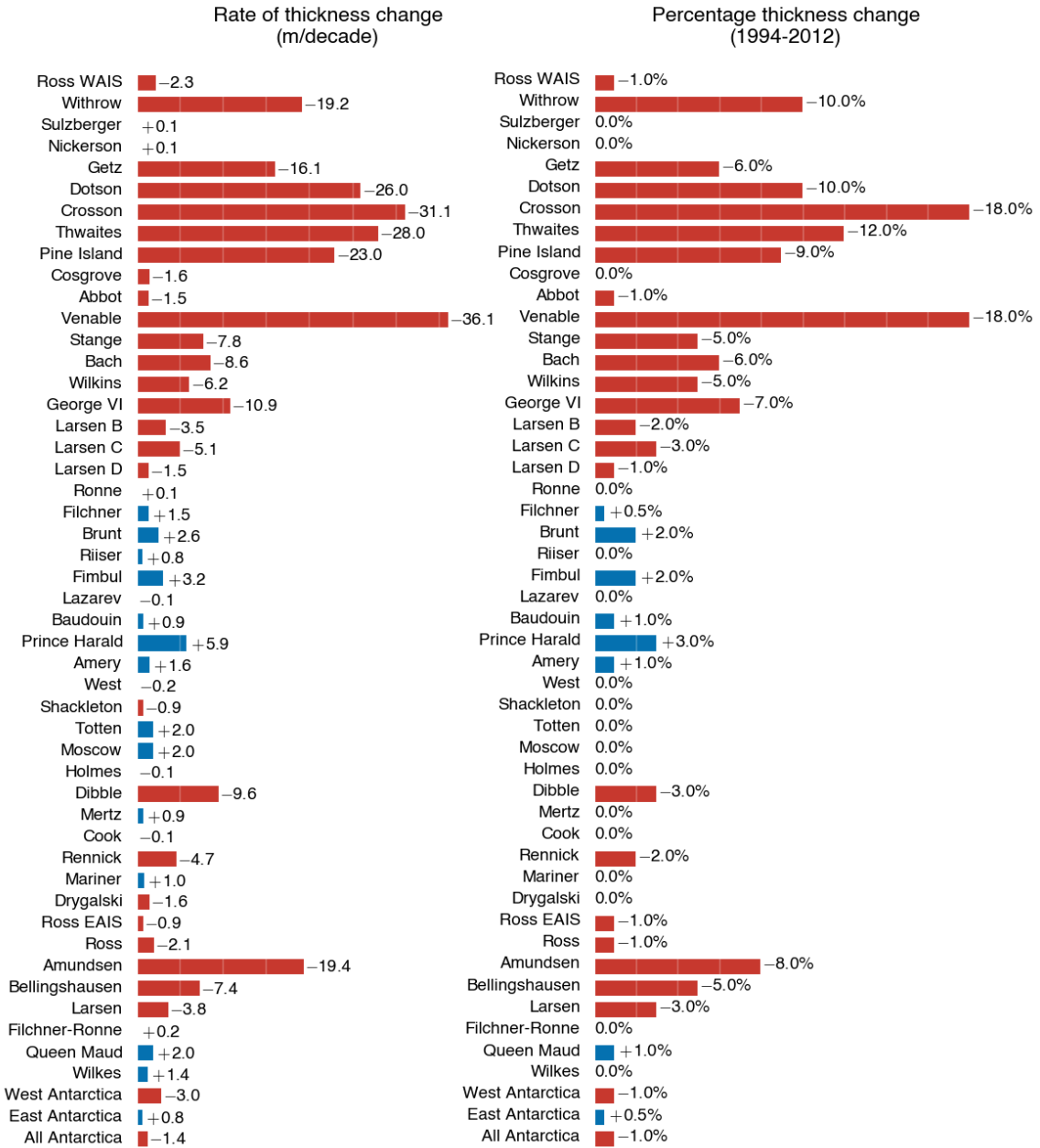


Figure 3.7: Average rate and total thickness change for each Antarctic ice shelf from 1994 to 2012. (left) Rate of thickness change (in m/decade) and (right) percentage thickness lost or gained in 18 years (values not significant at the 95% confidence level were set to 0%). Values are grouped as: West Antarctic ice shelves (top), East Antarctic ice shelves (middle) and regions (bottom). Red is thinning/loss and blue is thickening/gain. Locations are shown in Fig. 3.1.

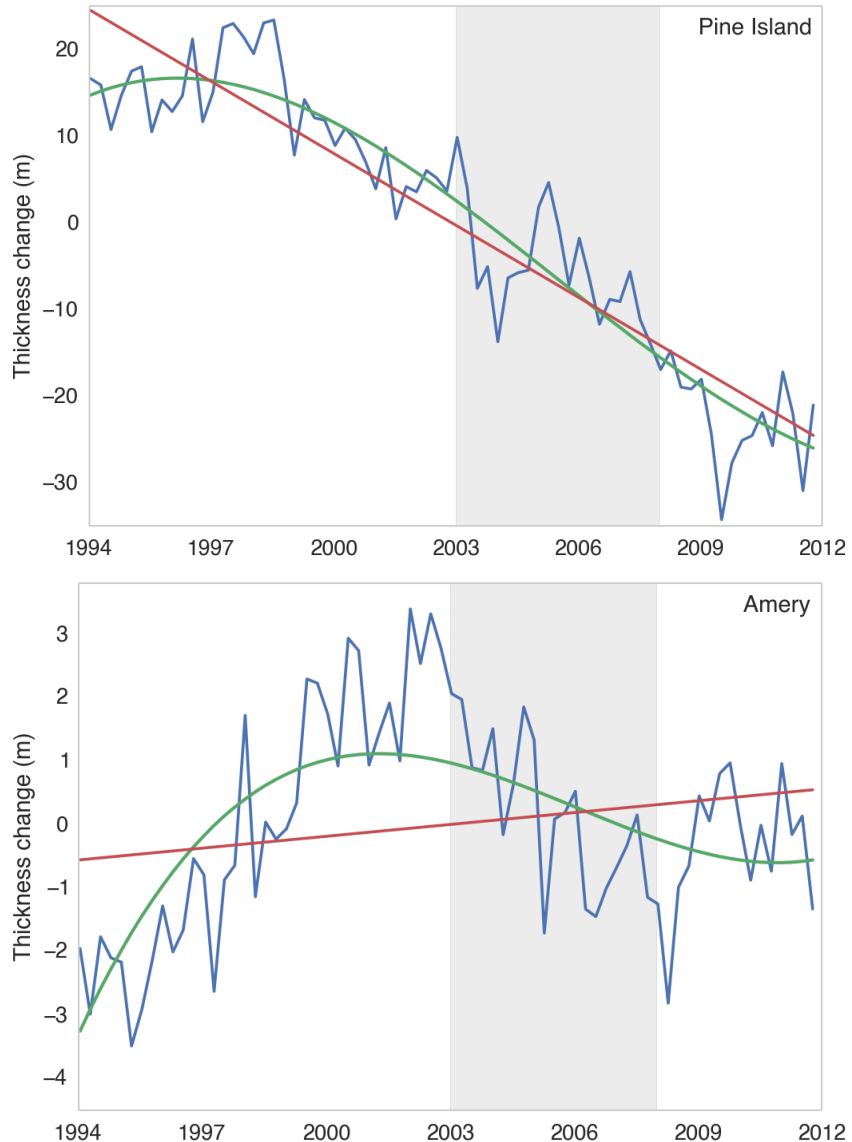


Figure 3.8: Polynomial versus line fit to 18-year-long records. Examples of discrepancies between polynomial regression (green) and straight-line fit (red) in representing long-term trends in thickness-change time series (blue). Two examples showing (top) Pine Island Ice Shelf and (bottom) Amery Ice Shelf, where the straight-line fit overestimates and underestimates, respectively, the trend. The shaded region (light gray) represents the time interval used in a previous ICESat-based study (2003–2008) [Pritchard et al. 2012].

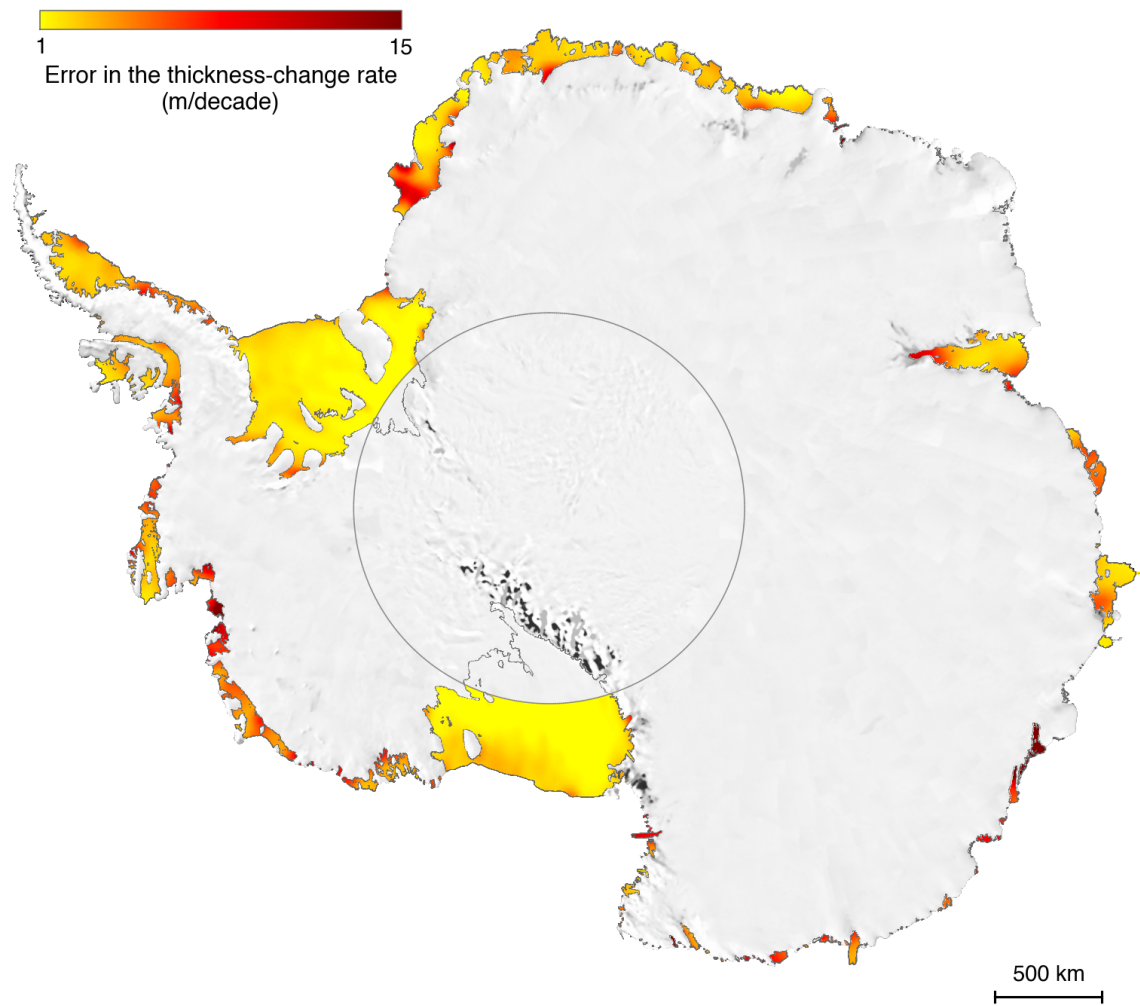


Figure 3.9: Error map for estimated rates of Antarctic ice-shelf thickness change. Map showing estimated uncertainties for individual (grid cell) decade-averaged rates of thickness change (map on Fig. 3.1). Uncertainties are two standard errors (95% confidence level) estimated using the bootstrap approach [see text; Efron and Tibshirani 1993].

Table 3.1: Average rates and total thickness change for Antarctic ice shelves from 1994 to 2012. Table summarizing estimated area, decade-averaged ice-shelf-wide and local-minimum thickness-change rates, volume-change rate and percentage-thickness change during 1994–2012, for each Antarctic ice shelf and region. Uncertainties are stated at the 95% confidence level. Total area refers to area under the satellite’s coverage (latitudinal limit of 81.5°S). Percentages have been rounded to the next integer or to ± 0.5 when below 1% (only significant values have been considered). Note: Small differences are due to values being computed independently (subject to different constraints on the regression analysis from individual datasets), and use of round-off values. All estimates are consistent within the formal errors.

Ice shelf	Area (Survey) (km ²)	Thickness rate (m/decade)	Local minimum (m/decade)	Volume rate (km ³ /year)	%–Change	
					1994–2012	
Ross WAIS	215,000 (97%)	-2.3 ± 1.0	-35.0 ± 10.0	-48 ± 22		-1
Withrow	650 (82%)	-19.2 ± 5.8	-19.2 ± 5.8	-2 ± 1		-10
Sulzberger	12,200 (78%)	0.1 ± 0.9	-6.8 ± 4.2	0 ± 1		—
Nickerson	6,600 (80%)	0.1 ± 1.3	-15.7 ± 3.0	0 ± 1		—
Getz	33,200 (85%)	-16.1 ± 1.5	-66.5 ± 9.0	-54 ± 5		-6
Dotson	5,400 (80%)	-26.0 ± 3.2	-64.5 ± 7.9	-14 ± 2		-10
Crosson	2,700 (78%)	-31.1 ± 5.4	-31.4 ± 8.6	-8 ± 2		-18
Thwaites	4,600 (75%)	-28.0 ± 4.1	-31.7 ± 4.4	-13 ± 2		-12
Pine Island	6,000 (60%)	-23.0 ± 3.8	-34.7 ± 4.7	-14 ± 2		-9
Cosgrove	3,000 (65%)	1.6 ± 2.0	-29.2 ± 8.2	0 ± 1		—
Abbot	30,100 (80%)	-1.5 ± 0.9	-19.2 ± 4.4	-4 ± 3		-1
Venable	3,100 (85%)	-36.1 ± 4.4	-64.4 ± 4.9	-11 ± 1		-18
Stange	7,700 (80%)	-7.8 ± 2.4	-15.1 ± 2.1	-6 ± 2		-5
Bach	4,600 (60%)	-8.6 ± 1.0	-12.9 ± 1.3	-4 ± 1		-6
Wilkins	13,500 (82%)	-6.2 ± 1.2	-19.9 ± 2.0	-8 ± 2		-5
George VI	23,200 (75%)	-10.9 ± 1.1	-31.3 ± 6.7	-25 ± 3		-7
Larsen B	2,500 (50%)	-3.5 ± 2.9	-5.5 ± 2.9	-1 ± 1		-2
Larsen C	46,500 (96%)	-5.1 ± 0.8	-16.6 ± 8.1	-24 ± 4		-3
Larsen D	25,000 (70%)	-1.5 ± 1.2	-22.5 ± 2.8	-4 ± 3		-1
Ronne	318,000 (98%)	0.1 ± 0.6	-10.0 ± 3.5	2 ± 19		—
Filchner	91,000 (95%)	1.5 ± 0.5	-12.7 ± 1.7	13 ± 4		0.5
Brunt	36,000 (78%)	2.6 ± 1.2	-24.5 ± 7.8	9 ± 4		2
Riiser	43,000 (90%)	0.8 ± 0.9	-3.7 ± 1.5	3 ± 4		—
Fimbul	40,500 (78%)	3.2 ± 1.1	-7.7 ± 2.5	13 ± 5		2
Lazarev	8,500 (75%)	-0.1 ± 0.7	-1.6 ± 1.5	0 ± 1		—
Baudouin	33,000 (80%)	0.9 ± 0.8	-7.0 ± 8.5	3 ± 2		1
Prince Harald	5,000 (50%)	5.9 ± 3.8	-0.3 ± 2.1	3 ± 2		3
Amery	60,000 (88%)	1.6 ± 1.1	-18.3 ± 9.2	9 ± 6		1
West	15,500 (50%)	-0.2 ± 1.7	-21.3 ± 5.7	0 ± 3		—

continues...

Table 3.1: Average rates and total thickness change for Antarctic ice shelves (continued).

Ice shelf	Area (Survey)	Thickness rate	Local minimum	Volume rate	%-Change
	(km ²)	(m/decade)	(m/decade)	(km ³ /year)	1994–2012
Shackleton	31,000 (48%)	-0.9 ± 1.0	-9.3 ± 9.2	-3 ± 3	—
Totten	6,000 (50%)	2.0 ± 7.5	2.0 ± 7.5	1 ± 5	—
Moscow	5,600 (50%)	2.0 ± 5.6	-5.7 ± 4.2	1 ± 3	—
Holmes	2,000 (40%)	-0.1 ± 7.0	-0.4 ± 7.4	0 ± 1	—
Dibble	1,500 (60%)	-9.6 ± 4.6	-9.6 ± 4.6	-2 ± 1	-3
Mertz	2,800 (55%)	0.9 ± 1.5	0.9 ± 1.5	1 ± 2	—
Cook	3,200 (35%)	-0.1 ± 3.9	-22.9 ± 4.0	0 ± 1	—
Rennick	3,200 (80%)	-4.7 ± 1.4	-17.1 ± 2.2	-2 ± 1	-2
Mariner	2,600 (55%)	1.0 ± 2.1	1.0 ± 2.1	0 ± 1	—
Drygalski	2,500 (50%)	-1.6 ± 4.3	-14.4 ± 11.2	0 ± 1	—
Ross EAIS	145,000 (98%)	-0.9 ± 0.4	-32.9 ± 8.3	-13 ± 6	-1
Ross	360,000 (98%)	-2.1 ± 0.5	-35.0 ± 10.0	-75 ± 19	-1
Amundsen	56,000 (80%)	-19.4 ± 1.9	-66.5 ± 9.0	-109 ± 11	-8
Bellingshausen	86,000 (78%)	-7.4 ± 0.9	-64.4 ± 4.9	-64 ± 8	-5
Larsen	75,000 (80%)	-3.8 ± 1.1	-22.5 ± 2.8	-28 ± 8	-3
Filchner-Ronne	410,000 (97%)	0.2 ± 0.5	-12.7 ± 1.7	5 ± 22	—
Queen Maud	224,000 (78%)	2.0 ± 0.8	-24.5 ± 7.8	44 ± 18	1
Wilkes	87,000 (55%)	1.4 ± 1.5	-22.9 ± 4.0	12 ± 13	—
West Antarctica	650,000 (90%)	-3.0 ± 0.5	-66.5 ± 9.0	-191 ± 32	-1
East Antarctica	600,000 (82%)	0.8 ± 0.5	-32.9 ± 8.3	45 ± 29	0.5
All Antarctica	1,250,000 (86%)	-1.4 ± 0.4	-66.5 ± 9.0	-166 ± 48	-1

Table 3.2: Comparison of our estimated thickness-change rates (m/year) with previous studies. Table comparing our estimates [Paolo et al. 2015b] with Pritchard et al. [2012], Shepherd et al. [2010] and Shepherd et al. [2004a]. Missing values correspond to either different ice-shelf boundary definition or ice shelf not reported. When required, we converted all the estimates to thickness change (in m/year) and rounded values to facilitate the comparison. Values not significantly different from zero were set to 0.0. See text for explanation on potential differences.

Ice shelf	Paolo <i>et al.</i> ¹	Pritchard <i>et al.</i> ²	Shepherd <i>et al.</i> ³	Shepherd <i>et al.</i> ⁴
	18 years (1994–2012)	5 years (2003–2008)	9 years (1992–2001)	14 years (1994–2008)
	0.0	0.3	—	—
Sulzberger	0.0	0.0	—	—
Nickerson	0.0	0.0	—	—
Getz	-1.6	-1.7	-1.6	-1.8
Dotson	-2.6	-5.2	-3.3	—
Crosson	-3.1	-3.3	-4.5	—
Thwaites	-2.8	-5.6	-5.5	-8.3
Pine Island	-2.3	-4.9	-3.9	-6.0
Cosgrove	-0.2	-0.6	-0.7	—
Abbot	-0.2	0.4	-0.6	—
Venable	-3.6	-2.5	—	-16.0
Strange	-0.8	-0.6	—	—
Bach	-0.9	-0.7	—	8.8
Wilkins	-0.6	-0.6	—	—
George VI	-1.1	-0.9	—	-0.8
Larsen B	-0.4	-2.3	—	—
Larsen C	-0.5	-0.9	—	-0.8
Larsen D	-0.2	0.4	—	—
Brunt	0.3	0.3	—	0.6
Riiser	0.1	0.3	—	—
Fimbul	0.3	0.0	—	-0.5
Lazarev	0.0	-0.6	—	—
Amery	0.2	-0.6	—	0.9
West	0.0	-1.1	—	—
Shackleton	0.0	-1.1	—	—
Totten	0.0	-3.8	—	—
Moscow	0.0	-1.0	—	5.4
Holmes	0.0	-2.8	—	—
Dibble	-1.0	-2.2	—	—
Mertz	0.0	0.3	—	—

continues...

Table 3.2: Comparison of our estimated thickness-change rates (continued).

Ice shelf	Paolo <i>et al.</i> ¹	Pritchard <i>et al.</i> ²	Shepherd <i>et al.</i> ³	Shepherd <i>et al.</i> ⁴
	18 years (1994–2012)	5 years (2003–2008)	9 years (1992–2001)	14 years (1994–2008)
Cook	0.0	1.1	—	—
Rennick	-0.5	-1.2	—	—
Mariner	0.0	0.2	—	—
Drygalski	0.0	-0.3	—	—
Ross	-0.2	0.1	—	0.2
Filchner-Ronne	0.0	0.2	—	0.5

¹Paolo *et al.* [2015b], Radar altimetry.²Pritchard *et al.* [2012], Laser altimetry.³Shepherd *et al.* [2010], Radar altimetry.⁴Shepherd *et al.* [2004a], Radar altimetry.

Acknowledgements

This work was funded by NASA [awards NNX12AN50H 002 (93735A), NNX10A-G19G, and NNX13AP60G]. This is ESR contribution 154. We thank J. Zwally's Ice Altimetry group at the NASA Goddard Space Flight Center for distributing their RA data sets for all satellite radar altimeter missions (<http://icesat4.gsfc.nasa.gov>). We thank C. Davis and D. Wingham for RA-processing advice. We thank A. Shepherd and anonymous reviewers for their comments on the manuscript.

Chapter 3, in full, is a reprint of the material as it appears in *Science* 2015. Paolo, Fernando S.; Fricker, Helen A.; Padman, Laurie. The dissertation author was the primary investigator and author of this paper.

References

- Borstad, C. P., E. Rignot, J. Mouginot, and M. P. Schodlok (2013). “Creep deformation and buttressing capacity of damaged ice shelves: theory and application to Larsen C ice shelf”. *The Cryosphere* 7, 1931–1947.
- Cook, A. J. and D. G. Vaughan (2010). “Overview of areal changes of the ice shelves on the Antarctic Peninsula over the past 50 years”. *The Cryosphere* 2002, 77–98.
- Davis, C. H. and A. C. Ferguson (2004). “Elevation change of the antarctic ice sheet, 1995-2000, from ERS-2 satellite radar altimetry”. *IEEE Transactions on Geoscience and Remote Sensing* 42, 2437–2445.
- Depoorter, M. A., J. L. Bamber, J. A. Griggs, J. T. M. Lenaerts, S. R. M. Ligtenberg, M. R. van den Broeke, and G. Moholdt (2013). “Calving fluxes and basal melt rates of Antarctic ice shelves”. *Nature* 502, 89–92.
- Dutrieux, P., J. D. Rydt, A. Jenkins, P. R. Holland, H. K. Ha, S. H. Lee, E. J. Steig, Q. Ding, E. P. Abrahamsen, and M. Schröder (2014). “Strong Sensitivity of Pine Island Ice-Shelf Melting to Climatic Variability”. *Science* 343, 174–178.
- Efron, B. and R. J. Tibshirani (1993). *An introduction to the Bootstrap*. Chapman and Hall/CRC.
- Favier, L., G. Durand, S. L. Cornford, G. H. Gudmundsson, O. Gagliardini, F. Gillet-Chaulet, T. Zwinger, A. J. Payne, and A. M. Le Brocq (2014). “Retreat of Pine Island Glacier controlled by marine ice-sheet instability”. *Nature Climate Change* 4, 117–121.
- Fretwell, P., H. D. Pritchard, D. G. Vaughan, J. L. Bamber, N. E. Barrand, R. Bell, C. Bianchi, R. G. Bingham, D. D. Blankenship, G. Casassa, G. Catania, D. Callens, H. Conway, A. J. Cook, H. F. J. Corr, D. Damaske, V. Damm, F. Ferraccioli, R. Forsberg, S. Fujita, Y. Gim, P. Gogineni, J. A. Griggs, R. C. A. Hindmarsh, P. Holmlund, J. W. Holt, R. W. Jacobel, A. Jenkins, W. Jokat, T. Jordan, E. C. King, J. Kohler, W. Krabill, M. Riger-Kusk, K. A. Langley, G. Leitchenkov, C. Leuschen, B. P. Luyendyk, K. Matsuoka, J. Mouginot, F. O. Nitsche, Y. Nogi, O. A. Nost, S. V. Popov, E. Rignot, D. M. Rippin, A. Rivera, J. Roberts, N. Ross, M. J. Siegert, A. M. Smith, D. Steinhage, M. Studinger, B. Sun, B. K. Tinto, B. C. Welch, D. Wilson, D. A. Young, C. Xiangbin, and A. Zirizzotti (2013). “Bedmap2: improved ice bed, surface and thickness datasets for Antarctica”. *The Cryosphere* 7, 375–393.
- Fricker, H. A. and L. Padman (2012). “Thirty years of elevation change on Antarctic Peninsula ice shelves from multimission satellite radar altimetry”. *Journal of Geophysical Research: Oceans* 117, C02026.

- Goldberg, D., D. M. Holland, and C. Schoof (2009). "Grounding line movement and ice shelf buttressing in marine ice sheets". *Journal of Geophysical Research: Earth Surface* 114, F04026.
- Holland, P. R., A. Brisbourne, H. F. J. Corr, D. McGrath, K. Purdon, J. Paden, H. A. Fricker, F. S. Paolo, and A. H. Fleming (2015). "Oceanic and atmospheric forcing of Larsen C Ice-Shelf thinning". *The Cryosphere* 9, 1005–1024.
- Jacobs, S. S., A. Jenkins, C. F. Giulivi, and P. Dutrieux (2011). "Stronger ocean circulation and increased melting under Pine Island Glacier ice shelf". *Nature Geoscience* 4, 1–5.
- Joughin, I. and R. B. Alley (2011). "Stability of the West Antarctic ice sheet in a warming world". *Nature Geoscience* 4, 506–513.
- Joughin, I., B. E. Smith, and B. Medley (2014). "Marine Ice Sheet Collapse Potentially Under Way for the Thwaites Glacier Basin, West Antarctica". *Science* 344, 735–738.
- Paolo, F. S., H. A. Fricker, and L. Padman (2015b). "Volume loss from Antarctic ice shelves is accelerating". *Science* 348, 327–331.
- Pritchard, H. D., S. R. M. Ligtenberg, H. A. Fricker, D. G. Vaughan, M. R. van den Broeke, and L. Padman (2012). "Antarctic ice-sheet loss driven by basal melting of ice shelves". *Nature* 484, 502–505.
- Rignot, E., S. Jacobs, J. Mouginot, and B. Scheuchl (2013). "Ice-Shelf Melting Around Antarctica". *Science* 341, 266–270.
- Rignot, E., J. Mouginot, M. Morlighem, H. Seroussi, and B. Scheuchl (2014). "Widespread, rapid grounding line retreat of Pine Island, Thwaites, Smith, and Kohler glaciers, West Antarctica, from 1992 to 2011". *Geophysical Research Letters* 41, 3502–3509.
- Scambos, T. A., J. A. Bohlander, C. A. Shuman, and P. Skvarca (2004). "Glacier acceleration and thinning after ice shelf collapse in the Larsen B embayment, Antarctica". *Geophysical Research Letters* 31, 2001–2004.
- Scambos, T., C. Hulbe, and M. Fahnestock (2003). "Climate-Induced Ice Shelf Disintegration in the Antarctic Peninsula". In: *Antarctic Peninsula Climate Variability: Historical and Paleoenvironmental Perspectives*. Ed. by E. Domack, A. Levente, A. Burnet, R. Bindschadler, P. Convey, and t. Kirby. American Geophysical Union, 79–92.
- Schoof, C. (2007). "Ice sheet grounding line dynamics: Steady states, stability, and hysteresis". *Journal of Geophysical Research: Earth Surface* 112, 1–19.

- Shepherd, A., D. Wingham, T. Payne, and P. Skvarca (2004a). "Correction to: Larsen Ice Shelf has progressively thinned". *Science* 303, 1612–1612.
- Shepherd, A., D. Wingham, D. Wallis, K. Giles, S. Laxon, and A. V. Sundal (2010). "Recent loss of floating ice and the consequent sea level contribution". *Geophysical Research Letters* 37, 1–5.
- Shepherd, A., E. R. Ivins, G. A. V.R. Barletta, M. J. Bentley, S. Bettadpur, K. H. Briggs, D. H. Bromwich, R. Forsberg, N. Galin, M. Horwath, S. Jacobs, I. Joughin, M. A. King, J. T. M. Lenaerts, J. Li, S. R. M. Ligtenberg, A. Luckman, S. B. Luthcke, M. McMillan, R. Meister, G. Milne, J. Mouginot, A. Muir, J. P. Nicolas, J. Paden, A. J. Payne, H. Pritchard, E. Rignot, H. Rott, L. S. Sørensen, T. A. Scambos, B. Scheuchl, E. J. O. Schrama, B. Smith, A. V. Sundal, J. H. van Angelen, W. J. van de Berg, M. R. van den Broeke, D. G. Vaughan, I. Velicogna, J. Wahr, P. L. Whitehouse, D. J. Wingham, D. Yi, D. Young, and H. J. Zwally (2012). "A Reconciled Estimate of Ice-Sheet Mass Balance". *Science* 338, 1183–1189.
- Sutterley, T. C., I. Velicogna, E. Rignot, J. Mouginot, T. Flament, M. R. van den Broeke, J. M. van Wessem, and C. H. Reijmer (2014). "Mass loss of the Amundsen Sea Embayment of West Antarctica from four independent techniques". *Geophysical Research Letters* 41, 2014GL061940.
- Thoma, M., A. Jenkins, D. Holland, and S. Jacobs (2008). "Modelling Circumpolar Deep Water intrusions on the Amundsen Sea continental shelf, Antarctica". *Geophysical Research Letters* 35, L18602.
- Tibshirani, R. (1996). "Regression shrinkage and selection via the lasso". *Journal of the Royal Statistical Society, Series B* 58, 267–288.
- Weertman, J. (1974). "Stability of the junction of an ice sheet and an ice shelf". *Journal of Glaciology* 13, 3–11.
- Wingham, D. J., D. W. Wallis, and A. Shepherd (2009). "Spatial and temporal evolution of Pine Island Glacier thinning, 1995–2006". *Geophysical Research Letters* 36, 5–9.
- Zwally, H. J., M. B. Giovinetto, J. Li, H. G. Cornejo, and M. A. Beckley (2005). "Mass changes of the Greenland and Antarctica ice sheets and shelves and contributions to sea level rise: 1992–2002". *Journal of Glaciology* 51, 509–509.

Chapter 4

Variability analysis of ice-shelf height

This chapter, in full, is currently being prepared for publication:

*Interannual variability in the Amundsen Sea ice-shelf height change linked to ENSO,
F.S. Paolo, H.A. Fricker, L. Padman*

4.1 Abstract

Atmospheric and sea-ice conditions around Antarctica, particularly in the Amundsen and Bellingshausen seas, respond to climate dynamics in the tropical Pacific Ocean on interannual time scales including the El Niño-Southern Oscillation (ENSO). It has been hypothesized that the mass balance of the Antarctic Ice Sheet, including its floating ice shelves, also responds to this climate signal; however, this has not yet been unambiguously demonstrated. We apply multivariate singular spectrum analysis (MSSA) to our 18-year (1994–2012) time series of ice-shelf height in the Amundsen Sea (AS) region. This advanced spectral method distinguishes between regular deterministic behavior (cycles) at sub-decadal time scale and irregular behavior (noise) at shorter time scales. Although the long-term trends of AS ice-shelf height changes are much larger than the range of interannual variability, the short-term rate of change ($\partial h/\partial t$) can vary about the trend by more than 50%. The mode of interannual variability in the AS ice-shelf height is strongly correlated with the low-frequency mode of ENSO (periodicity of ~ 4.5 years) as represented by the Southern Oscillation Index. The ice-shelf height in

the AS is expected to respond to changes in precipitation and to inflows of warm subsurface Circumpolar Deep Water (CDW) into the ocean cavities under the ice shelves, that then alter basal melt rates. Preliminary analyses indicate that ENSO-linked variability of ice-shelf height may be explained by changes in precipitation; however, further studies are needed to identify changes due to basal melting associated with CDW intrusions.

4.2 Introduction

Predicting sea-level rise requires understanding the Antarctic and Greenland ice sheets' response to projected future climate states. Current accelerated losses of ice-sheet mass suggest that this contribution will exceed that of thermal expansion in the future [Shepherd et al. 2012; Harig and Simons 2015; Velicogna 2009; Sutterley et al. 2014]. Extensive portions of the Antarctic Ice Sheet (such as the West Antarctic sector and the Totten basin in East Antarctica, which combined have a potential for ~6 m of sea-level rise [Fretwell et al. 2013]) are grounded below sea-level (*marine ice sheet*) and are, therefore, particularly susceptible to changes in oceanic conditions [e.g., Joungin et al. 2012].

It is through the ice shelves, the floating margins of the ice sheet, that variations in oceanic and atmospheric states impact the Antarctic land ice. Most of the ice-sheet mass is lost at the margins by submarine melting and calving of the ice shelves. At the same time, drag forces originating from the ice-shelf/bedrock interaction opposing the grounded-ice flow (*buttressing effect*¹) make the ice shelves a key component for the stabilization of ice-sheet loss. Climate-induced perturbations to the ice shelves potentially reduce this resistive stress and, therefore, have significant implications for the fate of the ice sheet. Large uncertainties remain, however, in our understanding of how the ice shelves, and therefore the ice sheet, respond to large-scale climate variability.

Over the past two decades, significant changes in Antarctic ice shelves have been observed [Cook and Vaughan 2010; Shepherd et al. 2010; Scambos et al. 2004; Scambos et al. 2009; Rignot et al. 2004; Rignot et al. 2014; Pritchard et al. 2012; Paolo et al. 2015b]. The largest changes have occurred in the Amundsen and Bellingshausen seas,

¹*Buttressing effect* is defined as the change in the state of stress at the grounding line after the ice shelf has been removed.

and these have been attributed predominantly to wind-driven fluxes of warm Circumpolar Deep Water (CDW) inducing increased melt. These changes were associated with substantial mass imbalances in the grounded ice sheet observed during the same period [Shepherd et al. 2012; Chen et al. 2009; Velicogna 2009; Harig and Simons 2015]. In addition to long-term ice-shelf changes (15+ years), Paolo et al. [2015b]; Paolo et al. [2015a] showed that there is considerable short-term fluctuation in Antarctic ice-shelf volume at interannual-to-decadal time scales. Dutrieux et al. [2014] presented evidence for the sensitivity of basal melting of Pine Island Ice Shelf to interannual-scale atmospheric/oceanic variability, linking observed changes in near-ice-shelf oceanic conditions to a La Niña event. Model results [Steig et al. 2012] and indirect measurements (oxygen isotopic composition of precipitation from ice cores as a proxy for temperature [Steig et al. 2013]) have suggested a link between changes in wind-driven CDW inflows onto the continental shelf and variability of sea-surface temperature in the tropical Pacific (El Niño/La Niña). Other studies [e.g., Yuan 2004; Turner 2004] have also discussed linkages between El Niño-Southern Oscillation (ENSO) and, for example, changes in sea-surface pressure over the Amundsen and Bellingshausen seas (Fig. 4.1) causing a reduction in sea-ice concentration over that region.

The ENSO phenomenon, a large-scale internal climate mode characterized by large changes of tropical sea-surface temperatures, is the strongest natural climate fluctuation at interannual time scales (Sup. Fig. 4.10). This sea-surface temperature anomaly is a response to changes in surface-air pressure (the Southern Oscillation) between the tropical eastern and the western Pacific Ocean waters, which recurs on average every four years [Latif and Keenlyside 2009; Philander 1989]. Although some evidence of ENSO can be found in the Antarctic meteorological and ice-core records, a direct link between this tropical Pacific phenomenon and variations in the mass balance of the Antarctic Ice Sheet has yet to be demonstrated. Studies discussing this teleconnection present circumstantial evidence either based on a few sparse measurements with short time duration off the ice sheet/shelf [e.g., Dutrieux et al. 2014], or an indirect assessment based on model experiments, ice cores and/or reanalysis products [e.g., Steig et al. 2013]. Here we present results from multivariate spectral analysis of fluctuations in ice-shelf height for the Amundsen Sea (AS), as a means of using direct observations to test the hypothesis that there is a connection between ENSO and

Antarctic ice-shelf variability. We seek to quantify the extent to which tropical Pacific conditions may influence interannual changes in ice-shelf and ice-sheet mass balances.

4.3 Methods

The 18-year record of changes in ice-shelf height presented by Paolo et al. [2015a] and [2015b] is the most comprehensive data set for studies of ice-shelf sensitivity to oceanic and atmospheric conditions available to date. Although more highly resolved in time (~ 3 months) and space (~ 30 km) in comparison with previous available data sets [e.g., Shepherd et al. 2010; Pritchard et al. 2012], these time series still

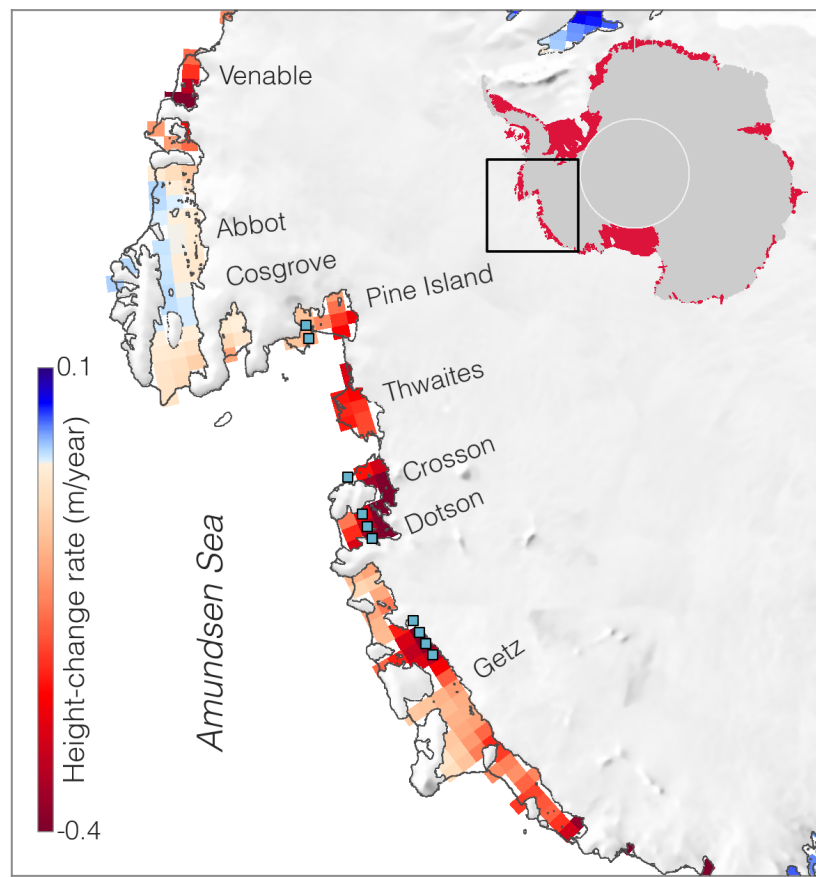


Figure 4.1: Amundsen Sea ice shelves in Antarctica. Map showing rate of change in surface-height (m/year) for the AS ice shelves. There are 140 30 km \times 30 km grid cells in the region, and the color represents the average $\partial h / \partial t$ for the period 1994–2012. Average height-change time series for each grid cell are analyzed in this chapter, and the ten blue squares show the locations of the time series used for stacking (see text).

contain high noise levels, inherent to (a) the complex satellite radar altimeter measurement over ice surfaces [Paolo et al. 2015a; Davis and Moore 1993; Arthern et al. 2001; Wingham and Wallis 2010; Remy et al. 2012] and (b) the wide range of time scales on which the ice shelves respond [Paolo et al. 2015a; Padman et al. 2003; Holland et al. 2015; Dutrieux et al. 2014]. In addition, the 18-year quarterly (3-month resolution) data is shorter and less well resolved in time compared with traditional climate records that typically span several decades at weekly/monthly resolution (see, for example, the NOAA Optimum Interpolation Sea Surface Temperature V2²). Hence, the challenge lies in analyzing a set of short, noisy and potentially non-stationary³ time series.

We used the orthogonal-component decomposition of a time series known as Singular Spectrum Analysis [SSA; Vautard et al. 1992; Golyandina and Zhitljavskiy 2013; Elsner and Tsonis 1996]. This technique has been applied extensively to the study of climate variability and other geophysical fields [Ghil et al. 2002, and references therein]; it was designed to handle the problem of describing cyclical behavior on short and noisy records, for which standard methods derived from Fourier analysis do not work well [Vautard and Ghil 1989; Ghil and Vautard 1991; Vautard et al. 1992; Groth and Ghil 2011]. The method is based on augmenting the original data set by constructing lagged versions of the original series (referred to as *embedding*) with time delays of $1, \dots, M - 1$, where M is the length of the observation window (time scale under consideration). The augmented (or *embedded*) data set can then be analyzed by standard Principal Component Analysis [PCA; Jolliffe 2002].

In the multivariate case, where there is more than one time series, the same principle applies, with the addition that the covariance matrix (\mathbf{C}) of the augmented data set (by embedding each series) includes cross-correlations, such that we can extract principal oscillations in time and space (common spectral properties). In particular, multivariate (or multichannel) SSA (MSSA) can separate distinct spectral components in a multivariate data set of limited length and in the presence of relatively high noise levels. The spectral decomposition by MSSA (Eq. 4.5) yields a set of eigenvectors (\mathbf{e}_k , mode of oscillation) and a set of corresponding eigenvalues (λ_k , variance in the direc-

²<http://www.esrl.noaa.gov/psd/data/gridded/data.noaa.oisst.v2.html>

³Stationarity means that statistical properties such as mean, variance and auto-correlation do not change with time.

tion of the eigenvector). Provided that pairs of eigenvectors correspond to the same period (*oscillatory pairs*), they are the data-adaptive equivalent of sine-and-cosine pairs in Fourier analysis: that is, they represent a temporal oscillation (phase-and-amplitude modulated in the case of MSSA; see Sup. material). The MSSA package used in this study also provides effective statistical tests to discriminate between potential oscillations from “white” noise (independent and identically distributed)—Monte-Carlo MSSA [Allen and Smith 1996]. Ghil et al. [2002] provide an overview and a comprehensive set of references to both the theory and applications of SSA and MSSA⁴.

We used the Southern Oscillation Index (SOI) as a measure of ENSO, which is a standardized time series of observed sea-level pressure differences between Tahiti and Darwin, Australia. The SOI is one measure of the large-scale fluctuations in air pressure occurring between the western and eastern tropical Pacific during El Niño and La Niña episodes. The negative phase of the SOI represents below-normal air pressure at Tahiti and above-normal air pressure at Darwin. Prolonged periods of negative (positive) SOI values coincide with abnormally warm (cold) ocean waters across the eastern tropical Pacific typical of El Niño (La Niña) episodes (NOAA/NCDC⁵).

To analyze the data we first removed the trend of each ice-shelf time series separately, by using the time-domain Hodrick-Prescott filter [Hodrick and Prescott 1997] with the parameter value $\lambda = 1600$, as recommended by these authors for detrending quarterly data (Fig. 4.2 and Sup. Eq. 4.6). A trend-independent analysis is particularly important in the case of AS ice shelves where a strong negative trend dominates the height-change signal (Fig. 4.2). Another reason for de-trending is that the trend varies (in some cases considerably) with location [Paolo et al. 2015b; Pritchard et al. 2012; Shepherd et al. 2010]. Next, we normalized each residual time series by its standard deviation so that the variance equals one. We do this to avoid giving the variables (time series) with higher variances a greater weight in the analysis. Variables with the highest sample variances will tend to be emphasized in the first few principal components (our goal is to analyze common oscillatory behavior among the time series regardless of their ranges). Since both the ice-shelf time series and the SOI were standardized

⁴Free software for implementation of SSA and MSSA, among other spectral techniques, is provided by the SSA-MTM Toolkit at <http://www.atmos.ucla.edu/tcd/ssa>

⁵<https://www.ncdc.noaa.gov/teleconnections/enso/indicators/soi>

(centered and normalized) we focused the analysis on relative values. To further reduce the noise content in the initial data set, a common procedure is to pre-filter the original time series with standard PCA and retain the few leading components that explain larger portions of the total variance. MSSA is then applied to these leading principal components. We reduced the original set of 140 time series (see locations in Fig. 4.1) to a set of 10 principal components (PCs) that explain over 47% of the total variance of the de-trended data set (Sup. Fig. 4.11).

The time scales under investigation are those characteristic of large-scale climate fluctuations at the interannual band. Therefore, our observation window (M) spans ~ 9 years (sub-decadal). Since no spectral estimation should rely on any particular method, we extend our analysis with the (spectral-domain) multi-taper [Thomson 1982] and maximum-entropy [Childers 1978] methods (MTM and MEM, respectively) to estimate spectral content of reconstructed series (see below).

4.4 Results and discussion

In addition to the observed strong thinning trend in the AS ice shelves, there are relatively large fluctuations at both the interannual and annual time scales (Fig. 4.2). Since an empirical ‘backscatter correction’ has been applied to the height time series being analyzed [Paolo et al. 2015a], we expect this correction to have removed much of the apparent seasonal signal that would have been observed in the uncorrected records (as an effect of fluctuations in backscatter due to changes in ice-shelf-surface properties). The same empirical correction also removes interannual signal that correlates with backscatter variations due to changes in surface state (rather than thickness). While we can explain (most of) the annual cycle by evoking the seasonal response of some ice-shelf-related mechanisms, such as surface accumulation, firn compaction, basal melting and changes in backscatter, we cannot yet directly attribute the interannual response to known interannual-scale climate processes. There are two reasons for this. First, there has been limited information, i.e., long-term and continuous observational records, on the ice-shelf state to allow inference of interannual variability [Paolo et al. 2015b]. Second, the link between known interannual-scale climate processes and variations in thickness of the grounded ice sheet and floating ice is not quite clear from observations

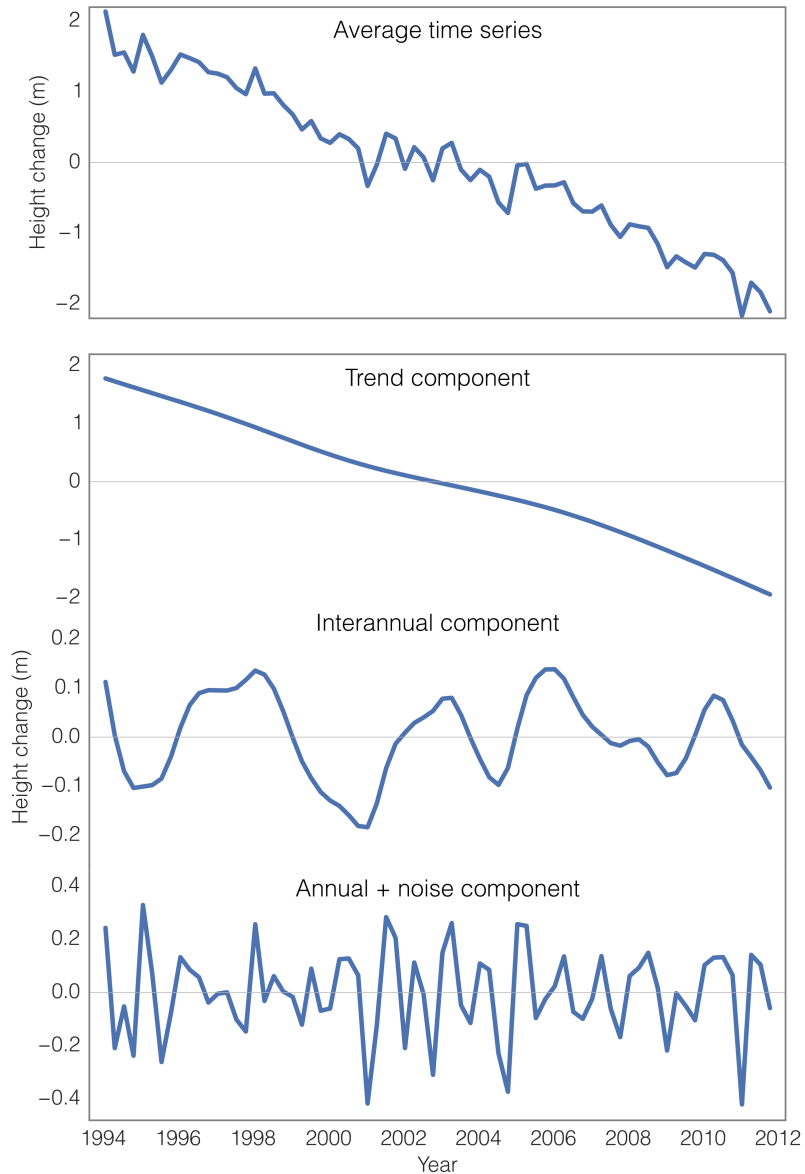


Figure 4.2: Decomposition of AS ice-shelf height time series. (top panel) Average of all (140) time series of ice-shelf height changes in the Amundsen region. (bottom panel) Decomposition of the average time series into its trend, interannual, and annual-plus-noise components. The Hodrick and Prescott [1997] filter was used to separate each component (see Supplementary material).

[e.g., Dutrieux et al. 2014; Steig et al. 2013; Turner 2004].

When decomposing the standardized records of ice-shelf height into modes of oscillation (eigenvectors or EOFs) and looking at the variance explained by each eigenvector (Fig. 4.3), there is a clear separation between the first four EOFs (eigenvalues of rank 1–4) and the remaining eigenvectors. Arranging the same modes into power

(equivalent to variance explained) versus the frequency that they represent, two facts become evident: 1) there is statistically-significant (90% level) energy content in two particular bands—around 1 year and around 2.5–5 years; 2) MSSA is able to group in pairs EOFs for these particular frequency bands (eigenvalues of nearly-equal power representing the same frequency), indicative of an oscillatory behavior (Fig. 4.3). We note that none of the other EOFs (represented by their respective eigenvalues) are able to rise above the noise background. The three most energetic pairs of EOFs can then be used to decompose (or reconstruct) the original time series into two interannual components (RC 1–2 and RC 3–4), and one annual component (RC 5–6) (Fig. 4.4).

Similarly, using all the significant components together (EOFs 1–2, 3–4 and 5–6) we reconstructed the ice-shelf height record (RC 1–6; Fig. 4.5), such that (a) we filtered out from the original time series all uncorrelated signals and measurement noise, and (b) we were able to estimate the power spectrum of the (significant) interannual and annual components (Fig. 4.5). Although we are particularly interested in identifying interannual fluctuations, we opted to retain the annual component in the reconstruction. This serves as a control for the MSSA procedure; since we know that ice shelves respond at the seasonal scale (e.g., precipitation-driven surface mass balance), we expect that this signal should be clearly detectable in our analysis. The MEM power spectrum of the reconstructed time series (Fig. 4.5) shows three peaks at frequencies ~ 0.2 , ~ 0.3 and ~ 1.0 cycles/year (~ 5 , 3 and 1 years, respectively). The MTM spectrum (Fig. 4.5) shows significant (95%) spectral peaks at frequencies 0.20–0.23 and 1.0 cycles/year (~ 5 –4.3 and 1 years, respectively). While the MEM approach is optimal when applied with low-resolution (low-order autoregression) to denoised series (reconstructed components), producing a smooth curve where only well-defined peaks “survive” [Penland et al. 1991], the MTM spectrum offers a good trade-off between high spectral resolution and statistical confidence levels that are independent of the spectral power [Mann and Lees 1996; Percival and Walden 1993]. In addition, the MTM implemented here [Mann and Lees 1996] makes use of a “robust” estimate of the background noise, and performs a harmonic test.

To obtain the ENSO signal we reproduced the analysis performed by Ghil et al. [2002] (univariate SSA) on the SOI time series, using an updated version of the

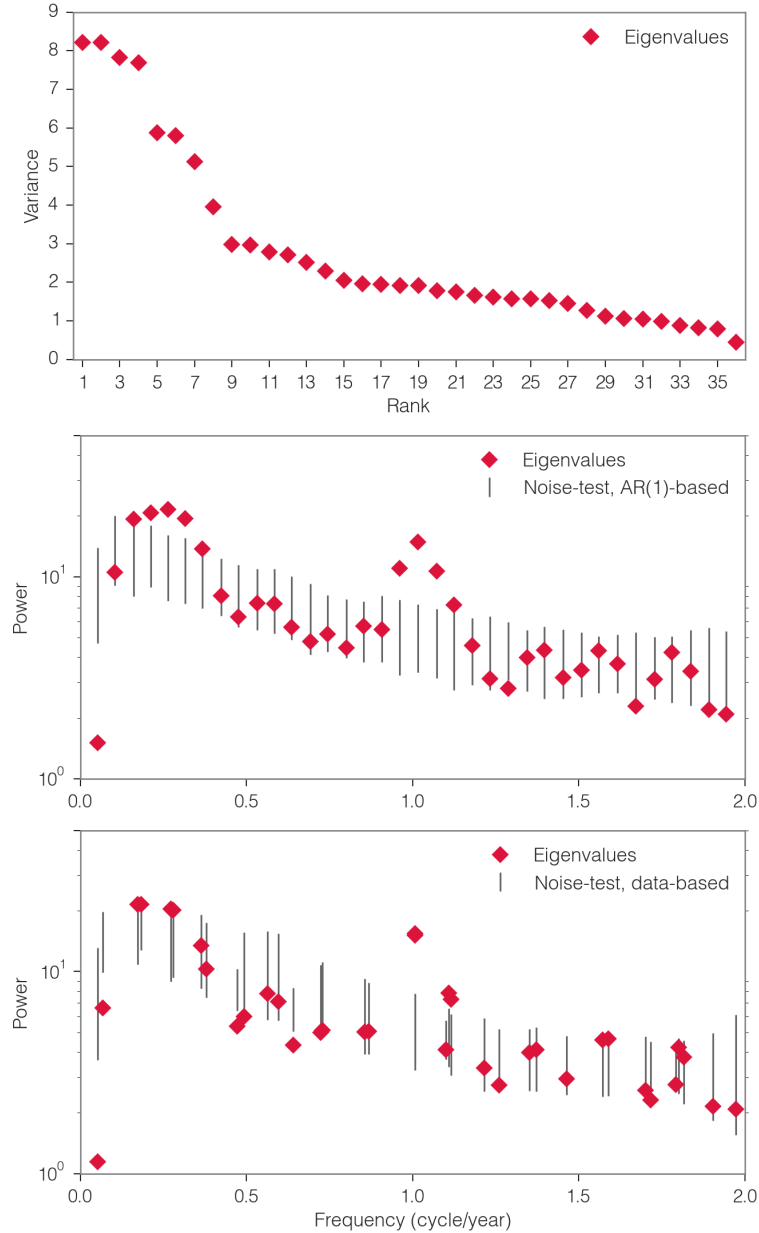


Figure 4.3: Singular spectrum of AS ice-shelf height time series. The ‘diamonds’ represent the eigenvalues of the auto-correlation matrix $\mathbf{C}^{(M)}$ (Eq. 4.5). The vertical bars are 90% confidence intervals for 100 red-noise realizations with the same variance and decorrelation time as the original series. The values that stand out above the error bars are statistically significant. (top) Variance vs. eigenvalue rank. (middle) Eigenvalue vs. dominant frequency of corresponding eigenvector, using an AR(1) model as basis (the frequencies are well defined). (bottom) Eigenvalue vs. dominant frequency using the data as basis, where the frequency of each eigenvector is obtained by least-square fitting the corresponding EOF to a sine function (the frequencies are approximated). Note that eigenvalues 1–4 (the interannual components) appear well separated from the remaining 5–36 (the seasonal-plus-noise components). The spectra were produce with Monte-Carlo MSSA using window width (number of lags) $M = 36$ (~ 9 years).

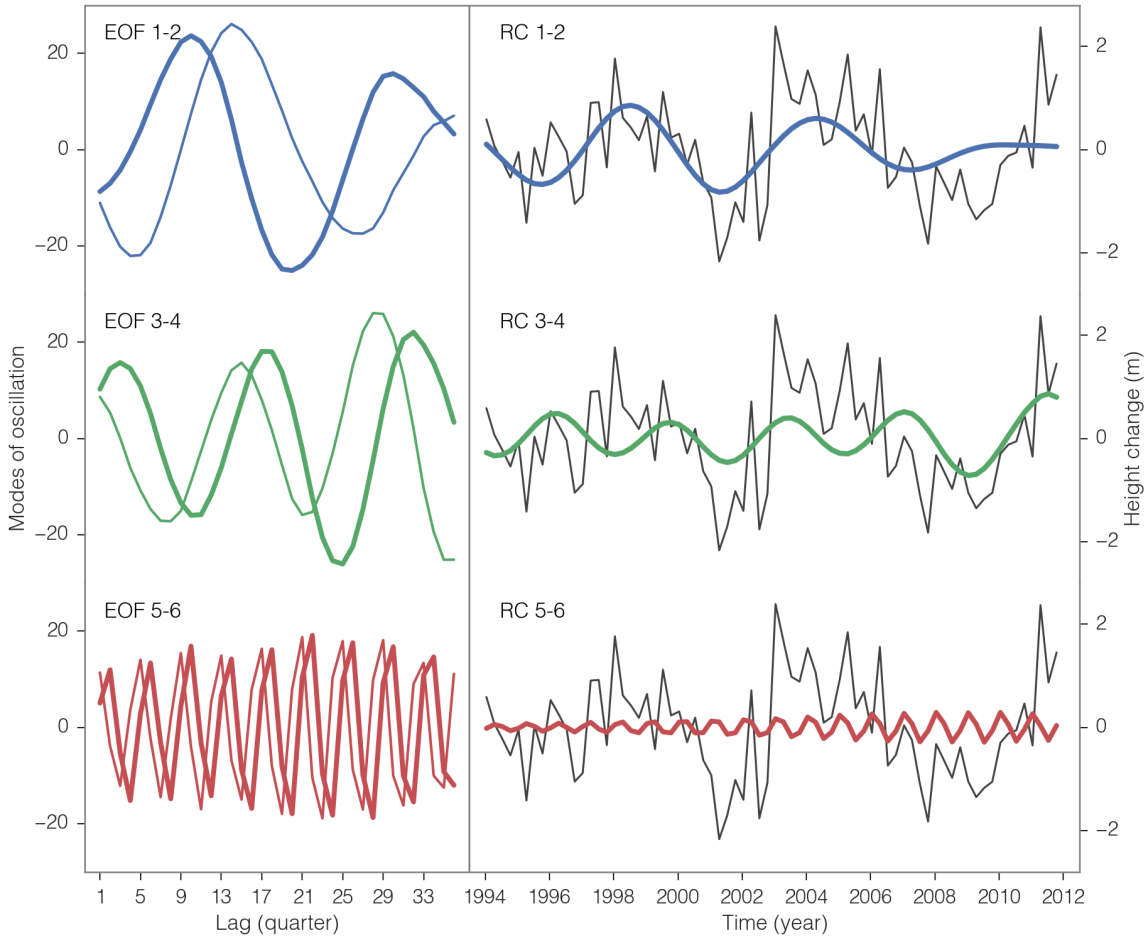


Figure 4.4: Modes of oscillation in the ice-shelf height RA time series. (left) The MSSA empirical orthogonal functions paired as EOFs 1–2, 3–4 (interannual components) and 5–6 (annual component). Note the phase quadrature ($\sim\pi/2$ shift, i.e., offset by approximately one-quarter cycle) between pairs, indicative of a temporal oscillation. (right) The reconstruction of each pair of modes in the time domain. This is equivalent to filtering the original time series (in gray) with respect to particular frequencies (periodicities). The reconstruction was done for each of the 140 individual grid-cell time series from the original RA-derived data set (this is one time series as example; see Fig. 4.12).

index (from NOAA⁶) spanning the period 1951 to 2015. The SSA spectrum of the SOI series (Fig. 4.6) clearly identifies two significant pairs of eigenvectors, which have been attributed to the low-frequency (4–5 years) and quasi-biennial (~ 2.5 years) modes of ENSO [e.g., Ghil et al. 2002; Philander 1989] (Fig. 4.6). We then reconstructed the SOI series using these two modes (RC 1–4; Fig. 4.7), and applied the MEM and MTM in the same way as done for the ice-shelf time-series reconstruction (Fig. 4.8).

The spectra of both reconstructions (ice-shelf height and SOI) show most of the

⁶<https://www.ncdc.noaa.gov/teleconnections/enso/indicators/soi/>

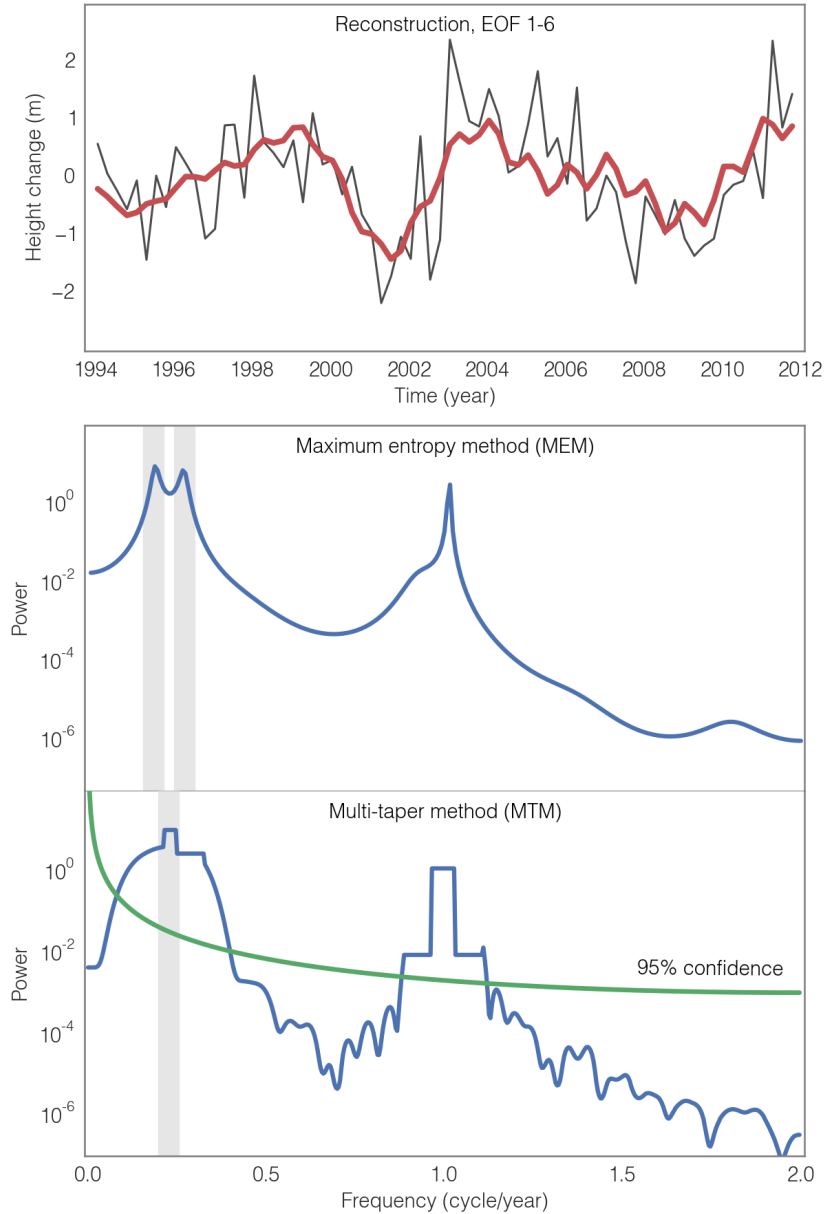


Figure 4.5: Power spectrum of the reconstructed RA-derived ice-shelf height time series. (top) Reconstruction of ice-shelf surface height series using the three leading pairs of EOFs (1–2, 3–4 and 5–6). (bottom) Power spectra by the maximum entropy and multi-taper methods (MEM and MTM, respectively). While the MEM spectrum is smooth (order 20) and focuses on the dominant frequencies, the MTM offers higher spectral resolution and confidence level of the estimated spectrum. The regular-shaped peaks represent the frequencies that passed a harmonic test, included in the MTM package. The gray stripes demarcate the dominant frequencies at the interannual band detected by each spectrum (0.18 and 0.26 cycle/year for MEM, 0.22 cycle/year for MTM).

energy in the frequency band of $\sim 0.2\text{--}0.4$ (2.5–5) cycle/year (years). While the MEM spectrum appears to identify two distinct oscillations (double peak; Fig. 4.5) the MTM

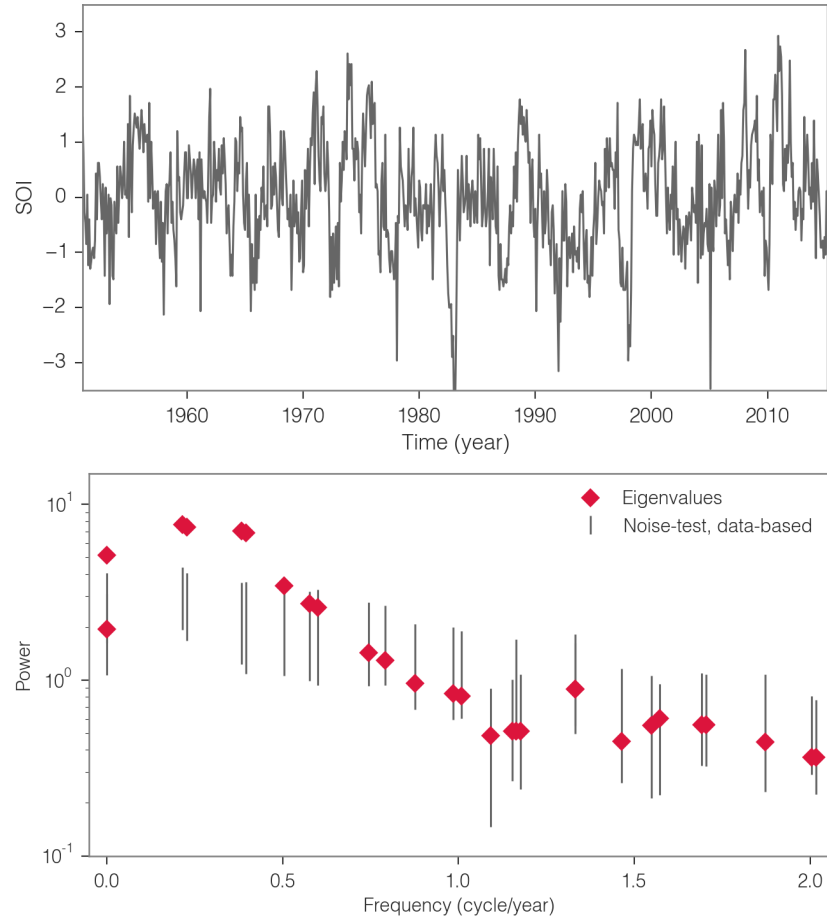


Figure 4.6: Singular spectrum of the SOI time series. (top) SOI time series from NOAA (1951–2015). (bottom) Singular spectrum analysis of the SOI time series ($M = 76$, ~ 6.3 years). The vertical bars are 90% confidence intervals for 100 red-noise realizations.

is not able to distinguish between these two components in the ice-shelf signal. Instead, the MTM shows significant (95%) spectral energy in one dominant frequency (~ 4.5 years).

We reconstructed all 140 individual grid-cell time series (the RA data) using the two leading pairs of EOFs (RC 1–4; Sup. Fig. 4.12). Since there is substantial coherent information within the RCs, we selected 10 of these reconstructions that display high amplitude and coherence (locations are shown in Fig. 4.1 and time series 40–49 are shown in Sup. Fig. 4.12) and stacked them in order to smooth out incoherent signals and enhance common fluctuations. To facilitate visual comparison, we multiplied the SOI RC 1–2 (the low-frequency mode of ENSO) by -1 (i.e., flipped the series upside-down), such that positive anomalies now represent El Niño events. We also centered

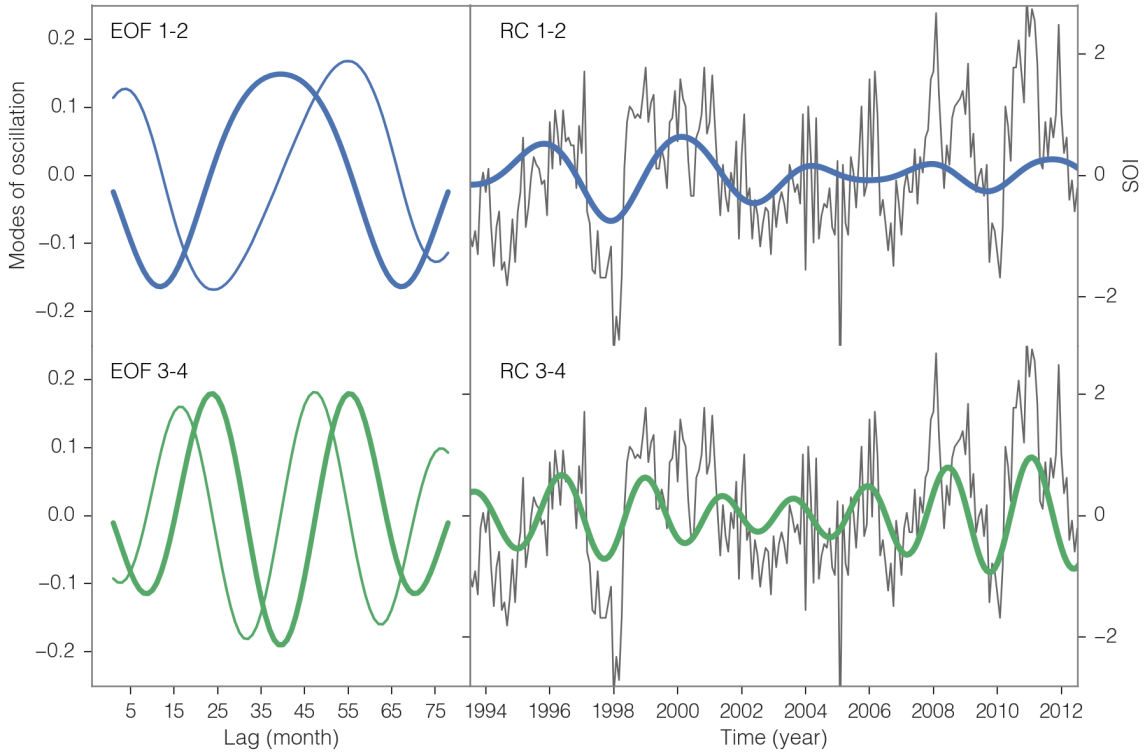


Figure 4.7: Modes of oscillation in the SOI time series. (left) Leading pairs of EOFs (1–2 and 3–4). (right) Reconstructions of the SOI series using the respective EOFs, corresponding to the low-frequency (blue) and quasi-biennial (green) modes of ENSO. In the background is the original SOI series.

and normalized both the ice-shelf height and SOI reconstructions.

The result reveals a strong correlation between the interannual signal for these 10 stacked ice-shelf-height reconstructions and the low-frequency mode of ENSO (the SOI reconstruction; Fig. 4.9). This implies that in the AS time-series decomposition by MSSA the two leading pairs of EOFs (eigenvectors 1–2 and 3–4) are, in fact, describing one dominant mode of variability (RC 1–4), an oscillation in the same frequency band as the \sim 4.5-year-mode of ENSO. The two reconstructions (ice-shelf height and SOI) show phase coherence and remarkable agreement in their amplitude modulation (peak-to-peak amplitude difference in the standardized series).

The apparent shift between the two time series is 2–6 months, with the height record lagging the (inverse) SOI. The positive correlation between the reconstructed ice-shelf height and inverse of the SOI reconstruction implies that there is a direct relationship between El Niño events and height increase in the AS ice shelves. The expected lag is complicated by the multiple processes and complex pathways by which

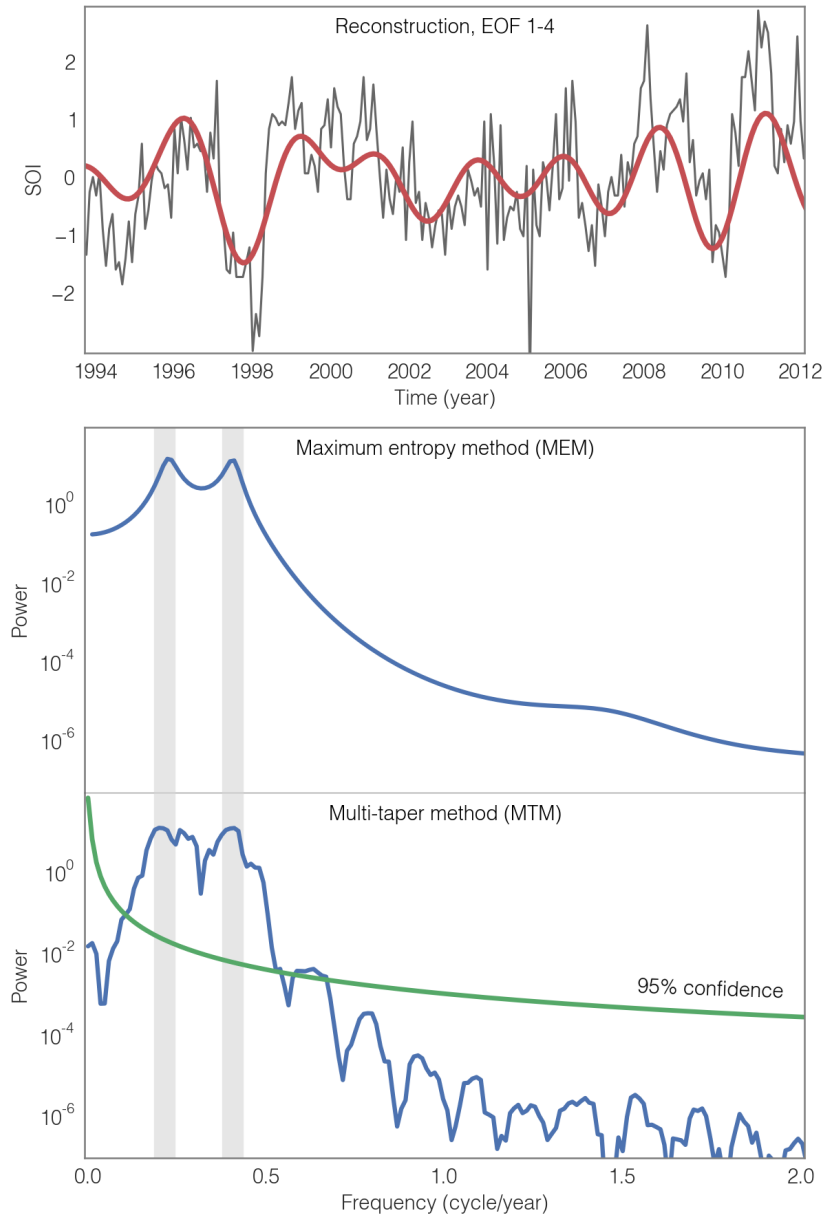


Figure 4.8: Power spectrum of the reconstructed SOI time series. (top) Reconstruction of SOI series using the two leading pairs of EOFs (1–2 and 3–4). (bottom) Power spectra by the maximum entropy and multi-taper methods (MEM and MTM, respectively). The gray stripes demarcate the dominant frequencies at the interannual band detected by each spectrum, which in this case are the same (0.21–0.22 and 0.40–0.41 cycle/year, or ~ 4.5 and ~ 2.5 years, respectively).

the atmospheric changes in the Amundsen Sea influence the ice-shelf thickness. There is, also, some uncertainty in the exact lag, given that the ice-shelf time series have lower resolution (quarterly) relative to the monthly values of SOI, and that the distribution of height measurements within each 3-month interval is heterogeneous [Paolo et al.

2015a].

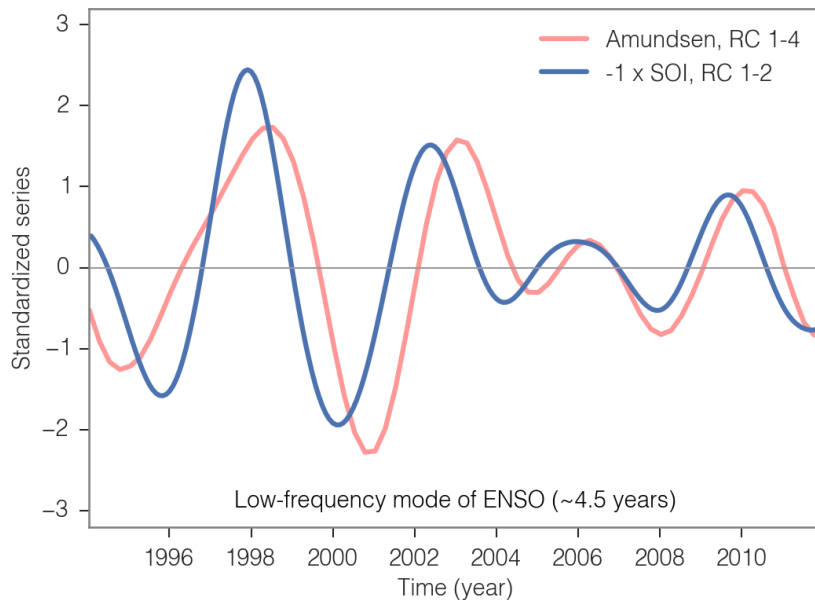


Figure 4.9: Dominant mode of interannual variability. Reconstruction of the dominant mode of interannual variability for the AS ice-shelf height and the SOI. Both series show the same dominant frequency of 0.20–0.23 cycle/year (periodicity of ~4.5 years), which corresponds to the low-frequency mode of ENSO.

Future analyses of these time series will consider the different mechanisms by which atmospheric variability, including the strong ENSO signal, can affect ice-shelf thickness and height. Here, we consider just one mechanism, the changing surface mass flux from snowfall.

The majority of precipitation in Antarctica comes from synoptic-scale⁷ storms (cyclones), which are most intense in winter. These cyclones form in mid-latitude ocean basins and, as they mature and intensify, they move southeast, picking up moisture from the surrounding seas. The influence of these cyclones is substantial along the Antarctic coast, particularly in West Antarctica where relatively low ice-sheet elevations permit easier transit of storms [Riffenburgh 2007]. As they move inland where temperatures are colder, the moisture freezes leading to heavy snowfalls. Cyclonic activity fluctuates interannually in association with climatic teleconnections such as ENSO, particularly in the Pacific sector of West Antarctica (see Sup. Fig. 4.10). Cyclonic activity tends to in-

⁷Synoptic scale, or cyclonic scale, is the horizontal scale typical of mid-latitude atmospheric depressions (e.g., extra-tropical cyclones); spatial scale on the order of 1000 km.

crease on the western side of the Antarctic Peninsula during El Niño events [Riffenburgh 2007]. Consistent with these dynamics, Kwok and Comiso [2002] found that surface temperatures over the eastern Bellingshausen Sea were positively correlated with the SOI, that is, temperatures were colder than normal during El Niño events. Cullather et al. (1996) showed that nearly 40% of the moisture flux into Antarctica occurred along the West Antarctic coast, where the precipitation variability correlated well with ENSO—with more moisture convergence during El Niño events. A strong positive correlation between ENSO and precipitation in the Amundsen Sea region was also found by Genthon and Cosme [2003]. The strongest correlations associated with the ENSO signal, however, appear to occur with the sea-ice extent anomaly in the Amundsen and Bellingshausen seas, where El Niño events generate a corresponding signal (decrease) in the ice extent 6 months later [Yuan and Martinson 2000; Turner 2004].

The correlation between the inverse of SOI and RA-derived ice-shelf height is broadly consistent with this view of changing moisture transport for differing ENSO states. Ice-shelf heights are highest following the peak of an El Niño event (warmer ocean surface in the tropical Pacific) during which we expect higher-than-average precipitation over the ice shelves and coastal regions of the grounded ice sheet. More work is required, however, to determine whether the measured interannual changes in ice-shelf height are consistent with the estimated change in surface mass balance between El Niño events and neutral or La Niña conditions. Furthermore, there is strong circumstantial evidence that some of the interannual variability in ice-shelf height is due to changing basal-melt rate as inflows of CDW under the AS ice shelves change, possibly due in part to variations in thermocline⁸ height [Dutrieux et al. 2014]. The CDW inflow and thermocline depth are both dependent on changes in the wind field, and so are expected to be correlated with the atmospheric changes influencing ice-shelf surface-mass balance.

Although the ENSO signal is clearly identified in our analysis, we emphasize that, over 18 years, the long-term trend actually overwhelms the interannual fluctuation in the AS ice-shelf height change signal by 1–2 orders of magnitude. On short periods of

⁸The thermocline is the transition layer between the mixed layer at the surface and the deep water layer. The definitions of these layers are based on temperature. The mixed layer is near the surface where the temperature is approximately that of surface water.

one to a few years, however, the rate of change of ice-shelf height ($\partial h/\partial t$) can vary about the trend by more than 50%, implying that height trends based on short satellite records and limited-duration field campaigns might also be in error by this amount. We note that the amplitude of the interannual variation, while explaining a larger portion of the total variance, is comparable to that of the seasonal-plus-noise fluctuation.

4.5 Conclusions

We have presented a signal-detection procedure that (a) optimizes the fundamental signal-to-noise ratio problem through the combination of multivariate singular spectrum analysis, principal component analysis, maximum entropy and multi-taper methods; and (b) tests assumptions regarding the detectability of signals immersed in background noise, which is of fundamental importance in analyzing short and noisy records. We have shown that there is significant variability in ice-shelf height in the AS sector, particularly at the interannual scale. This interannual response is strongly correlated with the low-frequency mode of El Niño-Southern Oscillation. Due to the convoluted nature of different modes of variability and lack of observations, an ENSO signature in Antarctica has been suggested but not unequivocally demonstrated so far. Thus, our results are the first direct observational evidence of a teleconnection between climate dynamics in the tropical Pacific Ocean and the mass balance of Antarctic ice shelves and, through the buttressing effect, the Antarctic Ice Sheet. These findings may ultimately allow us to understand the processes driving ice-shelf changes sufficiently to improve our models for predicting future ice loss.

4.6 Supplementary material

Singular Spectrum Analysis

SSA is essentially an application of the Karhunen-Loève spectral decomposition theorem in the time domain [Ghil et al. 2002, , and references therein]. The particular strength of SSA is that the basis functions in terms of which the data are decomposed, are determined from the time series itself (unlike the predefined orthonormal sine and

cosine bases as in the Fourier analysis [Blackman and Tukey 1958]). The basic assumption is that the information contained in a *continuous* variable and its first-to- $(M - 1)$ th derivatives can be approximated by a *discrete* time series and lagged copies of itself, by $1, \dots, M - 1$ time steps [Elsner and Tsonis 1996, chap. 4]. The multivariate version of SSA (MSSA) is an advanced data-adaptive method to analyze oscillatory spatio-temporal modes in multivariate time series. Thus, given a multivariate (or multichannel) time series:

$$\mathbf{x}(t) = \{x_l(t)\} \quad (4.1)$$

where $l = 1, \dots, L$ are the channels of length $t = 1, \dots, N$; one can represent the M -dimensional time-delayed embedding of each channel as:

$$\mathbf{X}_l(t) = \{x_l(t), x_l(t + 1), \dots, x_l(t + M - 1)\} \quad (4.2)$$

which gives the full augmented trajectory matrix:

$$\mathbf{X} = (\mathbf{X}_1 \ \mathbf{X}_2 \ \cdots \ \mathbf{X}_L) \quad (4.3)$$

from which information on the underlaying dynamics of the system is then extracted by dimensionality reduction to principal components.

The MSSA methodology combines two useful features: (i) it determines the data set's directions of dominant variability—with the help of principal component analysis; and (ii) it extracts major (shared) spectral components with the help of data-adaptive filters—*temporal* empirical orthogonal functions. MSSA first estimates all pairs of auto- and cross-correlation functions up to a predefined time lag M . With this information, a covariance matrix is constructed as:

$$\mathbf{C} = \frac{1}{N} \mathbf{X}^T \mathbf{X} \quad (4.4)$$

which is then decomposed into its eigenvalues and eigenvectors:

$$\Lambda = \mathbf{E}^T \mathbf{C} \mathbf{E} \quad (4.5)$$

where \mathbf{E} contains the eigenvectors \mathbf{e}_k (one per column) representing an orthonormal basis for the original phase space of the system (also referred to as EOFs), while Λ is

diagonal and contains the eigenvalues λ_k capturing the variance along each eigenvector. The subset of leading eigenvalues and corresponding eigenvectors usually describe larger portions of the variance in the system.

Projecting the data \mathbf{X} onto the eigenvectors \mathbf{E} gives principal components (modes). Reconstructing the time series \mathbf{x} with respect to each eigenvector \mathbf{e}_k gives reconstructed components (RCs), which is equivalent to a filtered time series. However, since MSSA looks for common spectral components contained in all time series, it gives a significant advantage over univariate smoothing algorithms (including single-channel SSA). MSSA is analogous to space-time PCA (ST-PCA), or the extended empirical orthogonal function analysis (EEOF) (though in typical EEOF applications, only a small number of lags are used).

In our analysis we used a maximum lag of $M = 36$ quarters. Thus our covariance matrix has a size of $N \times N$, with $N = LM = 360$, where $L = 10$ is the number of channels. These are the 10 leading principal components retained after pre-filtering with PCA the original data set of 140 time series. That is, PCA was performed twice: to pre-filter the original data set and internally by MSSA. It should be noted that we also tested different parameters for window size (M), number of components in the pre-PCA filtering, autorregression order for MEM estimation, and so on.

Maximum-Entropy Method

MEM is a *parametric* spectral estimation method [Childers 1978]. Under the assumption that a time series is generated by an autoregressive AR(n) process, the power spectrum is estimated by determining the most random (i.e., with the fewest assumptions) process with the same auto-correlation coefficients as the time series. In other words, the method looks for an autoregressive process that mimics the original time series. This is the notion of *maximal entropy* as defined in terms of information theory.

The MEM is efficient for detecting frequency lines in stationary time series. However, if the time series is non-stationary, misleading results can occur with little chance of being detected other than by cross-checking with supplementary techniques (hence the additional spectral methods used). The behaviour of the spectral estimate depends

on the appropriate choice of the order n of the auto-regression model. The number of spectral peaks will increase with the order n . The trade-off is, therefore, between high spectral resolution (high order) and few spurious peaks (low order). The MEM works well when applied with low n to denoised time series (e.g., SSA reconstructions) [Penland et al. 1991]. In our analysis we used low-order $n = 20$.

Multi-Taper Method

MTM is a *nonparametric* spectral estimation method, in that it does not prescribe an *a priori* (e.g., autoregressive) model for the process generating the time series under analysis [Thomson 1982; Percival and Walden 1993]. MTM attempts to reduce the variance of spectral estimates by using a small set of orthogonal tapers rather than the unique spectral window (data taper) used by standard Fourier transform methods (i.e., Blackman-Tukey). These tapers are constructed to minimize the spectral leakage due to the finite length of the time series. A set of independent estimates of the power spectrum is computed from the data pre-multiplied by each orthogonal taper. These estimates are then weight-averaged to reduce variance. The optimal tapers, or *eigentapers*, belong to a family of functions known as discrete prolate spheroidal sequences [see Percival and Walden 1993].

In practice, there is a trade-off between spectral resolution and variance in the spectral estimate. The choice of the band width $2pf_n$ versus number of tapers K represents the resolution-variance trade-off problem. Since only the first few tapers provide usefully small-spectral leakage, a number of tapers less than $2p - 1$ should be used ($p = 1$ and $K = 1$ is equivalent to the single-tapered discrete Fourier transform). In our analysis we used $p = 2$ and $K = 2-3$.

Hodrick-Prescott Filter

The HP-filter is a time-domain time-series decomposition technique widely used in the field of macroeconomics/business cycle theory [Hodrick and Prescott 1997]. The filter attempts to remove the cyclical component from the raw data by providing a smoothed-representation that is more sensitive to long-term than short-term fluctuations. Besides the practicality of operating in the time domain, the HP-filter offers the

advantage of being exceptionally simple; which is convenient for fast computations on large data sets. Assuming that a time series can be represented as $x_t = T_t + C_t$, where T is the trend component and C is the cyclical component, the filter can be described in terms of a minimization problem:

$$\min_T \left\{ \sum_{t=1}^m (x_t - T_t)^2 + \lambda \sum_{t=2}^{m-1} [(T_{t+1} - T_t) - (T_t - T_{t-1})]^2 \right\} \quad (4.6)$$

where m is the number of samples and λ is the smoothing parameter. The minimization occurs over all T_1, \dots, T_m . The first sum minimizes the difference between the time series and its trend component (which is its cyclical component). The second sum minimizes the second-order difference of the trend component (which is analogous to minimization of the second derivative of the trend).

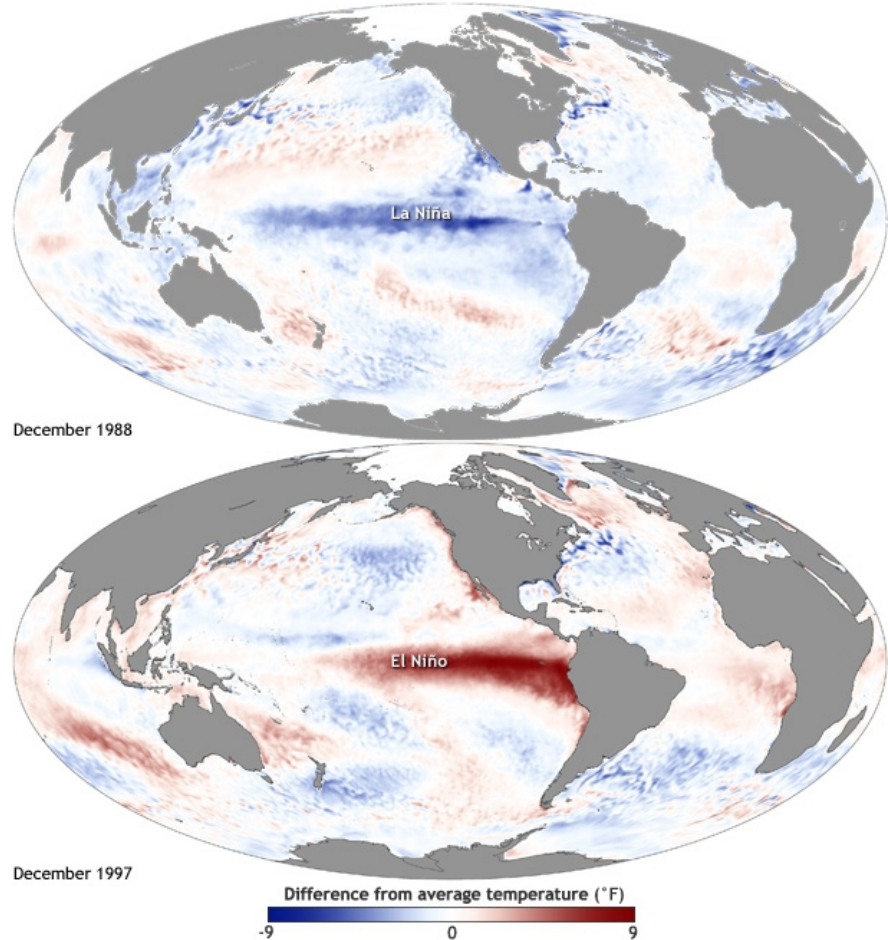


Figure 4.10: Maps of sea surface temperature (SST) anomaly in the Pacific Ocean during a strong La Niña (top, December 1988) and El Niño (bottom, December 1997). Red is warm and blue is cold. Note the warmer ocean surface (positive SST anomaly) in the Pacific all the way from the tropics to the Amundsen-Bellingshausen Sea during an El Niño event (in red). Maps by NOAA Climate.gov, based on data provided by NOAA View (<http://www.nvnl.noaa.gov/view/>).

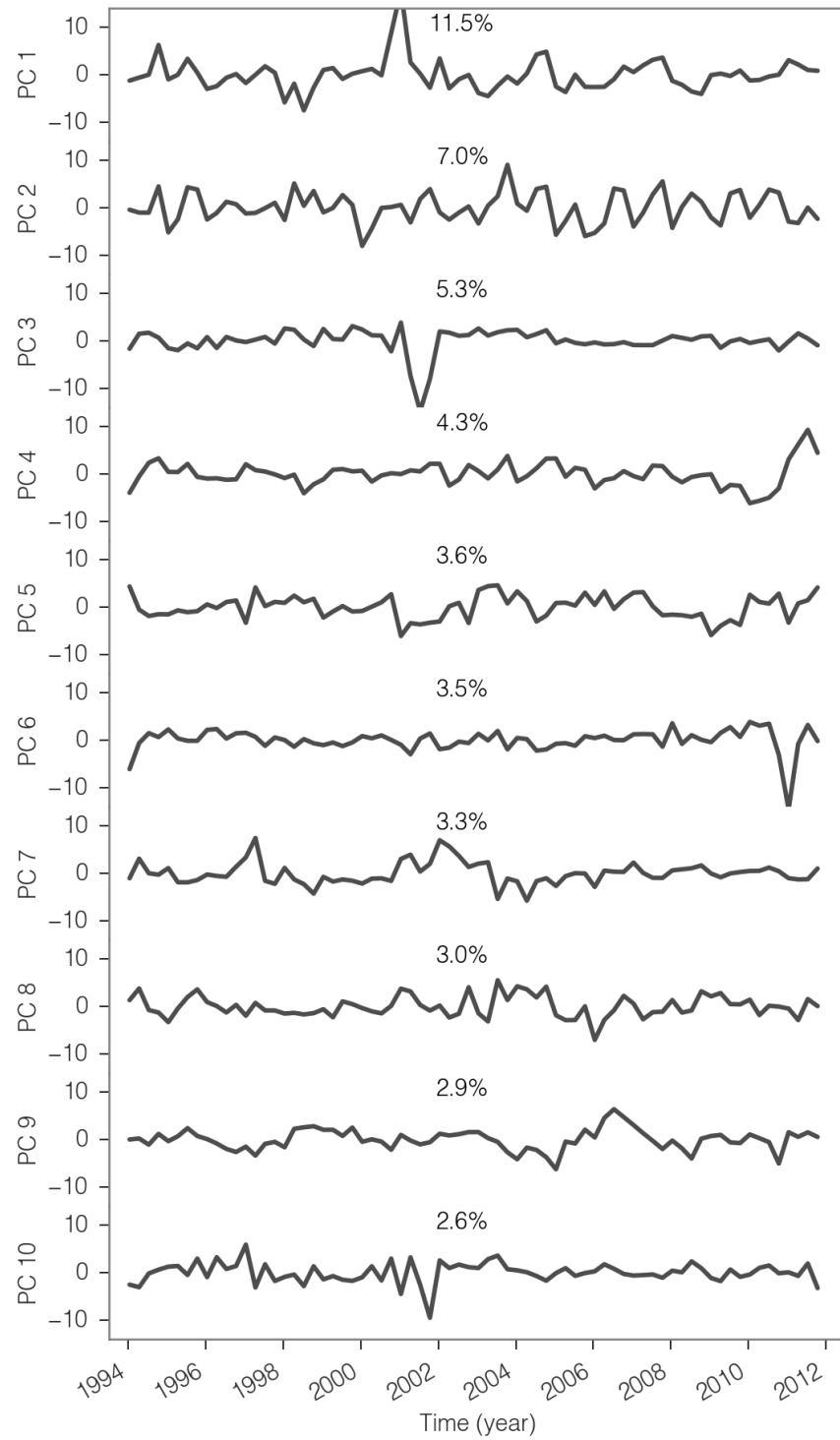


Figure 4.11: Principal components retained after pre-PCA filtering. The ten leading orthogonal components extracted from the original data set (140 time series) by standard PCA. MSSA was then applied to these spatial PCs (i.e., dimensionality was reduced from 140 non-orthogonal series to 10 orthogonal components).

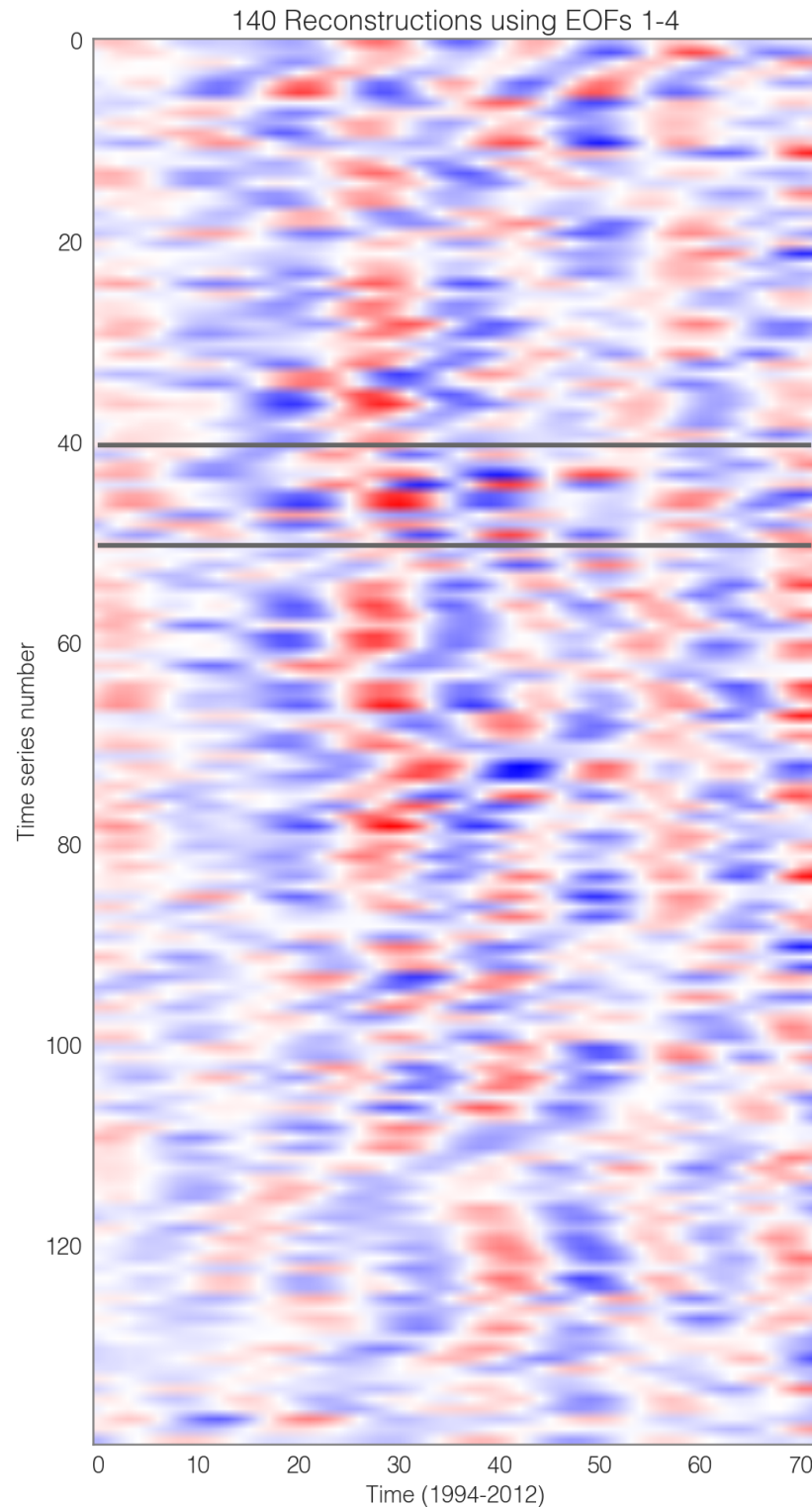


Figure 4.12: Time series reconstruction using EOF 1–4. Reconstruction of all 140 time series of ice-shelf height change for the Amundsen region. Red is negative and blue is positive. The gray lines show the ten reconstructions stacked to construct Fig. 4.9 (see locations in Fig. 4.1).

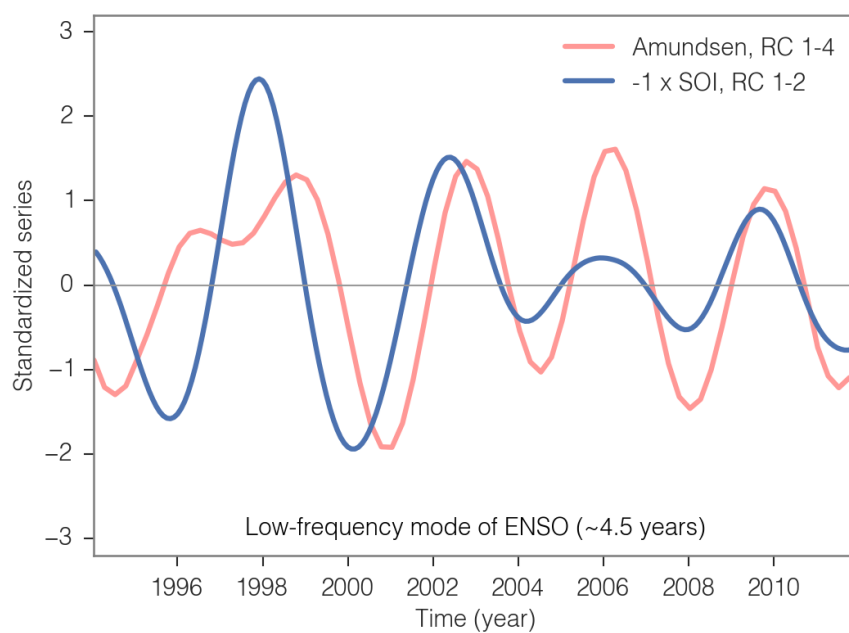


Figure 4.13: Dominant mode of interannual variability (all time series). Reconstruction of the dominant mode of interannual variability for the AS ice-shelf height and the SOI. This is the same as Fig. 4.9 but stacking all 140 reconstructions (instead of only 10). Both series show the same dominant frequency of 0.20–0.23 cycle/year (periodicity of ~ 4.5 years), which corresponds to the low-frequency mode of ENSO.

Acknowledgments

This work was funded by NASA [awards NNX12AN50H 002 (93735A), NNX10A-G19G, and NNX13AP60G]. This is ESR contribution XXX. We thank J. Zwally's Ice Altimetry group at the NASA Goddard Space Flight Center for distributing their RA data sets for all satellite radar altimeter missions (<http://icesat4.gsfc.nasa.gov>).

Chapter 4, in full, is currently being prepared for submission for publication of the material. Paolo, Fernando S.; Fricker, Helen A.; Padman, Laurie. The dissertation author was the primary investigator and author of this material.

References

- Allen, M. R. and L. A. Smith (1996). "Monte Carlo SSA: Detecting irregular oscillations in the Presence of Colored Noise". *Journal of Climate* 9, 3373–3404.
- Arthern, R. J., D. J. Wingham, and A. L. Ridout (2001). "Controls on ERS altimeter measurements over ice sheets: Footprint-scale topography, backscatter fluctuations, and the dependence of microwave penetration depth on satellite orientation". *Journal of Geophysical Research: Atmospheres* 106, 33471–33484.
- Blackman, R. B. and J. W. Tukey (1958). "The Measurement of Power Spectra from the Point of View of Communications Engineering — Part I". *Bell System Technical Journal* 37, 185–282.
- Chen, J. L., C. R. Wilson, D. Blankenship, and B. D. Tapley (2009). "Accelerated Antarctic ice loss from satellite gravity measurements". *Nature Geoscience* 2, 859–862.
- Childers, D. G. (1978). *Modern Spectrum Analysis*. New York: IEEE. 334 pp.
- Cook, A. J. and D. G. Vaughan (2010). "Overview of areal changes of the ice shelves on the Antarctic Peninsula over the past 50 years". *The Cryosphere* 2002, 77–98.
- Davis, C. H. and R. K. Moore (1993). "A combined surface- and volume-scattering model for ice-sheet radar altimetry". *Journal of Glaciology* 39, 675–686.
- Dutrieux, P., J. D. Rydt, A. Jenkins, P. R. Holland, H. K. Ha, S. H. Lee, E. J. Steig, Q. Ding, E. P. Abrahamsen, and M. Schröder (2014). "Strong Sensitivity of Pine Island Ice-Shelf Melting to Climatic Variability". *Science* 343, 174–178.
- Elsner, J. B. and A. A. Tsonis (1996). *Singular Spectrum Analysis: A New Tool in Time Series Analysis*. Springer Science & Business Media. 184 pp.
- Fretwell, P., H. D. Pritchard, D. G. Vaughan, J. L. Bamber, N. E. Barrand, R. Bell, C. Bianchi, R. G. Bingham, D. D. Blankenship, G. Casassa, G. Catania, D. Callens, H. Conway, A. J. Cook, H. F. J. Corr, D. Damaske, V. Damm, F. Ferraccioli, R. Forsberg, S. Fujita, Y. Gim, P. Gogineni, J. A. Griggs, R. C. A. Hindmarsh, P. Holmlund, J. W. Holt, R. W. Jacobel, A. Jenkins, W. Jokat, T. Jordan, E. C. King, J. Kohler, W. Krabill, M. Riger-Kusk, K. A. Langley, G. Leitchenkov, C. Leuschen, B. P. Luyendyk, K. Matsuoka, J. Mouginot, F. O. Nitsche, Y. Nogi, O. A. Nost, S. V. Popov, E. Rignot, D. M. Rippin, A. Rivera, J. Roberts, N. Ross, M. J. Siegert, A. M. Smith, D. Steinhage, M. Studinger, B. Sun, B. K. Tinto, B. C. Welch, D. Wilson, D. A. Young, C. Xiangbin, and A. Zirizzotti (2013). "Bedmap2: improved ice bed, surface and thickness datasets for Antarctica". *The Cryosphere* 7, 375–393.
- Genthon, C. and E. Cosme (2003). "Intermittent signature of ENSO in west-Antarctic precipitation". *Geophysical Research Letters* 30, 2081.

- Ghil, M. and R. Vautard (1991). "Interdecadal oscillations and the warming trend in global temperature time series". *Nature* 350, 324–327.
- Ghil, M., M. Allen, M. Dettinger, K. Ide, D. Kondrashov, M. Mann, A. Robertson, A. Saunders, Y. Tian, F. Varadi, and P. Yiou (2002). "Advanced spectral methods for climatic time series". *Reviews of Geophysics* 40, 3–41.
- Golyandina, N. and A. Zhigljavsky (2013). *Singular Spectrum Analysis for Time Series*. 2013 edition. Heidelberg ; New York: Springer. 120 pp.
- Groth, A. and M. Ghil (2011). "Multivariate singular spectrum analysis and the road to phase synchronization". *Physical review. E, Statistical, nonlinear, and soft matter physics* 84, 036206.
- Harig, C. and F. J. Simons (2015). "Accelerated West Antarctic ice mass loss continues to outpace East Antarctic gains". *Earth and Planetary Science Letters* 415, 134–141.
- Hodrick, R. J. and E. C. Prescott (1997). "Postwar U.S. Business Cycles: An Empirical Investigation". *Journal of Money, Credit and Banking* 29, 1–16.
- Holland, P. R., A. Brisbourne, H. F. J. Corr, D. McGrath, K. Purdon, J. Paden, H. A. Fricker, F. S. Paolo, and A. H. Fleming (2015). "Oceanic and atmospheric forcing of Larsen C Ice-Shelf thinning". *The Cryosphere* 9, 1005–1024.
- Jolliffe, I. T. (2002). *Principal Component Analysis*. Springer Science & Business Media. 524 pp.
- Joughin, I., R. B. Alley, and D. M. Holland (2012). "Ice-Sheet Response to Oceanic Forcing". *Science* 338, 1172–1176.
- Kwok, R. and J. C. Comiso (2002). "Southern Ocean Climate and Sea Ice Anomalies Associated with the Southern Oscillation". *Journal of Climate* 15, 487–501.
- Latif, M. and N. S. Keenlyside (2009). "El Niño/Southern Oscillation response to global warming". *Proceedings of the National Academy of Sciences* 106, 20578–20583.
- Mann, M. E. and J. M. Lees (1996). "Robust estimation of background noise and signal detection in climatic time series". *Climatic Change* 33, 409–445.
- Padman, L., M. King, D. Goring, H. Corr, and R. Coleman (2003). "Ice-shelf elevation changes due to atmospheric pressure variations". *Journal of Glaciology* 49, 521–526.
- Paolo, F. S., H. A. Fricker, and L. Padman (2015a). "Developing improved decadal records of Antarctic ice-shelf height change from multiple satellite radar altimeters". *Remote Sensing of Environment* in revision.
- (2015b). "Volume loss from Antarctic ice shelves is accelerating". *Science* 348, 327–331.

- Penland, C., M. Ghil, and K. M. Weickmann (1991). "Adaptive filtering and maximum entropy spectra with application to changes in atmospheric angular momentum". *Journal of Geophysical Research: Atmospheres* 96, 22659–22671.
- Percival, D. B. and A. T. Walden (1993). *Spectral Analysis for Physical Applications: Multitaper and Conventional Univariate Techniques*. Cambridge: Cambridge University Press.
- Philander, S. G. (1989). *El Nino, La Nina, and the Southern Oscillation*. Academic Press. 309 pp.
- Pritchard, H. D., S. R. M. Ligtenberg, H. A. Fricker, D. G. Vaughan, M. R. van den Broeke, and L. Padman (2012). "Antarctic ice-sheet loss driven by basal melting of ice shelves". *Nature* 484, 502–505.
- Remy, F., T. Flament, F. Blarel, and J. Benveniste (2012). "Radar altimetry measurements over antarctic ice sheet: A focus on antenna polarization and change in backscatter problems". *Advances in Space Research* 50, 998–1006.
- Riffenburgh, B. (2007). *Encyclopedia of the Antarctic*. Taylor & Francis. 1274 pp.
- Rignot, E., G. Casassa, P. Gogineni, W. Krabill, A. Rivera, and R. Thomas (2004). "Accelerated ice discharge from the Antarctic Peninsula following the collapse of Larsen B ice shelf". *Geophysical Research Letters* 31, L18401.
- Rignot, E., J. Mouginot, M. Morlighem, H. Seroussi, and B. Scheuchl (2014). "Widespread, rapid grounding line retreat of Pine Island, Thwaites, Smith, and Kohler glaciers, West Antarctica, from 1992 to 2011". *Geophysical Research Letters* 41, 3502–3509.
- Scambos, T. A., J. A. Bohlander, C. A. Shuman, and P. Skvarca (2004). "Glacier acceleration and thinning after ice shelf collapse in the Larsen B embayment, Antarctica". *Geophysical Research Letters* 31, 2001–2004.
- Scambos, T., H. A. Fricker, C. C. Liu, J. Bohlander, J. Fastook, A. Sargent, R. Massom, and A. M. Wu (2009). "Ice shelf disintegration by plate bending and hydro-fracture: Satellite observations and model results of the 2008 Wilkins ice shelf break-ups". *Earth and Planetary Science Letters* 280, 51–60.
- Shepherd, A., D. Wingham, D. Wallis, K. Giles, S. Laxon, and A. V. Sundal (2010). "Recent loss of floating ice and the consequent sea level contribution". *Geophysical Research Letters* 37, 1–5.
- Shepherd, A., E. R. Ivins, G. A. V.R. Barletta, M. J. Bentley, S. Bettadpur, K. H. Briggs, D. H. Bromwich, R. Forsberg, N. Galin, M. Horwath, S. Jacobs, I. Joughin, M. A. King, J. T. M. Lenaerts, J. Li, S. R. M. Ligtenberg, A. Luckman, S. B. Luthcke, M. McMillan, R. Meister, G. Milne, J. Mouginot, A. Muir, J. P. Nicolas, J. Paden, A. J. Payne, H. Pritchard, E. Rignot, H. Rott, L. S. Sørensen, T. A. Scambos, B. Scheuchl,

- E. J. O. Schrama, B. Smith, A. V. Sundal, J. H. van Angelen, W. J. van de Berg, M. R. van den Broeke, D. G. Vaughan, I. Velicogna, J. Wahr, P. L. Whitehouse, D. J. Wingham, D. Yi, D. Young, and H. J. Zwally (2012). “A Reconciled Estimate of Ice-Sheet Mass Balance”. *Science* 338, 1183–1189.
- Steig, E. J., Q. Ding, D. S. Battisti, and A. Jenkins (2012). “Tropical forcing of Circumpolar Deep Water Inflow and outlet glacier thinning in the Amundsen Sea Embayment, West Antarctica”. *Annals of Glaciology* 53, 19–28.
- Steig, E. J., Q. Ding, J. W. C. White, M. Küttel, S. B. Rupper, T. A. Neumann, P. D. Neff, A. J. E. Gallant, P. A. Mayewski, K. C. Taylor, G. Hoffmann, D. A. Dixon, S. W. Schoenemann, B. R. Markle, T. J. Fudge, D. P. Schneider, A. J. Schauer, R. P. Teel, B. H. Vaughn, L. Burgener, J. Williams, and E. Korotkikh (2013). “Recent climate and ice-sheet changes in West Antarctica compared with the past 2,000 years”. *Nature Geoscience* 6, 372–375.
- Sutterley, T. C., I. Velicogna, E. Rignot, J. Mouginot, T. Flament, M. R. van den Broeke, J. M. van Wessem, and C. H. Reijmer (2014). “Mass loss of the Amundsen Sea Embayment of West Antarctica from four independent techniques”. *Geophysical Research Letters* 41, 2014GL061940.
- Thomson, D. (1982). “Spectrum estimation and harmonic analysis”. *Proceedings of the IEEE* 70, 1055–1096.
- Turner, J. (2004). “The El Niño–southern oscillation and Antarctica”. *International Journal of Climatology* 24, 1–31.
- Vautard, R. and M. Ghil (1989). “Singular spectrum analysis in nonlinear dynamics, with applications to paleoclimatic time series”. *Physica D: Nonlinear Phenomena* 35, 395–424.
- Vautard, R., P. Yiou, and M. Ghil (1992). “Singular-spectrum analysis: A toolkit for short, noisy chaotic signals”. *Physica D: Nonlinear Phenomena* 58, 95–126.
- Velicogna, I. (2009). “Increasing rates of ice mass loss from the Greenland and Antarctic ice sheets revealed by GRACE”. *Geophysical Research Letters* 36, L19503.
- Wingham, D. J. and D. W. Wallis (2010). “The rough surface impulse response of a pulse-limited altimeter with an elliptical antenna pattern”. *IEEE Antennas and Wireless Propagation Letters* 9, 232–235.
- Yuan, X. (2004). “ENSO-related impacts on Antarctic sea ice: a synthesis of phenomenon and mechanisms”. *Antarctic Science* 16, 415–425.
- Yuan, X. and D. G. Martinson (2000). “Antarctic Sea Ice Extent Variability and Its Global Connectivity”. *Journal of Climate* 13, 1697–1717.